

ABSTRACT

Title of dissertation: POLYMER COMPOSITES FOR SENSING AND ACTUATION

Mark Paul Kujawski, Doctor of Philosophy, 2011

Directed By: Professor Elisabeth Smela
Department of Mechanical Engineering.

This thesis concerns materials for polymer actuators and mechanical sensors. Polymer actuators are a class of artificial muscle with promising actuation performance; however, they are currently limited by the materials used in their fabrication. The metal-foil type mechanical strain gauges are commercially available and well understood; however, typically have gauge factors less than 5.5^[1], cannot be patterned into custom shapes, and only monitor small areas. New materials provide opportunities to improve the performance of both polymer actuators and mechanical sensors. The aim of this research was to develop, characterize, and implement such materials. Specifically, this thesis describes novel composites of exfoliated graphite (EG) blended with elastomeric hosts. The mechanical and electrical properties of these composites were tailored for two specific applications by

modifying the EG loading and the elastomer host: compliant electrodes and strain gauges.

Compliant electrodes were demonstrated that had ultimate tensile strains greater than 300% and that could withstand more than 10^6 strain cycles. Composites fabricated with polydimethylsiloxane (PDMS) exhibited conductivities up to 0.2 S/cm, and having tangent moduli less than 1.4 MPa. This modulus is the lowest reported for loaded elastomers above the percolation threshold.

Conductivity was increased to more than 12.5 S/cm by fabricating composites with polyisoprene (latex) elastomers, and the tangent moduli remained less than 5 MPa. Actuation strains of polymer actuators were increased 3 fold using the composites as electrodes, compared to using carbon-grease electrodes. This was due to the composites ability to be spin-coated with thin insulating layers of PDMS, allowing 30% higher electric fields to be applied.

Strain gauges fabricated with these composites exhibited gauge factors (GFs) $> 27,000$, to the authors knowledge this is the highest GF ever reported. The effects of humidity, temperature and strain were investigated.

POLYMER COMPOSITES FOR SENSING AND ACTUATION

By

Mark Paul Kujawski

Dissertation submitted to the Faculty of the Graduate School of the
University of Maryland, College Park in partial fulfillment
of the requirements for the degree of
Doctor of Philosophy
2011

Advisory Committee:

Professor Elisabeth Smela, Chair
Professor Sreeramamurthy Ankem
Professor Sarah Bergbreiter
Professor Satyandra K. Gupta
Professor Oded Rabin
Professor Srinivasa R. Raghavan

© Copyright by
Mark Paul Kujawski
2011

Dedication

This work is dedicated to my advisor, Dr. Elisabeth Smela, and my dissertation committee members for their invaluable guidance, advice, and support. They say behind every great man, stands an even greater woman. From my experience, this is true. I would like to extend my dedication to my loving girlfriend, Megan, for having the virtue of patience and for putting up with countless living room experiments, late nights, early mornings, and long weekends. Thank you all.

Acknowledgements

I am especially grateful to my advisor, Dr. Elisabeth Smela, for her many years of continued guidance. She provided me with the tools necessary to become a successful and independent research scientist. Her wisdom has improved my ability to think critically, work diligently, and effectively overcome obstacles.

I would like to thank all of my dissertation advisory committee members for their support and guidance, Dr. Srinivasa Raghavan, Dr. Sreeramamurthy Ankem, Dr. Sarah Bergbreiter, Dr. Satyandra K. Gupta, and Dr. Oded Rabin

I would like to express my gratitude for the extended support from Dr. Hugh Bruck for his guidance and advice with modeling, and Dr. Oded Rabin for his advice on conducting experiments and analyzing data Dr. Srinivasa Raghavan for his advice, guidance, and initiation of the resistive heating application,.

A very special thanks goes to my colleagues for their conversations, suggestions for improving my research, and for helping develop my ideas, and improve presentations including Bavani Balakrishna, Justin Pearce, Timir Datta, Deepa Sritharan, Eugene Daneshvar (University of Michigan), Marc Dandin, and Dr. Mario Urdaneta.

I would like to thank my colleagues Dr. Jeff Burke and Dr. Disha Pant for their help with editing papers and for their invaluable advice and discussions.

I am also grateful to Dr. Mike Armani for his advice on business startups, proof reading executive summaries, and helping us rehearse business plan competition presentations.

I would like to thank those I trained and mentored, including Justin Pearse, Kate Miller, Sungmin Park, Brent Snyder, Tristan Neumann, Xavier Pelle, and for their willingness to learn, dedication, and hard work.

I must also thank Li-Chung (Larry) Lai, and Dr. Wen-An Chiou for their help with SEM imaging.

I would like to thank Dr. Fuhrer and Alex Curtin from the Physics Department for providing the necessary training, equipment, and materials for exfoliating graphite.

I would like to thank Charles Elder, Omkar Deer, Dr. Nabil, and everyone at Lawrence Technological University for allowing me to use their facilities and help with my research.

I would like to thank people outside of my work who helped me and supported me, especially to the assistant Director of Student Services in the Department of Materials Science and Engineering, Dr. Kathleen Hart, and the entire administrative staffs of the Departments of Aerospace Engineering, Materials Science and Engineering, and

Mechanical Engineering. Lastly, I have to thank Dr. Inder Chopra, the Micro Autonomous Systems and Technologies program (MAST) of the U.S. Army Research Labs, and the U.S. tax-payers for financially supporting my research.

Table of Contents

ABSTRACT.....	ii
Dedication.....	ii
Acknowledgements.....	iii
Table of Contents.....	vi
List of Figures.....	ix
List of Tables.....	xiv
Chapter 1: Motivation and background.....	1
1.1 Introduction.....	1
1.2 Background.....	2
1.3 Dielectric elastomer actuators.....	2
1.3.1 What are dielectric elastomer actuators?.....	2
1.3.2 Device types.....	5
1.3.3 Fabrication and actuation.....	6
1.3.4 Compliant electrodes.....	7
1.4 Literature review.....	8
1.4.1 Actuation strain.....	9
1.4.2 Actuation stress.....	11
1.4.3 Blocking force.....	12
1.4.4 Load curves.....	12
1.5 Mechanical sensors.....	15
1.6 Summary.....	16
1.7 Aims.....	16
1.8 Chapter 1 Appendix.....	17
1.9 Co-author contributions.....	19
1.9.1 Chapter 2.....	19
1.9.2 Chapter 3.....	19
1.9.3 Chapter 4.....	19
1.9.4 Chapter 5.....	19
Chapter 2: Comparison of three elastomers for dielectric elastomer actuators.....	21
2.1 Abstract.....	21
2.2 Introduction.....	21
2.3 Experimental.....	23
2.3.1 Elastomer preparation.....	23
2.3.2 DEA fabrication and electrical connection.....	24
2.3.3 Mechanical measurements.....	25
2.4 Results and discussion.....	26
2.4.1 Tangent modulus.....	26
2.4.2 Creep.....	28
2.4.3 Actuation strain as a function of electric field.....	29
2.4.4 Actuation response times.....	31

2.4.5	Actuation strain as a function of frequency	33
2.5	Conclusions.....	36
2.6	Acknowledgements.....	36
2.7	Chapter 2 Appendix	37
2.7.1	Experimental challenges	37
2.7.1.1	Sample sparking	37
2.7.1.2	Equipment limitations.....	38
2.7.2	Unsuccessful experiments.....	38
Chapter 3: Elastomers filled with exfoliated graphite as compliant electrodes.....		41
3.1	Abstract.....	41
3.2	Introduction.....	42
3.3	Experimental.....	44
3.3.1	Microwave Exfoliation	44
3.3.2	Characterization	45
3.3.3	Sample fabrication	46
3.3.4	Mechanical testing	48
3.3.5	Geometric corrections.....	49
3.4	Results and discussion	49
3.4.1	Exfoliation results.....	49
3.4.2	Modulus and strain.....	50
3.4.3	Modulus and strain versus EG loading	56
3.4.4	Strain to failure	58
3.4.5	SEM images of composites.....	60
3.5	Discussion.....	61
3.6	Conclusions.....	62
3.7	Acknowledgements.....	62
3.8	Chapter 3 Appendix	64
3.8.1	Alternative electrodes	64
3.8.2	Surfactants.....	76
3.8.2.1	Triton X-100 and DSPE-mPEG 5000	76
3.8.2.2	Triton X-100.....	76
3.8.2.3	Triton X- 45.....	77
3.8.2.4	Sodium cholate hydrate	78
3.8.3	Comparison of PDMS/EG to similar compliant electrode materials....	78
3.8.4	Basis of Using EG for Conductive Composites with Low Modulus....	79
3.8.5	Effects of voids on the tangent moduli	82
3.8.6	Uncertainty calculations for conductivity.....	83
3.8.7	Dynamic stress-strain characterization of the composites.....	85
3.8.8	Sample Fabrication	86
3.8.9	Power law model for conductivity as a function of EG loading.....	88
Chapter 4: PDMS/graphite stretchable electrodes for dielectric elastomer actuators		92
4.1	Abstract.....	92
4.2	Introduction.....	93

4.3	Experimental	95
4.3.1	Microwave exfoliation	95
4.3.2	Characterization	96
4.3.3	Sample fabrication	96
4.4	Electrical and mechanical characterization.....	100
4.5	Results and discussion	102
4.5.1	Mechanical characterization of PDMS/EG composites.....	102
4.5.2	Electro-mechanical characterization of PDMS/EG composites	104
4.5.3	Electro-mechanical characterization of DEAs.....	106
4.6	Conclusion	108
4.7	Acknowledgements.....	109
Chapter 5:	Paintable elastomeric strain sensors: Characterization and application	
	110	
5.1	Abstract	110
5.2	Introduction.....	111
5.3	Experimental	112
5.3.1	Composite formulation	112
5.3.2	Sample fabrication	113
5.3.3	Temperature-resistance measurements	115
5.3.4	Temperature-humidity measurements	116
5.4	Results and Discussion	117
5.4.1	Characterization of latex composites	117
5.4.2	Young's modulus as a function of EG loading.....	118
5.4.3	Resistance as a function of strain.....	121
5.4.4	Resistance as a function of temperature.....	124
5.4.5	Resistance as a function of humidity	126
5.5	Applications of the composites as sensors.....	128
5.5.1	Tactile sensor application	128
5.5.2	Structural health monitoring application	131
5.6	Conclusions.....	135
5.7	Acknowledgments.....	136
5.8	Chapter 5 Appendix	137
5.8.1	Electron tunneling and activation energy of latex/EG composites.....	137
Chapter 6:	Concluding remarks and suggestions for future work	140
6.1	Concluding remarks	140
6.2	Future work.....	140
Chapter 7:	Intellectual contributions	143
References	146

List of Figures

Figure 1. Schematic illustration of a typical dielectric elastomer actuator.....	3
Figure 2. DEA applications in a) a walking robot fabricated by Pelrine <i>et al.</i> ^[14] , b) an inchworm fabricated by the Sungkyunkwan University ^[15] , and c) a blimp fabricated by the Technical University of Berlin ^[16]	4
Figure 3. DEA device forms.....	6
Figure 4. Compliant electrodes made from a) carbon grease, b) patterned metals ^[22] , c) ion implantation ^[23] , d) elastomer composites with carbon filler particles ^[24]	7
Figure 5. a) Actuation strain as a function of device form, b) actuation strain/ \sqrt{E} as a function of device form. Circles represent acrylic elastomers, diamonds represent silicone elastomers, and the x symbols represent other elastomers.....	10
Figure 6. a) Actuation strain as a function of elastomer type, b) actuation strain/ \sqrt{E} as a function of elastomer type. Circles represent acrylics, diamonds represent silicones, and x's represent other elastomers.....	10
Figure 7. Actuation strain as a function of force for a) silicone tube DEA ^[33] , b) silicone membrane DEA ^[72] , c) silicone membrane DEA with a 3 mm diameter ^[73] , d) silicone membrane DEA with a 2 mm diameter ^[73] , e) silicone multipart DEA by Danfoss ^[71] , f) urethane tube DEA ^[33] , g) acrylic fold/stack DEA ^[74] , and h) acrylic multi-part DEA ^[75]	13
Figure 8. a) stress as a function of DEA elastomer type, b) force as a function of DEA elastomer type.....	14
Figure 9. a) stress divided by the square root of the applied electric field as a function of DEA elastomer type, b) force divided by the square root of the applied electric field as a function of DEA elastomer type.....	15
Figure 10. Device configuration and experimental setup.....	25
Figure 11. Stress as a function of strain for the three elastomers, measured at a strain rate of 0.1 mm/s.....	27
Figure 12. Strain as a function of time for the three elastomers under an applied stress of 75 kPa.....	29
Figure 13. Schematic of the elongation that results when a mass is applied to the free end of a free-film DEA.....	30
Figure 14. a) Actuation strain as a function of time for a TC-5005 DEA. The raw data (dotted line), the corresponding creep strain (dashed line), and the corrected	

actuation strain (solid line) are shown. b) Strain as a function of electric field for DEAs fabricated with the 3 elastomers. The applied stress was 75 kPa and averages represent at least 3 samples. The dashed lines are guides for the eye. 31

Figure 15. a) Actuation strain as a function of time for a voltage step on/off. Rise times are shown. b) Applied electric field, 27.5 V/ μm , as a function of time. 32

Figure 16. Actuation strain as a function of frequency for a) PDMS DEAs at 47.5 V/ μm , b) TC-5005 DEAs at 25.0 V/ μm , and c) VHB-4905 DEAs DEAs at 27.5 V/ μm . d) Gain as a function of frequency; solid lines show the best fit roll-off rates. 34

Figure 17. Schematic illustration of the voltage and current measuring system used to calculate DEA power consumption. 39

Figure 18. For a PDMS/carbon grease DEA, a) voltage, b) current, c) power, and d) actuation strain as functions of time. 40

Figure 19. a) Acid-washed graphite before (left) and after (right) microwave exfoliation. b) SEM image of worm-like EG structures. 45

Figure 20. Schematic of the testing configuration. 48

Figure 21. SEM of microwave exfoliated graphite (EG) after sonication in hexane at a) 1,000 times magnification, and b) 10,000 times magnification. 50

Figure 22. For a 15 wt% sample a) stress vs. strain for the first 15 cycles, b) Young's modulus at 10% strain vs. cycle number, c) conductivity vs. strain, and d) conductivity vs. cycle number. The first cycle is indicated by a dotted black line, cycles 2-14 by gray lines, and cycle 15 by a solid black line. The directions of increasing and decreasing strain are indicated by arrows, as are shifts with increasing cycling number. 51

Figure 23. Research results by others showing, versus filler material, a) the percolation threshold, b) the maximum conductivity (circles) and the loading at maximum conductivity (squares), and c) the Young's modulus (circles) and the modulus increase (squares). The + symbols show the values for PDMS/EG of the percolation threshold, maximum conductivity, and Young's modulus, while the \times symbols show the values of loading at maximum conductivity and the modulus increase. 55

Figure 24. a) Conductivity and b) Young's modulus vs. loading of EG in 20:1 PDMS. For the modulus, 4 points were taken for 5, 10, and 15 wt%, three points for 20 wt%, and one for 25 wt%. The average and standard deviation are also indicated in gray in (b). 57

Figure 25. Ultimate tensile strain for PDMS/EG samples as a function of loading. A 5 wt% 20:1 PDMS/EG film spin coated onto a 10:1 PDMS film and patterned with “UMD compliant electrodes” is shown at rest and at 100% strain.....	59
Figure 26. SEM images of a) PDMS without EG and b) PDMS with 15 wt% EG...	60
Figure 27. Images of PDMS DEAs with a) gold electrodes with the contact pads patterned on the same-side of the DEA, and b) gold electrodes with the contact pads patterned on the opposite-sides of the DEA.	65
Figure 28. Images of a) the spring connection for DEAs with patterned gold electrodes, and b) close up of the spring making contact with the top gold contact pad.	66
Figure 29. Images of a) the ski connection for DEAs with patterned gold electrodes, and b) close up of the ski making contact with the top gold contact pad.	66
Figure 30. Images of a) the magnet type connection used for DEAs with patterned gold electrodes, and b) close up of the magnet making contact with the top gold contact pad.	67
Figure 31. Image of a PDMS/graphite composite material.	68
Figure 32. Images of DEAs fabricated with PDMS/graphite electrodes.....	68
Figure 33. Image of a patterned PDMS/EG DEA showing the silver epoxy contact pads applied over non-overlapping areas of the top and bottom electrode layers.	69
Figure 34. Processing and fabrication sequence for elastomer/EG compliant electrodes.	70
Figure 35. SEM images of chemically exfoliated graphite a) in a 15 wt% composite with PDMS at 300 times magnification, b) at 2,500 times magnification, and c) at 100,000 times magnification.....	75
Figure 36. Average conductivity as a function of surfactant concentration (wt% in DI water) for latex/EG composites fabricated with Triton X-100 surfactants.....	77
Figure 37. Guth and Halpin-Tsai model predictions for the Young’s modulus as a function of aspect ratio f for $E_0 = 0.44$ MPa and $\phi = 0.15$	80
Figure 38. Conductivity and Young’s modulus as a function of weight% of EG for PDMS/EG composites.	82
Figure 39. Stress as a function of strain for 15 wt% PDMS/EG composite calculated using the measured sample geometry (circles) compared to the stress strain curves for the same sample that were calculated using adjusted geometries to account for 5 vol% voids (squares) and 20 vol% voids (diamonds).	83

Figure 40. a) Stress as a function of strain for a sample with 5 wt% loading. b) Stress as a function of strain for 25 wt% loading.....	86
Figure 41. Power law fit to the conductivity as a function of loading data, with the dotted line representing the fit for unstrained samples (squares) and the dashed line representing the fit for strained samples (circles). Each point represents one sample.	88
Figure 42. a) Acid-washed graphite flakes before microwave exfoliation, b) acid-washed graphite flakes after microwave exfoliation, c) SEM image of worm-like EG particles at 30 times magnification, and d) SEM image of worm-like EG particles at 150 times magnification.....	96
Figure 43. Schematic of a cross sectional view of a DEA sample and the DEA testing configuration.	98
Figure 44. PDMS/EG material patterned with “UMD compliant electrodes” showed at rest (left) and at 100% strain (right).....	100
Figure 45. PDMS/EG compliant electrode material (black diamonds) compared to 10:1 PDMS (gray circles) in terms of a) stress vs. applied strain and b) creep strain vs. time.	103
Figure 46. SEM images at 1000 times magnification of a) unloaded PDMS, and b) 15 wt% PDMS/EG with voids present.....	104
Figure 47. Conductivity (black diamonds) and Young’s modulus (gray circles) vs. strain cycle for the PDMS/EG electrode material.....	105
Figure 48. a) Actuation strains of a DEA made with PDMS/EG electrodes (black line marked by diamonds) vs. time under applied electric fields of 15, 17.5, and 20 V/ μm . The actuation strain was found by removing the creep strain from Figure 45b (middle solid line) from the raw data (gray line marked by circles). b) Actuation strain vs. electric field of PDMS/EG (diamonds) compared to the strain in a DEA with CG electrodes (crosses). The dashed line is a guide for the eye.	107
Figure 49. a) Actuation strains of DEAs made with PDMS/EG electrodes (diamonds) and CG electrodes (circles) vs. time under an electric field of 50 V/ μm showing the corresponding rise and relaxation times. b) Actuation strains vs. frequency under electric fields of 27.5 and 47.5 V/ μm showing the fall-off of the actuation strains with increasing frequency. The dotted lines are guides for the eye.	108
Figure 50. Sample configuration for temperature dependence measurements.	116
Figure 51. a) Young’s moduli of latex/EG as a function of EG loading. Each point represents an average of two samples, and the standard deviations are indicated. The dashed line shows the Guth model. b) Young’s moduli as a function of strain (dashed	

lines are linear guides for the eye). c) Stress-strain curves for latex and for 6 and 10 wt% latex/EG composites.	119
Figure 52. Particle count as a function of particle diameter for EG particles.....	120
Figure 53. Gauge factor as a function of strain for latex/EG composites with three EG loadings strained at a rate of 0.1 mm/s.	122
Figure 54. a) Resistance (solid line) vs. time for a 6 wt% latex/EG composite cycled 5 times b) from 0 to 5% strain (triangle wave).	124
Figure 55. Resistivity vs. temperature for latex/EG composites at increasing strains. Each point represents the average of 3 samples. EG loadings were 6 wt% (circles), 7 wt% (squares), 8 wt% (diamonds), 9 wt% (triangles-up), and 10 wt% (triangles-down).	125
Figure 56. Normalized resistance as a function of relative humidity for a) 8 wt% latex/EG composites at 0% strain, b) 8 wt% latex/EG composites at 5% strain, c) 10 wt% latex/EG composites at 0% strain, and d) 10 wt% latex/EG composites at 5% strain. The dotted lines are guides for the eye.	127
Figure 57. Image of a 20 wt% neoprene/EG tactile sensor patterned via airbrushing onto a nitrile glove.	129
Figure 58. Neoprene/EG tactile glove sensor. a) Resistance at rest. b) Resistance when gripping an object. c) Normalized resistance $\Delta R/R_0$ vs. time under applied forces.....	130
Figure 59. Schematic of the 1/2 scale box beam and sensor positions.	132
Figure 60. a) Latex/EG strain gauge painted on a concrete structure over b) a series of cracks, and c) a rolled edge.	132
Figure 61. a) Load applied by the hydraulic ram. b) Strain measured with a commercial strain gauge and the 8 wt% latex/EG strain gauge applied to a 1/2 scale concrete composite bridge beam strained to failure.	134
Figure 62. The natural logarithm of conductivity as a function of inverse absolute temperature for latex/EG composites with EG loadings of 6 (circles), 7 (squares), 8 (diamonds), 9 (triangles - up), and 10 wt% (triangles - down).	138
Figure 63. Activation energy of latex/EG composites as a function of EG loading.	139

List of Tables

Table 1. Materials and conditions of reported data in Figure 8 and Figure 9.....	17
Table 2. Cutoff frequencies and roll-off rates for the three types of DEA. (There are no previous literature reports of cut-off frequencies.)	35
Table 3. Modulus and conductivity of 15 wt% PDMS/EG and results from prior work on elastomers with conductive fillers.	56
Table 4. Host materials and references for Figure 5 in the main text. Reference numbers are those used in the main text.	79
Table 5. Measured length, width, thickness, and resistance of five 6 wt% latex/EG samples and the calculated averages and standard deviations.	84
Table 6. Critical exponents t for PDMS/EG compared with results from prior work on unstrained elastomers with conductive fillers.	90
Table 7. Bridge beam deformation rate and duration.	133

Chapter 1: Motivation and background

Combining two or more materials to form a composite may yield properties that are unique from those of the individual constituents. Composites have many advanced applications, ranging from non-stick coatings protecting medical devices from bacteria ^[2] to race-car parts having ultra high strength to weight ratios ^[3]. This thesis examines how elastomer composites can be engineered to provide improved performance in polymer actuators and mechanical sensors.

1.1 Introduction

Mechanical sensors and polymer actuators are electromechanical transducers that convert mechanical or electrical inputs into electrical or mechanical outputs, respectively. The aim of this research was to **develop, characterize, and implement** novel composites for improved performance of polymer actuators, tactile sensors, and strain gauges. This thesis is organized into chapters discussing the steps taken to complete the objectives of this research.

- Chapter 1 of this thesis provides a review of the literature and background information for DEAs, as well as some general information on dielectrics, compliant electrodes, and sensors (further information on these subjects is provided in Chapters 2 through 5).

- The dielectric, mechanical, and actuation performances of DEAs fabricated with three commonly used elastomers are compared in Chapter 2.
- Chapter 3 presents the processing and fabrication of a new compliant electrode material intended for applications such as DEAs.
- Chapter 4 discusses the implementation of the compliant electrode material into DEAs and determines their effectiveness as a replacement for carbon grease.
- Chapter 5 examines applications of the compliant electrode material as tactile sensors and strain gauges.

Chapters 1-3 and 5 are followed by an appendix, providing additional information.

1.2 Background

This section provides basic information about the polymer actuators in this research, specifically dielectric elastomer actuators (DEAs), their reported actuation performance, and the main issues limiting their application. Elastomer materials, device forms, and experimental techniques used by researchers in the field are also presented.

1.3 Dielectric elastomer actuators

1.3.1 What are dielectric elastomer actuators?

Dielectric elastomer actuators (DEAs) are electromechanical transducers consisting of an elastomeric dielectric sandwiched between two compliant electrodes. When an electric

field is applied to the compliant electrodes, electrostatic forces are generated that compress the elastomer in the z -direction and expand it in the x and y -directions (Figure 1).

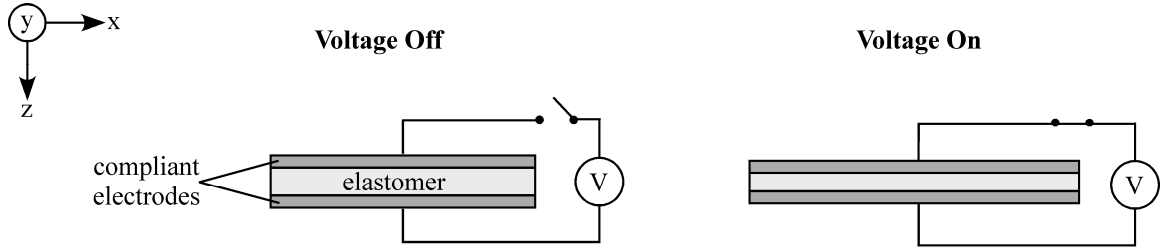


Figure 1. Schematic illustration of a typical dielectric elastomer actuator.

DEAs have received much interest and research since their inception nearly a decade ago by the Pelrine and Carpi group. At first, DEA research focused on device configurations. More recently, the focus has shifted towards investigating material properties to improve actuation performance.

The electrostatic pressure generated by DEAs is proportional to the square of the electric field. The electrostatic pressure, commonly known as Maxwell stress, is written as ^[4]:

$$\text{Eq. 1} \quad P_{el} = \frac{1}{2} \varepsilon \varepsilon_0 E^2 = \frac{1}{2} \varepsilon \varepsilon_0 (V/t)^2,$$

where P_{el} is the electrostatic pressure, ε is the dielectric constant of the elastomer, ε_0 is the vacuum permittivity (8.854×10^{-12} F/m), E is the electric field, V is the voltage, and t is the elastomer thickness. In the literature, the $\frac{1}{2}$ in Eq. 1 is commonly neglected due to an assumed expansion in electrode area caused by like charge repulsion ^[5]; however, this has not been experimentally observed in our investigations, and therefore have chosen to

maintain the $\frac{1}{2}$ in the Maxwell stress equation. Actuation pressure is related to actuation strain for unconstrained DEAs through the Young's modulus Y of the dielectric elastomer [6, 7].

$$\text{Eq. 2} \quad s_z = -p_z / Y, \text{ and}$$

$$\text{Eq. 3} \quad s_x = s_y = -\nu s_z.$$

where s_x , s_y , and s_z are the x -, y -, and z -direction strains, and ν is the Poisson's ratio of the elastomer. Combining Eq. 1 - Eq. 3 provides an equation for the x -direction strain:

$$\text{Eq. 4} \quad s_x = ((\frac{1}{2} \epsilon \epsilon_0 E^2) / Y) \nu.$$

DEAs have been reported with actuation strains up to 300% [8], stresses of up to 7 MPa [9], and estimated energy densities of over 3 J/g [9]. Demonstrated applications include artificial muscles for robotics [10], tunable optics [11], loudspeakers [12], and tactile sensors for Braille displays [13]. Figure 2 illustrates some examples of DEAs functioning in robotics applications. The reported actuation performance metrics have attracted much attention over the past decade as potential replacements or substitutes for DC electric motors, piezoelectric transducers, and shape memory alloys.

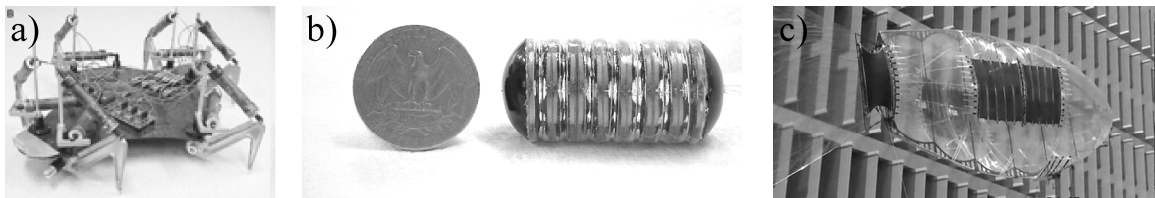


Figure 2. DEA applications in a) a walking robot fabricated by Pelrine *et al.* [14], b) an inchworm fabricated by the Sungkyunkwan University [15], and c) a blimp fabricated by the Technical University of Berlin [16].

1.3.2 Device types

DEAs are fabricated in a variety of shapes and forms, some of which are illustrated in Figure 3. In the literature, the primary DEA device forms are stretched film and free film, comprising more than 50% of all DEAs^[5]. Free-film DEAs (Figure 3a) consist of a DEA with one end fixed and the other end free to strain. Free film DEAs do not require rigid frames and can be attached to external loads directly, allowing work to be achieved without the use of additional linkages and attachments. Stretched Film DEAs (Figure 3b) use rigid frames to support pre-straining of the device. Diaphragm and membrane DEAs (Figure 3c) are pre-strained elastomers fixed to a rigid frame, similar to the stretched film DEAs. These forms do not strain in the x-direction like free or stretched films; rather, they bend or buckle out of plane. Multi-part DEAs (Figure 3d) consist of a stretched film DEA attached to mechanical linkages, such as the scissor-jack mechanism. Multi-part DEAs can be used to amplify either the force or the stroke produced by a DEA.

Free films produce movement without frames, mechanical linkages, or transmissions.

Free films have been demonstrated having actuation strains of up to 20% strain^[17], which was achieved using a silicone elastomer (Sylgard 182) under an electric field of 50 V/um.

Mechanical linkages can amplify actuation strain or force. Plante *et al.*^[18] fabricated a scissor-jack type frame with acrylic DEAs pre-strained between the linkages that achieved 150% strain. The actuation strain reported was not the strain exhibited by the DEA, but rather multiplied many times by the frame design.

Tube DEAs comprise only 5% of the DEA research ^[5] but are a promising device form. These devices are either single elastomer tubes ^[19] or stacked DEAs rolled together ^[20].

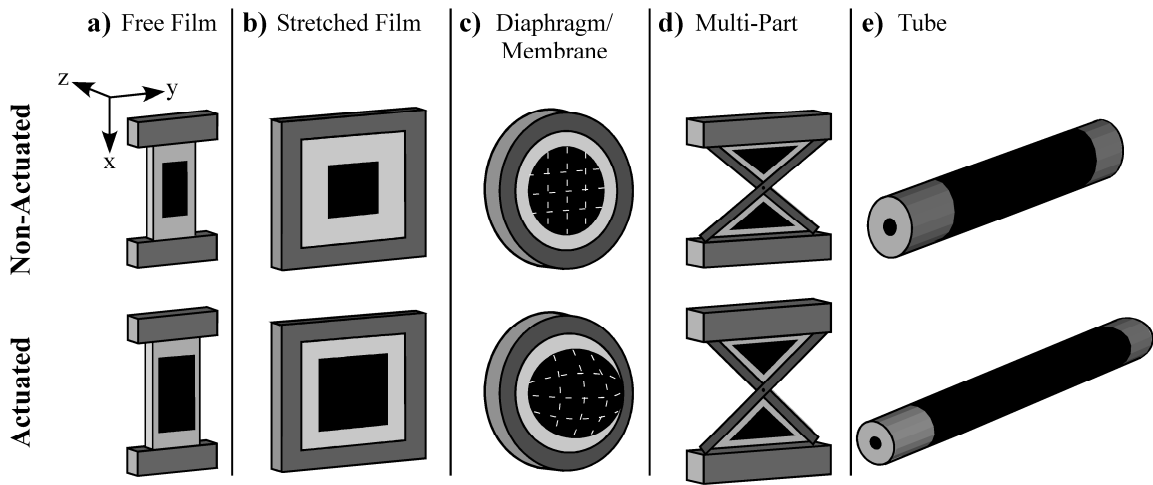


Figure 3. DEA device forms.

1.3.3 Fabrication and actuation

DEAs are fabricated by applying the compliant electrode to a cured elastomer. The most common compliant electrode is carbon grease ^[5]. Carbon grease electrodes are typically smeared over a stencil, and the stencil is removed leaving the desired pattern. Wires are then placed into the grease for connections to high voltage equipment. For tube DEAs, the carbon grease is forced into the center of the tube and also coated onto the surface of the tube to form the DEA. The dielectric materials used are either 1) pre-cured films, sheets or tapes, or 2) un-cured liquids that can be cast, spin coated, or otherwise processed and cured by solvent evaporation or vulcanization into solid elastomers. A major drawback for DEAs is the high voltages required for actuation, which often exceed 10 kV. When actuated, DEAs “push” which is the opposite of natural muscle.

1.3.4 Compliant electrodes

A major problem with DEAs is the lack of an ideal compliant electrode. For DEAs to achieve the largest actuation strains possible, the compliant electrode must have a low Young's modulus (or tangent modulus^[21] above stresses where Hook's law is invalid) so they do not impede actuation. It would also be beneficial for compliant electrodes if they were easily fabricated without requiring specialized equipment and if they could be patterned. A variety of materials and fabrication methods have been implemented, some of which are shown in Figure 4.

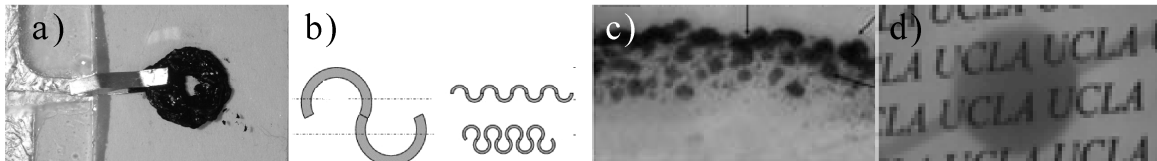


Figure 4. Compliant electrodes made from a) carbon grease, b) patterned metals^[22], c) ion implantation^[23], d) elastomer composites with carbon filler particles^[24].

Carbon grease is the most common electrode material because it is electrically conductive, is easy to apply, and has a low stiffness. The disadvantages of carbon grease are that it smears and rubs off, patterns distort when actuated, and dries out over time. One alternative is patterned metals. Patterned metals have much higher conductivity than carbon grease (10^6 S/cm vs. 10^{-1} S/cm) and can be applied to polymer and elastomer surfaces in intricate patterns; however, patterned metal electrodes, such as the serpentine patterns shown in Figure 4b, bend out of plane when stretched. The out-of-plane displacement results in a decrease in the stiffness by as much as 10^3 compared to the bulk stiffness^[22]. It is reasonable to suppose that the out-of-plane displacement required to

reduce the stiffness of the patterned metal electrodes may restrict DEAs from being fabricated into stacks or multi-layered systems.

Ion implanted electrodes are an excellent alternative to carbon grease because they provide electrical conductivity while maintaining the mechanical properties of the host elastomers^[23]. In this method, metal ions are generated under a high electric field and accelerated into a target surface. There are two problems with ion implantation: 1) specialized equipment is required, and 2) carbonization, chain scission and increased surface roughness occur due to damage created by the dissipation of the incoming ion energy^[23].

Perhaps the most promising alternative compliant electrode materials are elastomer composites. In this method, elastomers are blended with conductive filler particles above the percolation threshold to impart electrical conductivity^[25]. Maintaining the mechanical properties of the host elastomers remains an issue. Such materials have many additional applications including anti-static coatings^[26] and flexible electronics^[27].

1.4 Literature review

The following section provides an overview of DEA performance reported in the literature. When possible, actuation strains and forces have been normalized to the electric field and data were arranged by device form and elastomer material (silicone, acrylic, and other). From this section, the dissimilarities in DEA performances published

from group to group will become evident, justifying the need for the DEA comparison provided in Chapter 2.

1.4.1 Actuation strain

To effectively determine which DEA elastomers and configurations (as published in literature) have the best performance, it is necessary to level the playing field. For this, actuation strains have been arranged in terms of their device type (stretched-film, roll, multi-part, free film, tube, fold/stack, and other) in Figure 5a and by elastomer type (acrylic, silicone, and other) in Figure 6a. The actuation strain data were taken from [8, 9, 17-19, 28-71]. Actuation strains are plotted per unit electric field in Figure 5b and Figure 6b by dividing the actuation strain values by the square root of the reported electric field (Eq. 1) in $V/\mu\text{m}$.

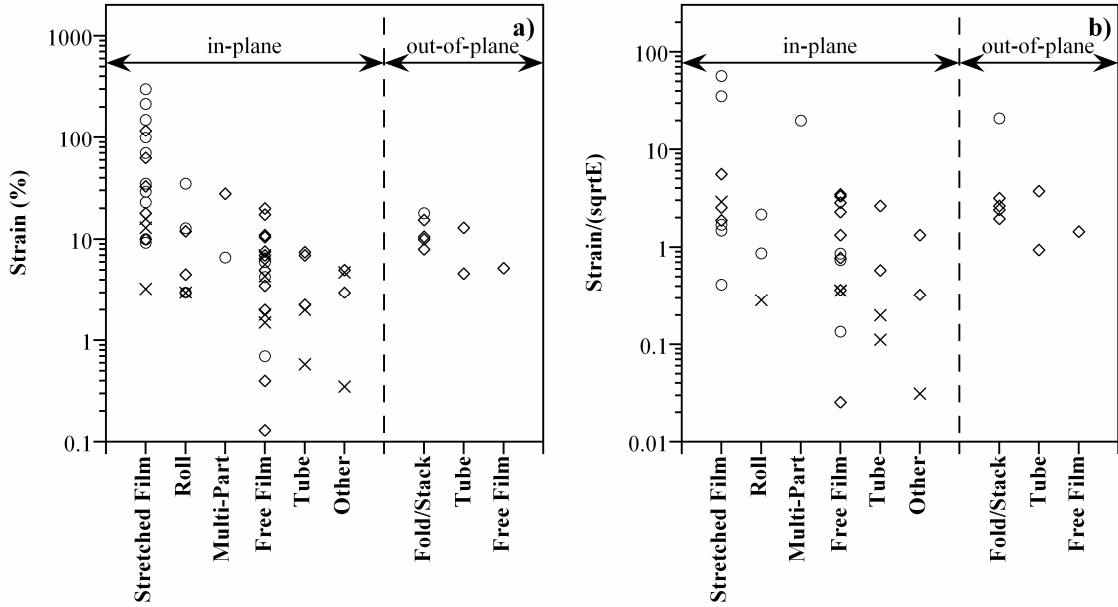


Figure 5. a) Actuation strain as a function of device form, b) actuation strain/ \sqrt{E} as a function of device form. Circles represent acrylic elastomers, diamonds represent silicone elastomers, and the x symbols represent other elastomers.

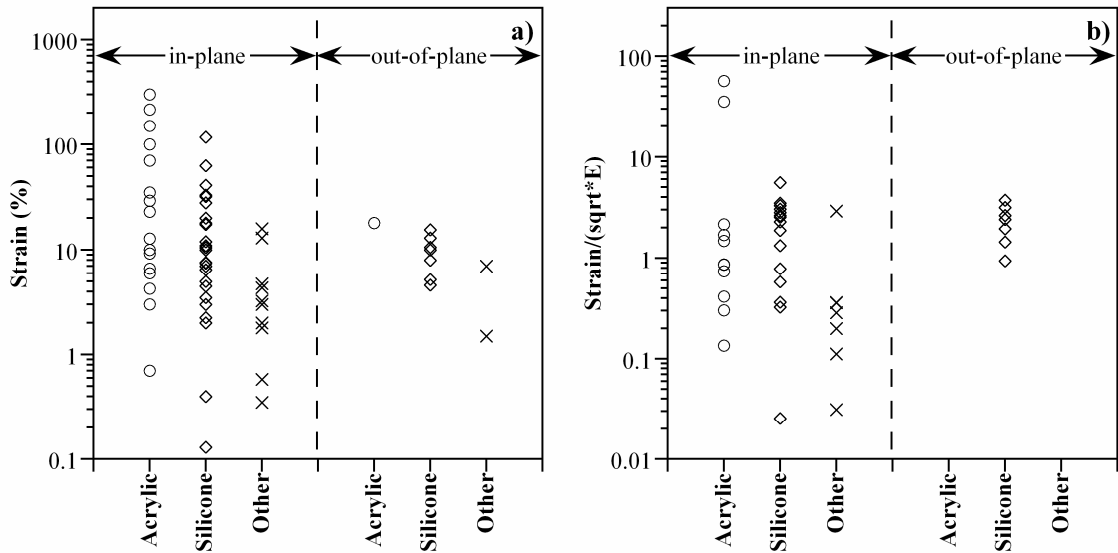


Figure 6. a) Actuation strain as a function of elastomer type, b) actuation strain/ \sqrt{E} as a function of elastomer type. Circles represent acrylics, diamonds represent silicones, and x's represent other elastomers.

The average out-of-plane (z -direction, Figure 3) actuation strains achieved by DEAs fabricated with acrylic, silicone, and other elastomers are 52.3%, 16.7%, and 6.3% respectively. The average in-plane (x and y -directions, Figure 3) actuation strains achieved by DEAs fabricated with acrylic, silicone, and other elastomers are 13.3%, 5.9%, and 4.3% respectively. These values correspond well with those measured in Chapter 2.

DEAs are tested under a wide range of experimental parameters, including the applied electric field. As shown in Figure 5b and Figure 6b, when the actuation strains are divided by the square root of the reported electric fields, the average in-plane actuation strain achieved by DEAs fabricated with acrylic, silicone, and other elastomers are 8.3% (only 0.7% when the two outliers discussed above are omitted), 1.9%, and 0.6% per unit electric field, respectively. These results signify that, excluding the two outliers, silicone provides the greatest actuation strain per unit electric field.

1.4.2 Actuation stress

Actuation stress is another important metric used to characterize DEA performance. In the analysis below, only data in which DEAs were actuated with attached loads were considered. Stress is defined as the ratio of the applied force and cross-sectional area of the DEAs. Work is defined as the product of the applied force and the distance it moved when actuated.

1.4.3 Blocking force

Blocked force is an applied force at which a DEA can no longer produce actuation strain. For example, imagine a stretched frame DEA with a weight hanging from the center of the active area. When the weight is increased, there will come a point where the actuator will not be able to lift the weight. Free strain is the actuation strain with no applied load. Free strain and blocked force make up the two extremes of a load curve.

1.4.4 Load curves

Load curves, which are used to characterize actuator performance, plot actuation strain as a function of applied force. Load curves convey a great deal of information including free strain (zero force), blocked force (zero strain), and work (area under the curve). Figure 7 shows the load curves from the load data but most of these plots have two points.

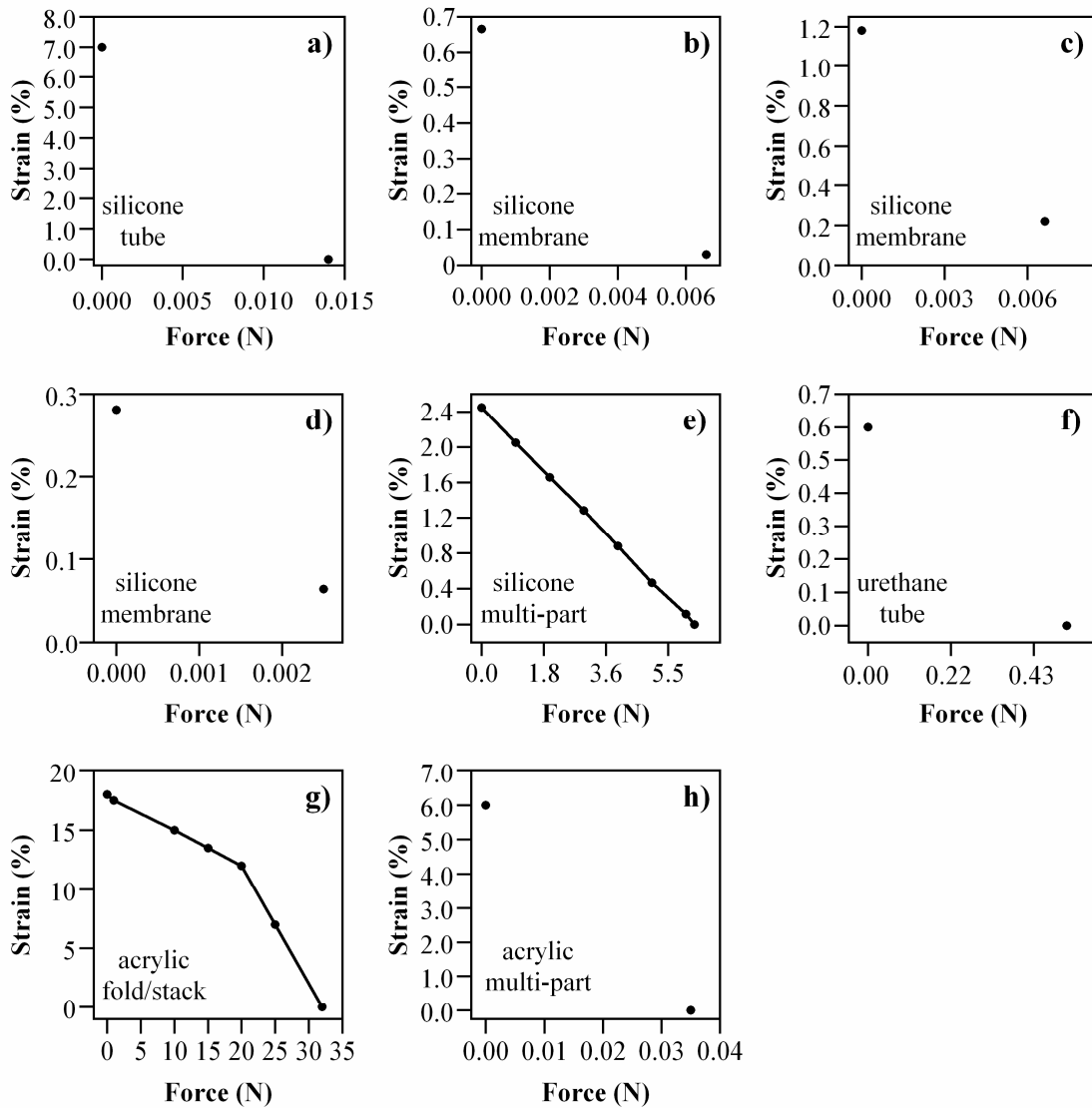


Figure 7. Actuation strain as a function of force for a) silicone tube DEA ^[33], b) silicone membrane DEA ^[72], c) silicone membrane DEA with a 3 mm diameter ^[73], d) silicone membrane DEA with a 2 mm diameter ^[73], e) silicone multi-part DEA by Danfoss ^[71], f) urethane tube DEA ^[33], g) acrylic fold/stack DEA ^[74], and h) acrylic multi-part DEA ^[75].

Ideally, units of stress are preferred to units of force since stress is independent of sample geometry; however, the majority of publications that present results in units of force do not include the necessary information to convert to stress. Calculated and reported

stresses (Figure 8a) and forces (Figure 8b) are plotted as a function of elastomer type. When the electric field was provided, the actuation stress and force was divided by the square root of the electric field to allow for direct comparison. Figure 8 and Figure 9 portray the same data from four different perspectives. Only data with the necessary information for the conversion from force to stress were plotted. Table 1 in the Appendix for this chapter lists the references for the data in Figure 8 and Figure 9, elastomer, initial elastomer thickness, actuator dimensions, pre-strains, elastomer thickness after pre-strain, in-plane or out-of-plane strain, and the applied voltage or electric field.

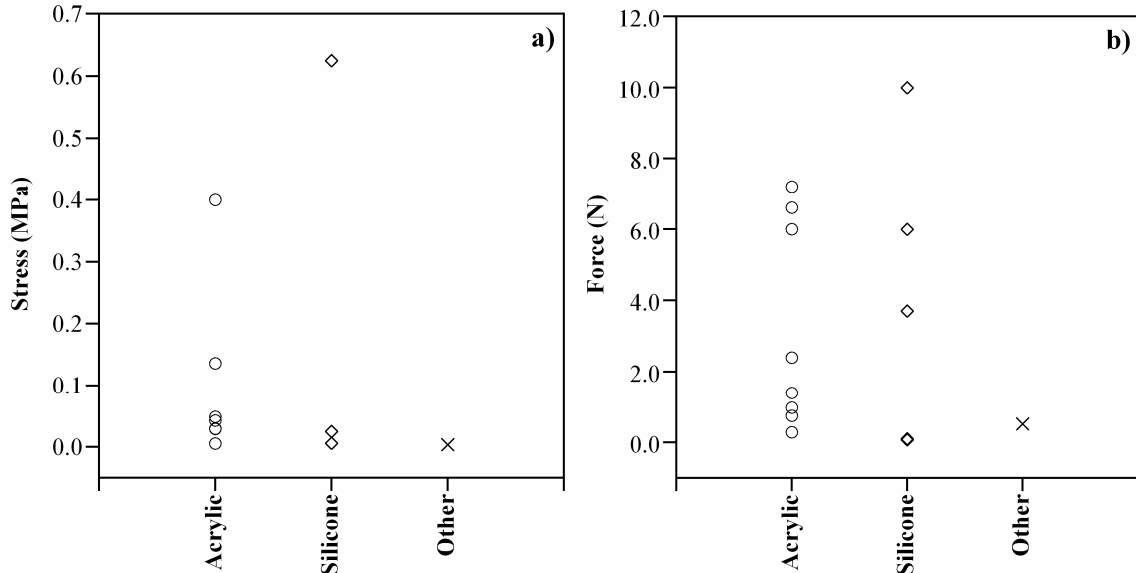


Figure 8. a) stress as a function of DEA elastomer type, b) force as a function of DEA elastomer type.

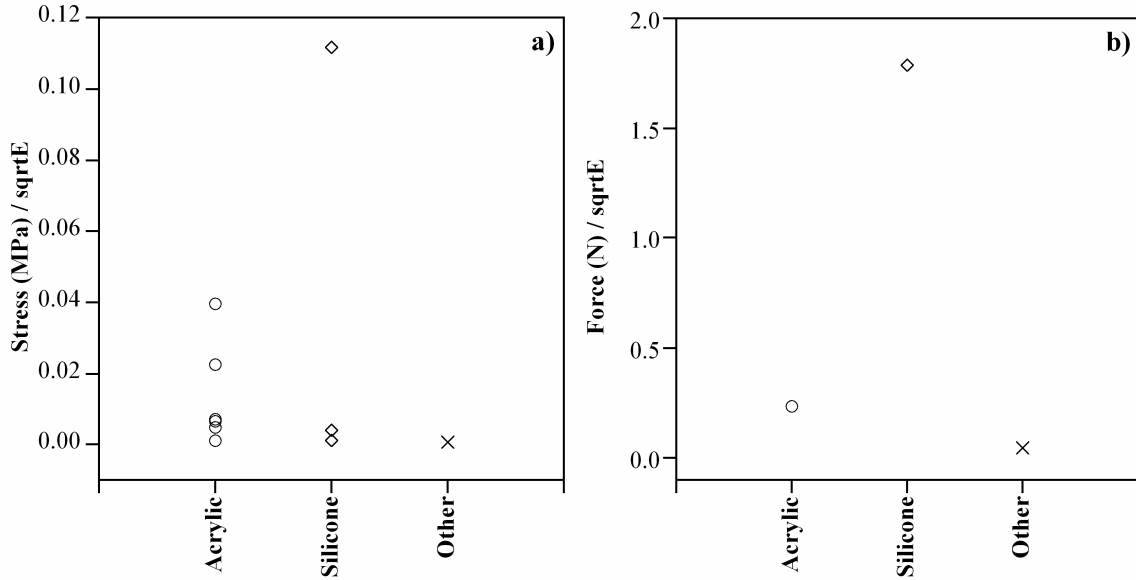


Figure 9. a) stress divided by the square root of the applied electric field as a function of DEA elastomer type, b) force divided by the square root of the applied electric field as a function of DEA elastomer type.

1.5 Mechanical sensors

Sensors provide feedback on environmental and other dynamic parameters, and are used for applications ranging from airbag deployment^[76] to robotics^[77]. There are many types of sensors, including optical^[78], chemical^[79], and mechanical^[80]. In this thesis, mechanical sensors are investigated for the detection of strain and pressure.

Some limitations of commercial sensors include small monitoring areas (i.e. strain gauges are generally $< 50 \text{ mm}^2$ ^[81]), lengthy installation^[81], and single parameter sensing (i.e. strain or pressure). In addition, some applications impose multiple requirements on sensors. For example, devices like micro-air vehicles (MAVs) may require multi-parameter feedback such as altitude, wing displacement, and contact for landing. The

current solution would be to install multiple single-parameter sensors to meet each of the requirements. Having a multiple-parameter sensor would reduce weight and system complexity. Further, irregular shaped and low stiffness sensors may be required because of the small size of the MAV and the potential of the sensing device impeding the deformation being monitored (i.e. wing displacements). Therefore, it will be beneficial to have a light weight, multi-parameter, patternable sensor with a low stiffness to reduce weight and system complexity.

1.6 Summary

DEAs are light weight, soft actuators capable of producing large actuation strains. DEAs are potential substitutes for DC electric motors, piezoelectric transducers, and shape memory alloys; however, several challenges need to be overcome for DEAs to reach widespread use in consumer products. One of the most important is the development of a compliant electrode material suitable for all elastomers and within reach of all researchers. Composite materials are one potential solution.

1.7 Aims

The objective of this research was to advance the fields of mechanical sensors and polymer actuators by developing and implementing new composite materials. The disparate data outlined in the above chapter shows a need for a direct comparison of DEA materials and actuation performance, which is provided in Chapter 2. For the field of DEAs to advance, a replacement for carbon grease electrodes needs to be developed.

Advancements in the field of sensors are also possible through new materials with multi-functionality (i.e. the same material capable of being applied as a strain gauge or as a temperature sensor. Control sensors would be required to remove undesired sensing modes if more than one are present simultaneously.) that simplify installation while maintaining or exceeding current performance. The environmental factors affecting the electrical properties of such materials are provided in Chapter 5.

1.8 Chapter 1 Appendix

Table 1. Materials and conditions of reported data in Figure 8 and Figure 9.

Reference	Initial elastomer thickness (mm)	Form	Width (mm)	Reported elastomer thickness (mm)	Voltage (V)	E (V/ μ m)	Stress (MPa)
[60]	1.00	free film	19	N.A.	N.A.	27	0.0053
[41]	0.05	free film	20	0.043	N.A.	38	0.0292
[41]	0.05	free film	20	0.043	N.A.	21	0.0295
[41]	0.05	free film	20	0.046	N.A.	37	0.0429
[41]	0.05	free film	20	0.040	N.A.	49	0.049
[30]	0.50	roll	117	0.086	3000	34.8	0.1356
[82]	N.A.	stretched	60	N.A.	N.A.	102	0.4
[83]	0.45	stretched	N.A.	N.A.	N.A.	24	0.0058
[84]	0.08	tube	N.A.	N.A.	N.A.	30	0.025
[71]	0.08	free film	200	N.A.	2500	N.A.	0.625
[60]	1.00	free film	19	N.A.	N.A.	27	0.0037
[85]	N.A.	stretched	190	N.A.	4000	N.A.	N.A.
[86]	1.50	stretched	N.A.	N.A.	10000	N.A.	N.A.
[87]	N.A.	multi-part	N.A.	N.A.	8000	N.A.	N.A.

[88]	0.10	stretched	N.A.	N.A.	5500	N.A.	N.A.
[89]	1.50	stretched	N.A.	N.A.	9400	N.A.	N.A.
[90]	1.00	stretched	200	N.A.	5400	N.A.	N.A.
[57]	1.00	multi-part	N.A.	N.A.	3400	N.A.	N.A.
[19]	N.A.	tube	N.A.	N.A.	1420	N.A.	N.A.
[91]	N.A.	roll	N.A.	N.A.	2500	N.A.	N.A.
[71]	N.A.	free film	N.A.	N.A.	2500	N.A.	0.625
[71]	N.A.	free film	N.A.	N.A.	2500	N.A.	0.025
[33]	N.A.	tube	N.A.	N.A.	N.A.	125	N.A.

1.9 Co-author contributions

Chapters 3 and 4 are reprints of published papers, and chapters 2 and 5 are modifications of drafts of journal papers that will be submitted. Therefore, they have additional authors who were responsible for parts of the research. This section outlines their contributions.

1.9.1 Chapter 2

B. Balakrishna, J. D. Pearse, and myself contributed equally to the data collection and analysis, and all three of us contributed text to the manuscript draft. For this chapter, I have re-written their text so that it is entirely in my own words.

1.9.2 Chapter 3

J. D. Pearse assisted with sample fabrication and conductivity measurements. I performed the data analysis and wrote the paper.

1.9.3 Chapter 4

J. D. Pearse assisted with sample fabrication, modulus measurements, and conductivity measurements. I performed the data analysis and wrote the paper.

1.9.4 Chapter 5

K. Miller assisted with sample fabrication and temperature-resistance measurements. T. Neumann fabricated the tactile sensors and performed the experiments in section 5.5.1. C. Elder and O. Dear fabricated the bridge beam and collected the data from the

commercial strain gauges and the force sensor in section 5.5.2. I performed the data analysis and wrote the paper.

Chapter 2: Comparison of three elastomers for dielectric elastomer actuators

Sensors and Actuators, full article, draft

M. Kujawski¹, J. D. Pearse², and E. Smela^{2*}

¹Dept. of Materials Science and Engineering, University of Maryland, College Park, MD 20742

²Dept. of Mechanical Engineering, University of Maryland, College Park, MD 20742

*smela@eng.umd.edu; tel: 301-405-5265; fax: 301-314-9477

2.1 Abstract

A variety of elastomers have been used as the dielectric layer in dielectric elastomer actuators (DEAs). However, the performance of DEAs varies substantially depending on the experimental conditions, making the evaluation and selection of elastomers for a particular application challenging. In this paper, the mechanical and electrical properties (tangent moduli, dielectric constants, and creep under load) of three elastomers – PDMS, TC-5005, and VHB-4905 – are compared under similar conditions. DEAs fabricated with these elastomers are next evaluated in terms of actuation strain and frequency response.

2.2 Introduction

Dielectric elastomer actuators (DEAs) are electro-mechanical transducers capable of producing actuation strains of greater than 100% ^[9]. As recently reviewed ^[92], DEAs have potential applications in robotics, haptics, tactile displays, and adaptive optics. A

DEA consists of an electrically insulating elastomer sandwiched between two compliant electrodes. When an electric field is applied to the electrodes, they are attracted together by Coulomb forces, producing a contraction in the z -direction (Figure 10) and expansions in the x and y -directions.

Three commonly used elastomers for DEAs are polydimethylsiloxane (PDMS, a silicone), TC-5005 (another silicone), and VHB-4905 (an acrylic). However, a thorough comparative study of the actuation performance and the mechanical and electrical properties of the elastomers has not yet been conducted, although power consumption and hysteresis have been evaluated^[93]. A direct comparison using literature data is difficult because dissimilar experimental conditions have been employed, such as device form factor, extent of pre-strain, and applied electric field.

In this paper the tangent moduli, creep strain under load, and dielectric constants of these three elastomers are measured under similar conditions, as well as their actuation performance in free-film DEAs as a function of electric field strength and frequency. We show that TC-5005 and VHB-4905 elastomers more than doubled in length within 2 hrs of applying a small pre-stress of 75 kPa. Free-film DEAs produced with TC-5005 gave the greatest actuation strains ($> 4\%$) and mechanical energy densities (0.3 J/kg at 27.5 V/ μm). Recommendations for potential DEA applications are provided based on the results obtained.

2.3 Experimental

2.3.1 Elastomer preparation

As noted above, PDMS (Sylgard 184, Dow Corning) and TC-5005 (BJB Enterprises) are silicones, and VHB-4905 (3M) is an acrylic. The VHB-4905 is commercially available in the form of a tape 12.5 mm wide and 500 μm thick. PDMS and TC-5005 are prepared by combining a pre-polymer and curing agent.

Sylgard 184 pre-polymer and curing agent were mixed at a 10:1 weight ratio and vacuum-desiccated for 30 min to remove air bubbles. To form films, the mixture was spin-coated onto 75 mm x 50 mm x 1.2 mm glass microscope slides at 1000 rpm for 60 sec, followed by vacuum-desiccation for 5 min and baking on a hotplate at 95 °C for 5 min. A second identical coat was applied, followed by degassing for 5 min and baking at 95 °C overnight. Forming the PDMS elastomers in two layers helped minimize air bubble formation. The PDMS films were 127 ± 21 μm thick as measured using a surface profiler (Dektak3 ST). These samples were kept thin to allow them to reach comparable strains under load as the other elastomers, which were softer.

TC-5005 elastomers were also prepared by mixing a 10:1 weight ratio of resin and curing agent. TC-5005 was not spin coated because it will not cure in thin films in the presence of oxygen. Instead, TC-5005 was vacuum-desiccated for 30 min to remove air bubbles, cast into polyethylene dishes, and cured at room temperature for 48 hrs. TC-5005

samples were $830 \pm 40 \mu\text{m}$ thick as measured with a handheld micrometer (L.S. Starrett Co., No. 120AM).

All three elastomers were cut into 50 mm long, 12.5 mm wide strips. One end of each strip was glued onto a glass microscope slide, and the other end was glued onto a 15 mm x 15 mm piece of a polyester (modulus $> 2 \text{ GPa}$ ^[94]) transparency sheet (3M) using a photo-curable adhesive (Loctite 3108), leaving a 25 mm long, 12.5 mm wide section in the center that was free to stretch (Figure 10).

2.3.2 DEA fabrication and electrical connection

The experimental setup is shown in Figure 10. Carbon grease (MG Chemicals) was applied manually to a thickness of approximately 1 mm to form the electrodes for the DEAs. The active area of the DEA, i.e. the area, A , between electrodes on both the top and bottom of the film, was held constant at 40 mm^2 . Stencils $20 \pm 2 \text{ mm}$ long and $2 \pm 0.2 \text{ mm}$ wide were used to pattern the carbon grease electrodes. Carbon grease was applied using a spatula over the stencil, and then the stencil was removed. Top and bottom electrode stencils were aligned by eye. Electrical connections to the grease were made using 5 cm long, 2 mm wide strips of Al foil that were gently pressed onto the grease electrode on one end and connected to a high voltage power supply (UltraVolt, Inc.) on the other using alligator clips.

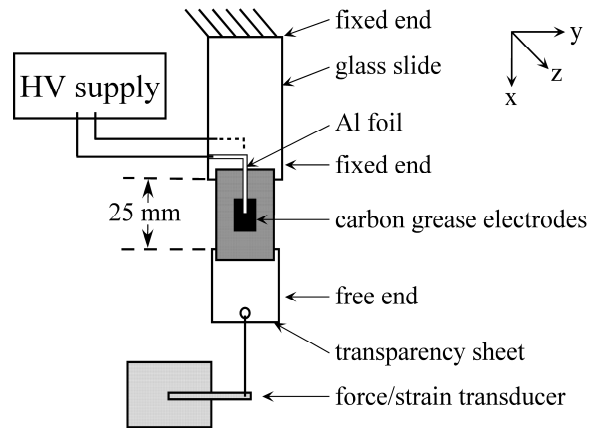


Figure 10. Device configuration and experimental setup.

2.3.3 Mechanical measurements

A force/strain transducer (Aurora Scientific Inc., model 3000LR) was used to apply and measure forces and displacements, which were then converted to stress and strain using the measured elastomer dimensions and transducer arm displacements. Elastomers and DEAs were suspended vertically by clamping the glass slides above the transducer. The transparency sheets were connected to the transducer arm using silk suture threaded through small holes in the transparency and transducer arm. A 2 gram force (corresponding to 6.2 kPa for PDMS, 0.94 kPa for TC-5005, and 1.6 kPa for VHB-4905) was applied by the transducer to hold the elastomer or DEA samples straight at the start of the measurement.

2.4 Results and discussion

2.4.1 Tangent modulus

For small strains (< 20%) and assuming constant volume (Poisson's ratio $\nu = 0.5$), the out-of-plane (i.e. in the z-direction) actuation stress σ_z (or pressure p_z) in a DEA is commonly modeled as the Maxwell stress, written as ^[4]:

$$\text{Eq. 5} \quad P_{el} = \frac{1}{2} \epsilon_r \epsilon_0 E^2 = \frac{1}{2} \epsilon_r \epsilon_0 (V/d)^2,$$

where ϵ_r is the relative dielectric constant, ϵ_0 is the permittivity of free space, E is the applied electric field, S_z is the strain in the z-direction, Y is the Young's modulus of the elastomer, V is the applied voltage and d is the thickness. While stress is directly proportional to the Young's modulus, rearranging shows that the strain is inversely proportional to the modulus:

$$\text{Eq. 6} \quad S_z = -\left(\frac{\epsilon_r \epsilon_0}{Y}\right)\left(\frac{V}{d}\right)^2,$$

The Young's modulus is the slope of the stress-strain curve of the elastomers in the range of strain for which Hook's law is valid (< 1%) and represents the elastomer stiffness. For larger strains (> 1%), Hook's law is no longer valid, and the slope of the stress-strain curve is defined as the tangent modulus ^[21]. While the tangent moduli of the three elastomers have previously been reported ^[43, 95-99], the moduli can vary with preparation conditions ^[100] and so needed to be determined for our samples. The force/strain transducer applied increasing displacements to the elastomers at a rate of 0.1 mm/sec while the force was measured. Tangent moduli were calculated from the slope of the

stress-strain curve at 5% strain (the observed actuation strain region). A minimum of three films of each elastomer were tested, and typical curves are shown in Figure 11.

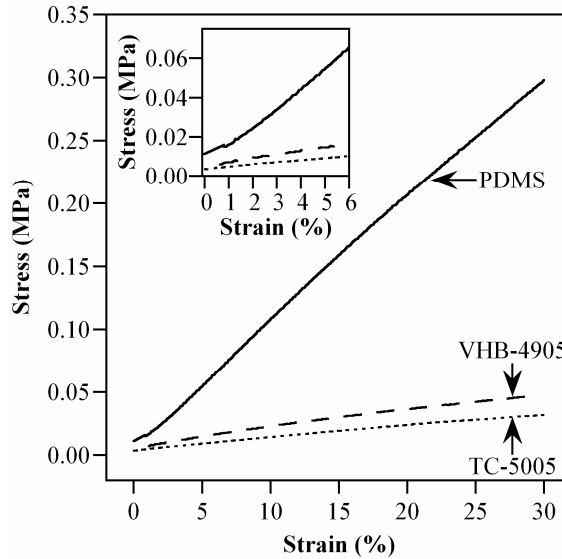


Figure 11. Stress as a function of strain for the three elastomers, measured at a strain rate of 0.1 mm/s.

PDMS, with a modulus of 1.06 ± 0.02 MPa, was an order of magnitude stiffer than TC-5005 (0.103 ± 0.004 MPa) and VHB-4905 (0.165 ± 0.002 MPa). These moduli compare with previously reported values of 0.75 - 2.6 MPa for PDMS^[95, 96], 0.062 - 0.095 MPa for TC-5005^[43, 97], and 0.182 - 0.8 MPa for VHB-4905^[98, 99]. As shown in the inset in Figure 11, the modulus of PDMS consistently showed a knee at 1% strain, increasing from 0.48 MP to 1.06 MPa, whereas the moduli of TC-5005 and VHB-4905 were linear between 1 and 30% strain. Depending on the strain range used for a particular application, this strain hardening may need to be taken into account.

2.4.2 Creep

Creep is the tendency of a solid material to keep deforming in response to a continuously applied stress ^[101]. In this report, total creep refers to the combination of creep (unrecoverable) and viscoelastic deformations (recoverable, also referred to elastic creep). Creep behavior for these elastomers have not previously been reported, but creep can pose potential problems for DEAs: depending on the device configuration and application, creep could require continuous counteracting adjustment of the voltage and introduces memory effects that complicate actuation repeatability.

Creep was determined using a modified version of the ASTM D945-06 testing procedure. A stress of 75 kPa was applied to the elastomer films and the resulting strain was measured over 10 hrs (Figure 12). For PDMS, the 75 kPa stress was sufficient to induce creep without exceeding the 10 mm stroke limitation of the force/strain transducer. TC-5005 and VHB-4905 elastomers stretched more than 10 mm, and the experiments were paused periodically in order to reposition the sample relative to the transducer arm. Creep recovery (the amount of strain recovered after removing the stress) was not investigated. Future investigations should include removal of the applied stress to determine the separate extents of the plastic and elastic creep.

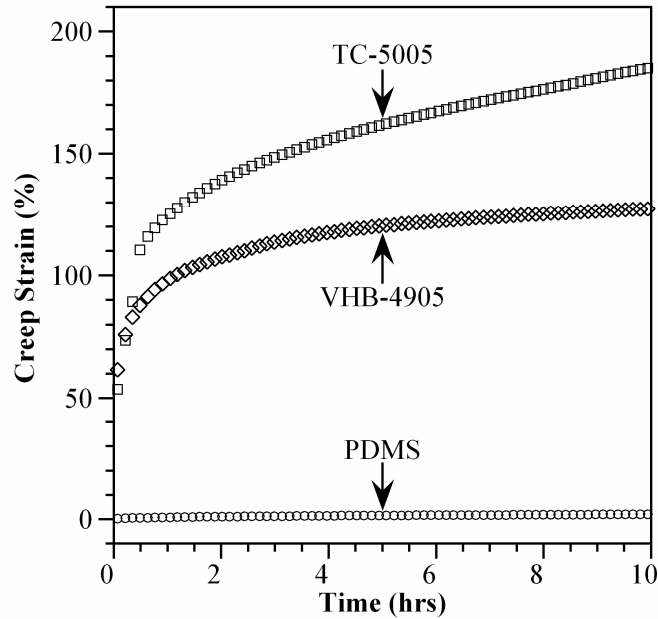


Figure 12. Strain as a function of time for the three elastomers under an applied stress of 75 kPa.

The total creep after 10 hrs was 2% for PDMS, but it was 185% for TC-5005 and 130% for VHB-4905. For the latter two, total creep was rapid during the first hour; thereafter it slowed but continued. For PDMS, the creep slowed after 5 min. Creep rates after 6 hours were 0.08%, 4.5%, and 1.3% /hr, respectively.

2.4.3 Actuation strain as a function of electric field

Strain, stress, and speed are the most important actuator metrics, the product of the first two determining work and the product of all three determining power. To measure strain as a function of electric field, the DEAs were placed under a small constant stress of 75 kPa at $T = 0$. Electric fields were applied in three sets of 30 sec on/off square waves increasing in $2.5 \text{ V}/\mu\text{m}$ increments. A minimum of three samples of each elastomer type

were tested. Pre-stressed elastomer thicknesses were used to determine the electric field corresponding to each applied voltage.

Under the increasing fields, the DEAs eventually failed. To prevent shorting, and allow potential re-use of the actuators, electric fields were reduced to 90-95% of the field at which the ratio of the number of samples that failed to the number of samples that didn't was $> 30\%$ (50, 27.5, and 32.5 V/ μm for PDMS, TC-5005, and VHB-4905 DEAs, respectively). Failure was accompanied by visible sparking around the sides of the elastomers, and not from dielectric breakdown in the electrode areas. (TC-5005 and VHB-4905 DEAs stretched when the pre-stress was applied, reducing the distance from the electrode to the elastomer edge to < 2 mm, from initial edge distances of < 5 mm with zero pre-stress). The sparks would burn the elastomer, ruining the DEAs (see Figure 13).

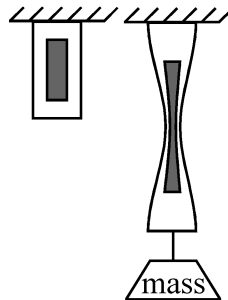


Figure 13. Schematic of the elongation that results when a mass is applied to the free end of a free-film DEA.

Creep strains were subtracted from the raw actuation strain data to give the reproducible actuation strain, as shown in Figure 14a. The creep strain slopes were taken from Figure 12 at the same time relative to the pre-stress being applied to the DEAs. For example, the creep measured 10 min after applying the 75 kPa pre-stress was subtracted from the

actuation strain measured 10 min after applying the 75 kPa pre-stress to a DEA. Due to the lower tangent moduli, at 27.5 V/ μm , actuation strains for DEAs made with TC-5005 (4.0%) were ten-fold those for PDMS (0.3%) and three-fold those for VHB-4905 (1.3%) DEAs.

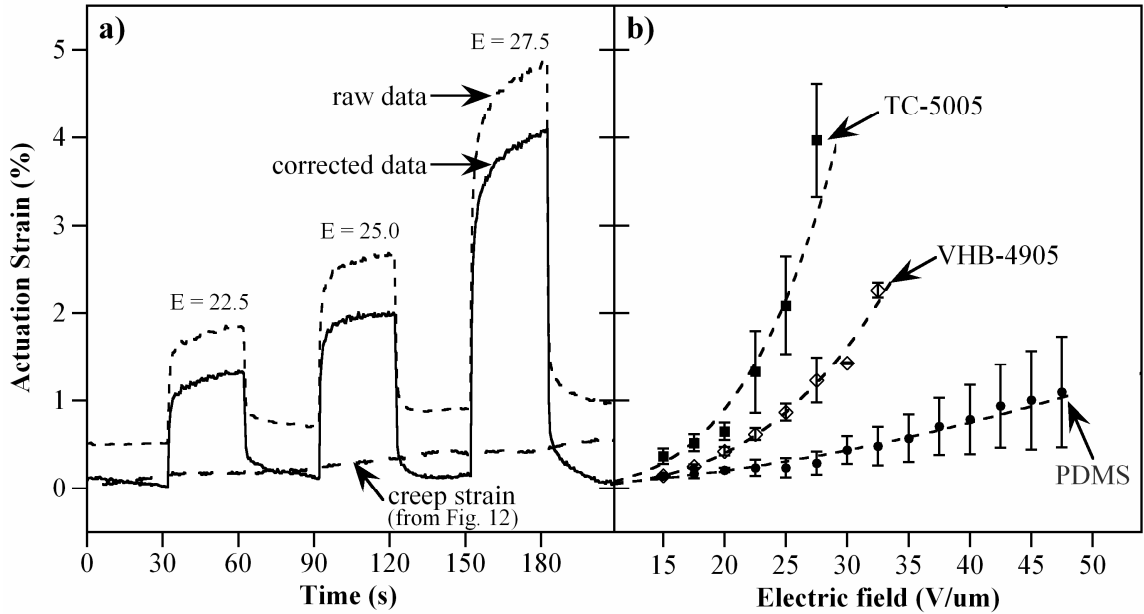


Figure 14. a) Actuation strain as a function of time for a TC-5005 DEA. The raw data (dotted line), the corresponding creep strain (dashed line), and the corrected actuation strain (solid line) are shown. b) Strain as a function of electric field for DEAs fabricated with the 3 elastomers. The applied stress was 75 kPa and averages represent at least 3 samples. The dashed lines are guides for the eye.

2.4.4 Actuation response times

Another way to examine speed is through the rise and fall (relaxation) times, defined as the times it takes for the actuator to reach 90% of its final positions. For these measurements, the DEAs were pre-stressed at 75 kPa and actuated by applying a DC square wave as in section 2.4.5, using the same fields with on/off times of 30 sec (Figure 15). The measured actuation strains were normalized to the maximum strains achieved at

the applied electric field: 0.3% for PDMS, 3.9% for TC-5005, and 1.2% for VHB-4905 DEAs. PDMS exhibited the shortest rise time t_r and fall time t_f : 0.8 and 18 sec, respectively. This is consistent with the step response data in Figure 14, showing PDMS to be the fastest. TC-5005 had $t_r = 9.4$ sec and $t_f = 2.4$ sec. While the rise time was 10x longer, the fall time was shorter. For VHB-4905, $t_r = 11.2$ sec and $t_f > 80$ sec, a comparable rise time to TC-5005, but a substantially longer fall time. (Note that unlike the PDMS and VHB DEAs, the rise time was longer than the fall time for TC-5005 DEAs. The reason for this is unclear, and requires further investigation). The discharge time of the high voltage power supply may be affecting the response of the DEAs at higher frequencies, and is currently being investigated.

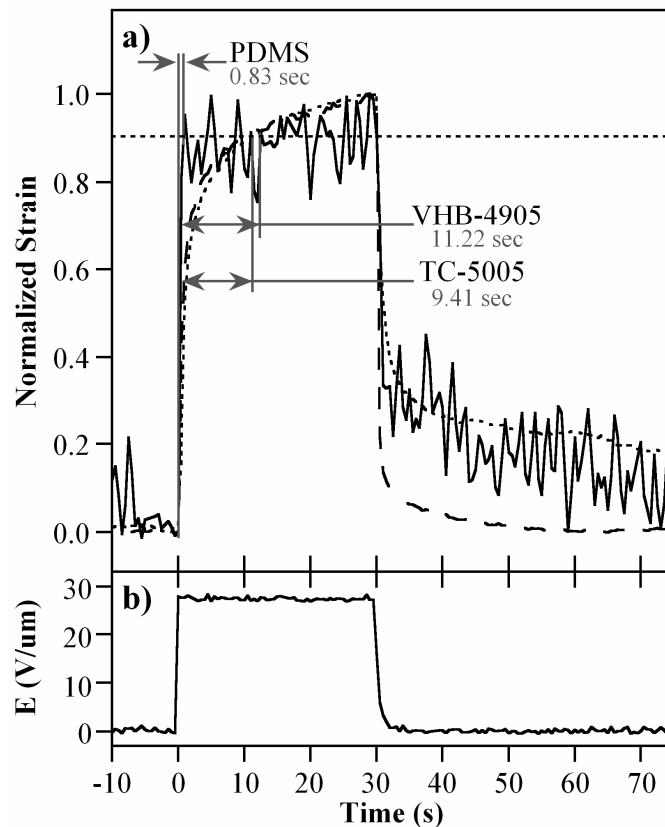


Figure 15. a) Actuation strain as a function of time for a voltage step on/off. Rise times are shown. b) Applied electric field, 27.5 V/ μm , as a function of time.

To provide some context for these numbers, they were compared to the electrical time constants, since DEAs are elastomeric capacitors. The RC time constants τ were estimated from the measured resistance of the carbon grease electrodes, obtained with a two-point probe, and the electrical leads (10Ω) and the measured capacitance of the DEAs (obtained using the relation $C = 1/(2\pi fZ'')$ ^[102] where Z'' is the imaginary part of the impedance) at 100 Hz and 0 kPa pre-stress. The electrical time constants are 11 orders of magnitude smaller than the mechanical ones, showing that the mechanical relaxation is the rate-limiting process, and not capacitor charging. Mechanical time constants between 1 ms and 500 ms have been reported by Rosset et al. ^[73, 103] for PDMS diaphragm DEAs. The mechanical response times are believed to be dominated by viscoelasticity and polymer chain relaxation ^[103, 104].

2.4.5 Actuation strain as a function of frequency

While DEAs have been described as operating up to kHz rates ^[63, 103, 105, 106], only a few curves showing strain versus frequency have been published ^[75, 103, 105-107]. The DEAs were therefore pre-stressed at 75 kPa and actuated by applying square waves at 90 - 95% of the maximum for each material (47.5 V/ μm for PDMS, 25.0 V/ μm for TC-5005, and 27.5 V/ μm for VHB-4905 DEAs) between 0.1 and 10 Hz (Figure 16a-c). These values gave the maximum strains achievable without significant risk of device failure, and it was assumed that the frequency response was not significantly affected by the field strength. (The actuation strains in Figure 16 are lower than those in Figure 14 because the electric fields were lower.) The actuation strains, normalized to those at 0.1 Hz, are shown in Figure 16d. (The strains at 0.1 Hz, $\varepsilon_{0.1}$, for PDMS, TC-5005, and VHB-4905 DEAs were

0.6%, 1.9%, and 0.9%, respectively.) It is possible that pre-straining the VHB and TC-5005 material may improve their rise and relaxation times, which is evident from their applications as loudspeakers [12, 108].

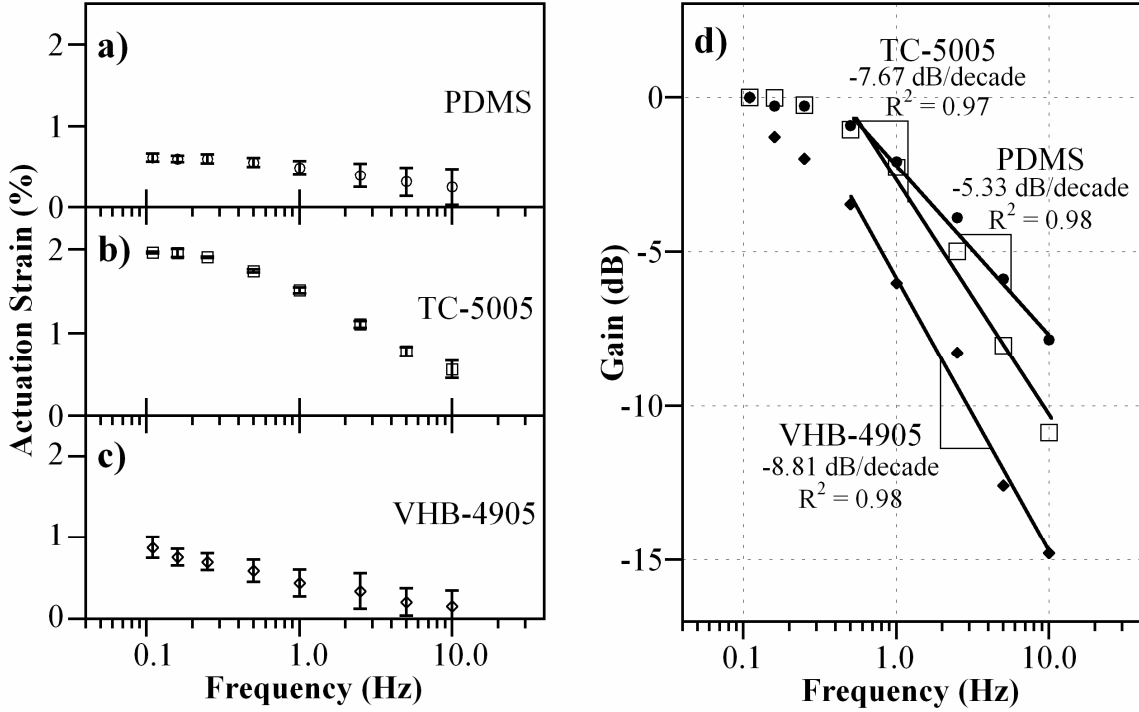


Figure 16. Actuation strain as a function of frequency for a) PDMS DEAs at 47.5 V/μm, b) TC-5005 DEAs at 25.0 V/μm, and c) VHB-4905 DEAs at 27.5 V/μm. d) Gain as a function of frequency; solid lines show the best fit roll-off rates.

The cut-off frequency f_c is defined as the frequency at which an input signal is attenuated by half (-3 dB, where the decibel value is given by $20\log M$, which is equivalent to the magnitude being reduced to 0.707), and the roll-off gives the rate at which the response decays with frequency above f_c [109]. The frequency dependences of the strains are shown in Figure 16, and the cut-off frequencies and roll-offs are given in Table 2. PDMS and TC-5005 had similar f_c , operating at > 1 Hz with a $< 25\%$ reduction in actuation strain. PDMS had the highest f_c (1.5 Hz) and lowest roll-off (-5.3 dB/decade) yielding the least

attenuation with increasing frequency, and making it the most suitable for high frequency applications. VHB-4905 exhibited the largest attenuation rate with frequency (-8.8 dB/decade).

Table 2. Cutoff frequencies and roll-off rates for the three types of DEA. (There are no previous literature reports of cut-off frequencies.)

Elastomer	Cutoff Frequency (Hz)	Roll-Off (dB/decade)	Previously Reported Roll-Offs (dB/decade)
PDMS	1.5	-5.3	-5.3 ^[106]
TC-5005	1.1	-7.7	no reports
VHB-4905	0.4	-8.8 (46% uniaxial pre-strain)	-10.4 (35% uniaxial pre-strain) ^[41] -20.0 (300% biaxial pre-strain) ^[107]

Strain as a function of frequency has previously been reported for PDMS and VHB DEAs. Pimpin *et al.*^[106] examined PDMS membrane DEAs, Carpi *et al.*^[41] studied VHB free-film DEAs, and Loverich *et al.*^[107] investigated VHB membrane DEAs. From their plots, we obtained cut-off frequencies and roll-offs for their devices (Table 2). Our results are close to those values. Further analysis of VHB data presented by Carpi *et al.*^[41] and Loverich *et al.*^[107] indicated that roll-offs increase with pre-strain, reaching a first order response when the DEAs were biaxially pre-strained $\geq 300\%$ ^[107]. Higher actuation frequencies may be achieved by exploiting resonance; resonant frequencies between 1 kHz and 1.4 kHz have been observed for silicone DEAs^[63, 105, 106].

2.5 Conclusions

Mechanical and dielectric properties, and electromechanical responses of DEAs, were investigated for three elastomers. It is shown that pre-stresses of 75 kPa produced creep strains in all three elastomers, which were negligible for PDMS ($< 2\%$), and quite large for TC-5005 and VHB-4905 ($> 100\%$). All three DEA types show potential for high-strain responses at high electric fields; however, the responses exhibit significant frequency dependence, particularly for VHB-4905 DEAs.

2.6 Acknowledgements

This research was supported by the US Army Research Laboratory under the MAST CTA program in the Center for Microsystem Mechanics.

2.7 Chapter 2 Appendix

2.7.1 Experimental challenges

There were many obstacles that needed to be overcome to conduct the experiments in this chapter. Two of the main issues were sample sparking and equipment limitations.

Sparking is an electrical discharge between electrodes.

2.7.1.1 *Sample sparking*

Samples failed by sparking from electrode to electrode around the edge of the elastomer.

To prevent sparking, the spacing between the edges of the elastomers and the electrodes needed to be adjusted. The spacing depended on the applied voltage, elastomer thickness, creep strain, and pre-stress.

The dielectric breakdown of air reported in the literature to be $\sim 3 \text{ MV/m}$ ^[110] which depends on environmental factors such as altitude, temperature, and humidity. We experimentally determined that the dielectric breakdown at 64°F and 32% RH was 1.5 MV/m by applying a 10 kV potential between two electrodes. The electrodes were moved closer together until, at a distance of 6.5 mm, sparking occurred; this corresponds to 1.5 V/ μm . The high voltage power supply used in this thesis was limited at a maximum output voltage of 10,000 V. Based on these data, at the maximum possible applied voltage, the electrodes needed to have a minimum distance between 1.5 mm and 3 mm to prevent sparking around the wall of the elastomer. By having a minimum spacing of 2 mm between the edge of the elastomer and electrode (multiplied by 2 for the

top and bottom) and with an elastomer thickness of 0.1 mm, the separation distance was 4.1 mm. Electrode patterning position and orientation were critical to ensure this separation was maintained on the elastomers that exhibited large creep strains. When pre-stressed TC-5005 and VHB-4905 elastomers continuously narrowed the separation distance as the elastomer became longer and narrower. This resulted in many device failures and is a notable reason for the use of alternative compliant electrodes that can be coated with thin insulating layers to help prevent sparking, like the PDMS/EG material.

2.7.1.2 Equipment limitations

The 1 N force limitation of the force-strain transducer, the elastomer tangent moduli, and elastomer cross-sectional areas were the determining factors for the applied pre-stresses. The 10 mm stroke limitation of the force-strain transducer, the elastomer tangent moduli, and resulting creep strains were the determining factors for applied stresses used for the creep strain experiments. These limitations dictated the experimental protocol.

2.7.2 Unsuccessful experiments

Electromechanical efficiency is seldom reported. Electromechanical efficiency is the ratio of the electrical energy given to the system to the mechanical energy produced by the system (work). To calculate the electrical energy given to the system, the applied voltage and resulting current need to be measured. The charge buildup on the electrodes occurs rapidly ($\sim 10^{-11}$ sec) after applying the voltage, so the voltage and current need to be sampled at high frequencies in order to accurately map the power consumed in this phase of the actuation. High voltages can destroy instrument, so we needed to design a

data collection system to handle this. A schematic illustration the system employed is shown in Figure 17. To provide the high sampling rate, a data acquisition card (National Instruments, USB-6008) was used to measure the voltage drop across a resistor. The resistance of the resistor was measured before testing, and the resistor was selected to produce a voltage drop between 3 and 7 V, depending on the applied electric field and elastomer thickness. Because of the high rate of failure for DEAs with carbon grease electrodes, an operational amplifier was used to mirror the measured voltage drop of 3-7 V. The operational amplifier would short out if the DEA failed and sent the 10,000 V directly to the resistor, and protect the more expensive data accusation card form being damaged. Using Ohm's law, $V = IR$, the current passing through the DEA, or current leakage, could be calculated.

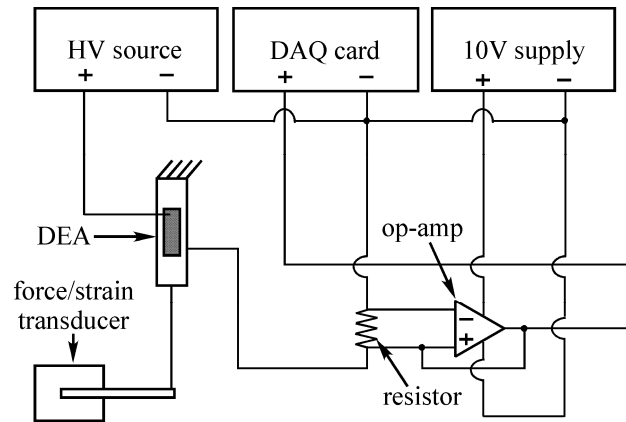


Figure 17. Schematic illustration of the voltage and current measuring system used to calculate DEA power consumption.

Due to the many variables (applied voltage, elastomer thickness, elastomer type, resistor value, resistor loss, and operational amplifier type) this method did not give reproducible results. An example of the data collected is shown in Figure 18. The peak at the start of

each actuation cycle is the charge buildup on the electrodes. The negative peaks at the ends of the actuation cycles are that same charge returning to the power supply. This charge/discharge could possibly be collected with circuitry and would therefore not contribute to the power consumption of DEAs, rather the current leakage through the elastomer that consumes the power. Improved electronic circuits are required to more accurately measure power consumption of DEAs.

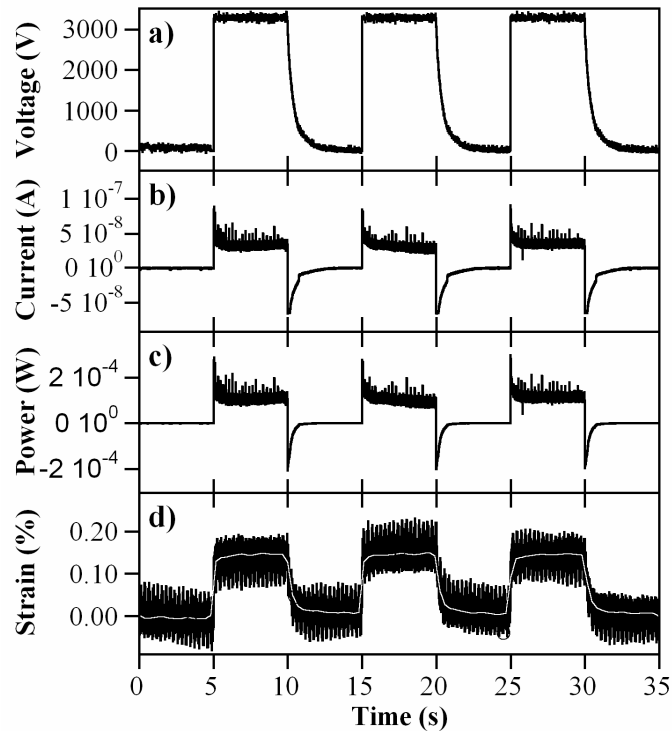


Figure 18. For a PDMS/carbon grease DEA, a) voltage, b) current, c) power, and d) actuation strain as functions of time.

Chapter 3: Elastomers filled with exfoliated graphite as compliant electrodes

Published in Carbon, 48(9) 2409-2417 (2010).
Reproduced by permission of Elsevier

M. Kujawski¹, J. D. Pearce², and E. Smela^{2*}

¹Dept. of Materials Science and Engineering, University of Maryland, College Park, MD 20742

²Dept. of Mechanical Engineering, University of Maryland, College Park, MD 20742
*smela@eng.umd.edu; tel: 301-405-5265; fax: 301-314-9477

3.1 Abstract

A compliant electrode material has been realized by blending an insulating polydimethylsiloxane (PDMS) elastomer with a conductive exfoliated graphite filler, which was produced by microwave irradiation. The conductivity and stiffness of the electrodes were determined as a function of filler concentration. These materials exhibited a low percolation threshold: above 3 wt% loading they became conductive, with conductivities reaching as high as 0.4 S/cm. They remained elastomeric upon loading up to 25 wt%, having a Young's modulus of only 1.4 MPa. This modulus (corresponding to a 220% increase compared to the unloaded PDMS) is the lowest reported for loaded elastomers above the percolation threshold. Scanning electron microscopy showed that the composites contained small voids, unlike unloaded PDMS, which might be responsible for the low modulus. The performance of these electrodes is comparable to that of PDMS loaded with carbon nanotubes, but the exfoliated graphite material can be produced at a fraction of the cost.

3.2 Introduction

Compliant electrodes that can undergo significant stretching while maintaining good conductivity are needed in applications such as strain gauges, flexible displays, wearable electronics, and dielectric elastomer actuators. However, the development of a really good compliant electrode material has proven to be challenging because of the numerous, sometimes incompatible, requirements on it. As implied by the name, the two most important requirements are mechanical compliance, which equates to a low Young's modulus, and high electrical conductivity. Other characteristics required by particular applications may include extended strain cycling, high ultimate tensile strain, negligible creep, ease of fabrication, low material costs, and resistance to wear, rubbing off, and delamination.

Much of the compliant electrode research over the past decade has focused on two-phase composites composed of conductive filler particles within an insulating polymer matrix [111-121]. Conductive filler materials include carbon black (CB) [111, 112], carbon fibers [112], multi-wall carbon nanotubes (MWCNTs) [113-116], and single wall carbon nanotubes (SWCNTs) [117-121]. Unfortunately, there is normally a dramatic increase in stiffness with loading of the conductive filler [116, 117, 122]. Stiffness increases can be minimized by using a lower percentage of the filler, but if the loading is too low then the material remains insulating. The loading at which the material becomes conductive is known as the percolation threshold, at which a conductive pathway through the host matrix is formed by the filler particles.

Graphite, which can be easily obtained and is relatively inexpensive, has also been used as a filler ^[123-126]. Graphite is composed of individual sheets, called graphene, of sp² hybridized carbon arranged in a hexagonal lattice; the sheets are stacked along the c-axis and bound together by van der Waals forces. Graphite is electrically conductive in the plane of the graphene layers.

Molecules can readily be introduced between the graphene sheets. Acids can be intercalated, for example. If the graphite particles are then rapidly heated, the acids are vaporized, generating enough force to overcome the van der Waals binding and expanding the graphite flakes along the c-axis ^[124, 127-129]. The expanded structures are sonicated in a solvent to break them into sheets. Separation of the layers is known as exfoliation, and it can be done either in a furnace ^[130] or by using microwave radiation ^[124, 128, 129, 131]. However, the production of pure single sheet graphene is difficult with these methods: exfoliation is generally incomplete, resulting in a combination of graphite and graphene.

In this paper we demonstrate that exfoliated graphite (EG) can be used to produce low modulus composites having good conductivities at low loadings. Using polydimethylsiloxane (PDMS) as the elastomer, we produced a material that can be cast or spin coated into films, as well as patterned. PDMS/EG sample preparation consisted of a simple two step process that can be repeated in virtually any lab: 1) exfoliate the graphite and 2) mix the resulting EG into the PDMS and cure.

3.3 Experimental

3.3.1 Microwave Exfoliation

The exfoliation methods employing microwave irradiation presented by Falcao *et al.* [128] and Wei *et al.* [132] were used in this work. Our starting material was acid-washed graphite flake (Asbury Graphite Mills, Inc.). The microwave oven (Kenmore) had a power of 1100 W and an operating frequency of 2.45 GHz. Flexible silicone tubing (MasterFlex® HV-96410-18) was fed through the rear vent so that the enclosure could be filled with forming gas (97% nitrogen, 3% hydrogen). The particles must be in close proximity to one another for exfoliation to occur. Therefore, graphite flake (2 g) was placed into an 18 mL glass vial in the center of the microwave. The forming gas was turned on for 10 minutes at a flow rate of 1 L/min prior to applying full power for 60 sec. Due to the conductivity of the graphite, large sparks were generated between particles during microwave irradiation, and the expanded material glowed orange-red. The exfoliation appeared to be complete after only a few seconds, as evidenced by a 200-300 fold increase in volume (Figure 19a).

The resulting worm-like particles (Figure 19b) were filtered by stirring them into hexane, in which they floated; large unexfoliated particles sank. The exfoliated particles were collected from the surface and dried on a hot plate overnight at 150 °C.

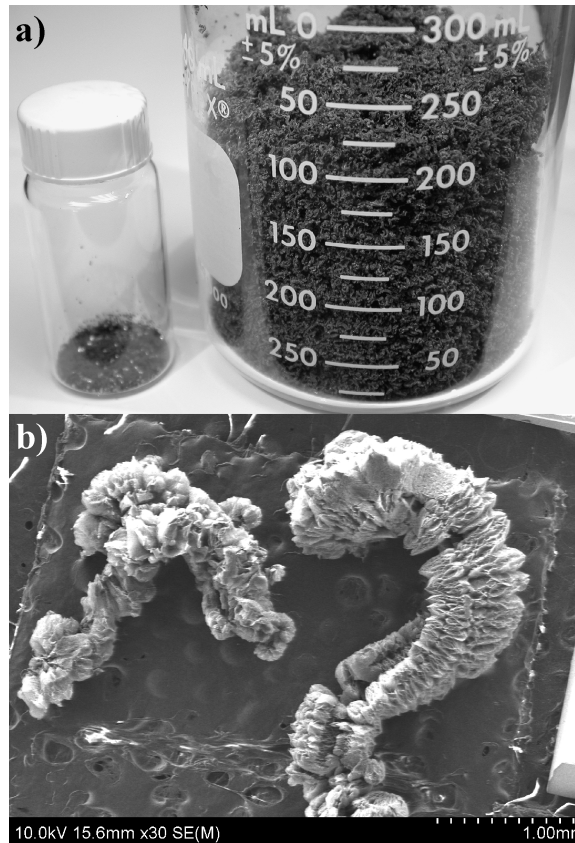


Figure 19. a) Acid-washed graphite before (left) and after (right) microwave exfoliation. b) SEM image of worm-like EG structures.

3.3.2 Characterization

SEM images of composite samples were obtained with a Hitachi SU-70 SEM at an acceleration voltage of 10 kV and a working distance of 15 mm, where unloaded PDMS samples were imaged using a Hitachi S-3400N variable pressure SEM at an acceleration voltage of 15 kV, a working distance of 15 mm, and a pressure of 100 Pa. No conductive coatings were used.

3.3.3 Sample fabrication

The PDMS used in this work was Sylgard 184 (Dow Corning). (The term PDMS encompasses a family of silicone elastomers, and these materials range in stiffness by a factor of 10. In this paper, “PDMS” refers to Sylgard 184). While the standard ratio of resin to cross-linking agent is 10:1, a ratio of 20:1 was used to produce a more compliant host matrix.

Hexane was used to disperse the EG particles, since PDMS is miscible with hexane. The EG was mixed with 120 parts by weight of hexane and sonicated (Branson 1510) at a frequency of 40 kHz for a minimum of 3 hours, until the particles appeared to be separated by visual inspection. The EG/hexane solution was then heated to 150 °C on a hot plate to drive off excess solvent until a 1:30 ratio (w/w) of EG to hexane was reached. (Solvent to particle ratios larger than 1:30 reduced the time required to break down the exfoliated structures, but as the solvent evaporated from the cast films (see below) it carried particles to some areas of the surface, resulting in inhomogeneous EG concentrations. Too little solvent resulted in poor particle wetting and thus difficulties in mixing.)

The PDMS resin was added, followed by sonication for another 30 minutes, and lastly the curing agent was added followed by sonication for a further 10 minutes. Samples were prepared containing between 2 and 25 wt% EG. The mixtures were cast into polyethylene dishes, vacuum desiccated for 2 hours to remove air bubbles and to completely evaporate the remaining solvent, and baked on a hot plate at 75 °C overnight

to cure. Once cured, the PDMS/EG composites could be easily handled without shedding of particles.

Spin coating the uncured mixture onto glass slides allowed the formation of thin films with a thickness that could be varied by controlling the spin speed. However, samples less than 20 μm thick formed through-holes (holes spanning the entire thickness of samples) and had lower conductivity. To form films that were thick enough to remove from the glass and handle, samples were formed by casting.

The cast samples ranged from 100 to 500 μm in thickness and were cut into strips 10 mm wide with a minimum length of 38 mm. Conductive silver epoxy (Chemtronics, CircuitWorks CW2400) was painted onto the samples for electrical connection. Each sample was prepared with four 2 mm wide rectangular contact pads spaced 10 mm apart. Before the epoxy cured, a 200 mm long fine stainless steel wire (43 gauge, California fine Wire co.) was placed into each epoxy pad to provide electrical connections that would not interfere with stress-strain measurements. (This configuration was also implemented by Rosset *et al.* ^[23], who also monitored conductivity versus strain.)

It was necessary to control the moisture content of the composites because the conductivity nearly doubled in humid environments. The samples were therefore dried in an oven at 75 °C for 24 hours prior to electrical and mechanical testing.

3.3.4 Mechanical testing

Mechanical testing was performed using a force/strain transducer (Aurora Scientific Inc., model 3000LR) with a custom LabView program. A schematic of the sample configuration is shown in Figure 20. One end of the sample (the fixed end) was attached to a 3" x 1" x 1.2 mm glass microscope slide (VWR, Cat No. 16004-424) using a photo-curable adhesive (Loctite® 3108), and the other (the moving end) was attached to a 12 mm wide, 16 mm long section of transparency sheet (3M CG3300). This configuration left a 10 mm x 10 mm section in the center of the sample that was free to stretch. The sample was suspended vertically to prevent the composite film from sagging. Silk suture thread (CP Medical, 675S) connected the sample to the force/strain transducer arm via a small hole drilled into the transparency sheet and a small hole at the tip of the arm.

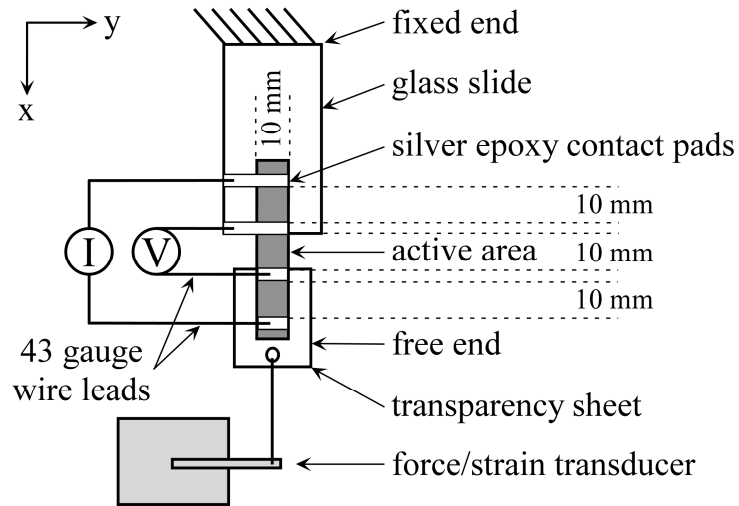


Figure 20. Schematic of the testing configuration.

The force/strain transducer applied a constant strain rate (0.1 mm/s) and recorded the resulting stress. This strain rate allowed a sufficient number of data points to be collected by the digital multimeter (Craftsman Professional, model no. 82324, 1 Hz sampling rate),

which simultaneously recorded resistance using a 4-point probe technique that was a modified version of ASTM D4496-87. (Contact resistances were on the order of 70 Ω .) An Autolab potentiostat/galvanostat (Eco Chemie, PGSTAT30) provided a constant current to the two outermost contact pads. The current ranged from 10⁻³ to 10⁻⁶ A, depending on the EG loading and sample thickness. Lower currents were selected for high resistivity samples to prevent excessive voltage. The conductivity was calculated from the voltage drop between the two innermost contact pads and the sample dimensions.

3.3.5 Geometric corrections

The calculation of the electrical conductivity (from the measured voltage, known applied current, and original dimensions) took into account the changing size of the sample under strain. The corrections assumed a Poisson ratio of 0.5. A detailed explanation of the equations used and an example of the calculations can be found in the Supplementary Information.

3.4 **Results and discussion**

3.4.1 Exfoliation results

Figure 21 shows SEM images of the graphite after it was microwave exfoliated and sonicated in hexane. The exfoliation process resulted in particles that were 10 to 200 nm thick, which is comparable to the 80 to 150 nm in previously made EG^[124, 130]. In addition, based on the transparency of flakes such as the one shown in Figure 21b, a

fraction of the material appears to be in the form of one to several sheets. The particle diameters mostly lie within the range of 5-20 μm , with an average of approximately 10 μm .

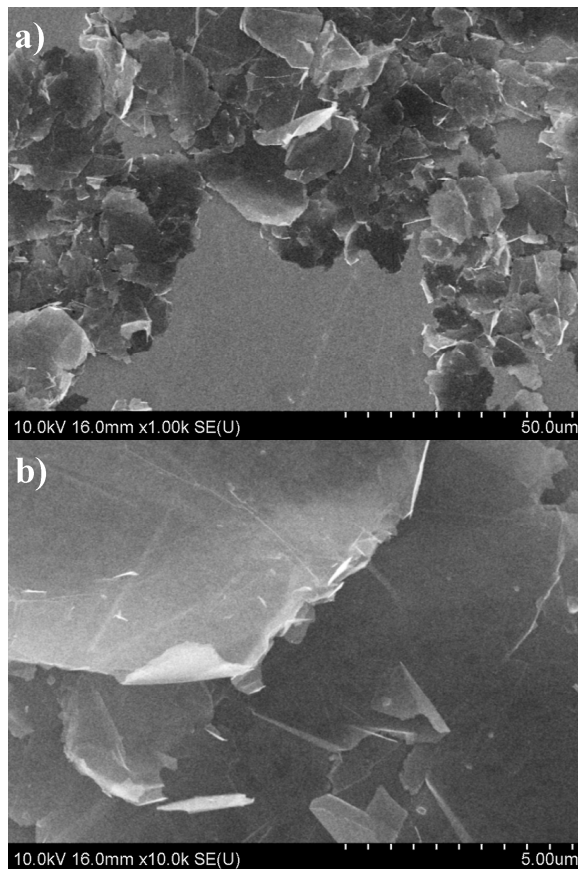


Figure 21. SEM of microwave exfoliated graphite (EG) after sonication in hexane at a) 1,000 times magnification, and b) 10,000 times magnification.

3.4.2 Modulus and strain

As discussed above, the two most important metrics for compliant electrodes are the Young's modulus and the conductivity. The stress-strain curves, from which the Young's modulus was derived, are shown in Figure 22a for PDMS (Sylgard 184, 20:1 resin:crosslinker) loaded with EG to 15 wt%. The slopes for the increasing and decreasing strain directions were almost the same, but there was some hysteresis

(separation of the curves). The stress dropped slightly with increasing cycle number, indicating a softening of the material. For samples with lower EG loadings, there was less change with cycle number. (additional stress-strain data for composites with other EG loadings can be found in the Chapter 3 Appendix.)

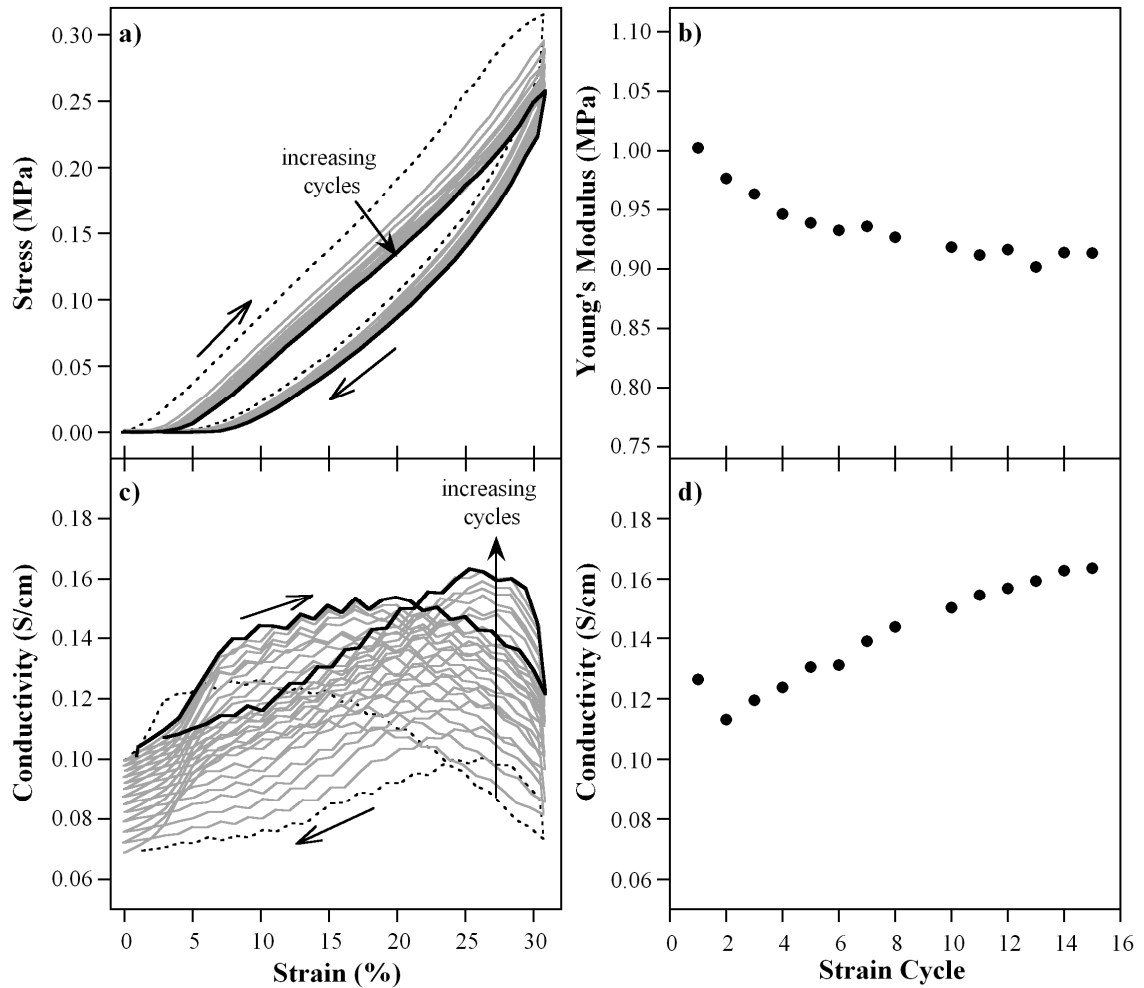


Figure 22. For a 15 wt% sample a) stress vs. strain for the first 15 cycles, b) Young's modulus at 10% strain vs. cycle number, c) conductivity vs. strain, and d) conductivity vs. cycle number. The first cycle is indicated by a dotted black line, cycles 2-14 by gray lines, and cycle 15 by a solid black line. The directions of increasing and decreasing strain are indicated by arrows, as are shifts with increasing cycling number.

During the first strain cycle, all samples experienced non-recoverable plastic deformation. This was evidenced by the slope of zero between 0 and 2-3% strain in later cycles: since the sample permanently elongated in the first cycle, a strain of ~3% was needed just to make it taut again, and above that it was stretched.

The Young's modulus was taken as the slope of the stress-strain curves at 10% strain. The moduli are plotted as a function of cycle number in Figure 22b. The modulus begins at 1 MPa and settles to 0.9 MPa with cycling. Therefore, we achieved the goal of retaining a low modulus for these composites. For comparison, Sylgard 184 mixed at a ratio of 10:1 resin to cross-linking agent has a reported Young's modulus of 1.8 MPa at 25% strain. It should be noted that the Young's modulus of PDMS depends on several factors, including sample thickness and geometry, fabrication techniques, testing conditions such as temperature, humidity, and strain rate, and the strain at which the modulus is measured.

The conductivity was measured simultaneously with the stress, and these data are shown for the same sample in Figure 22c. Conductivities for a loading of 15 wt% were on the order of 10^{-1} S/cm. As the strain increased, so did the conductivity, but as the strain increased further the conductivity dropped again. The maximum conductivity was reached between 15 and 30% strain for all samples. On the return scan, the conductivity peaked again before dropping, but at a higher value of strain. The fall in conductivity with strain is understandable from a percolation model of conductivity: as the distance between particles increases, the number of paths available for electron hopping decreases.

Above 25% this effect starts to dominate. The initial increase is, however, puzzling. One hypothesis is that it's due to reorientation of the particles upon elongation of the material so that their sheet faces begin to lie parallel to the strain direction, decreasing the out-of-plane particle separation and allowing the formation of new particle-particle contacts.

Un-strained samples had a higher conductivity than samples that had been strained, but for the latter the conductivity steadily increased with cycle number (after the second strain cycle), as shown in Figure 22d. For this sample, the never-cycled conductivity was 0.40 S/cm. When the sample was strained for the first time, the maximum conductivity dropped to 0.13 S/cm, and then it climbed back to 0.16 S/cm by the 15th cycle.

The initial drop in conductivity during the first strain cycle is presumably due to broken contacts between particles that are initially in weak contact with neighboring particles. Those routes for electron hopping are permanently lost. The subsequent increase in conductivity with cycling suggests that the EG rearranges within the PDMS matrix over time. Perhaps the plates are taking on a more in-plane alignment (along the stretch direction) that would be favorable to the in-plane conductivity that was measured.

The increase in conductivity under strain cycling has been reported previously in a variety of conductive-filler/insulating-host composites^[112, 122, 133-135]. This behavior has been postulated to be due to the formation of additional conductive pathways through the material by removal of matrix material between the EG particles^[136].

To put these results in context, moduli and conductivities that have previously been obtained for elastomer-filled composites are compared with our results in Figure 23. (A list of the starting materials and filler particles for the composites used in Figure 23 can be found in the Supplementary Information.) Numbers for those materials with properties that are similar to our PDMS/EG composite are shown in Table 3. Our results are most comparable to those for SWCNTs in PDMS. The exfoliated graphite has, however, the advantage of lower cost than SWCNTs.

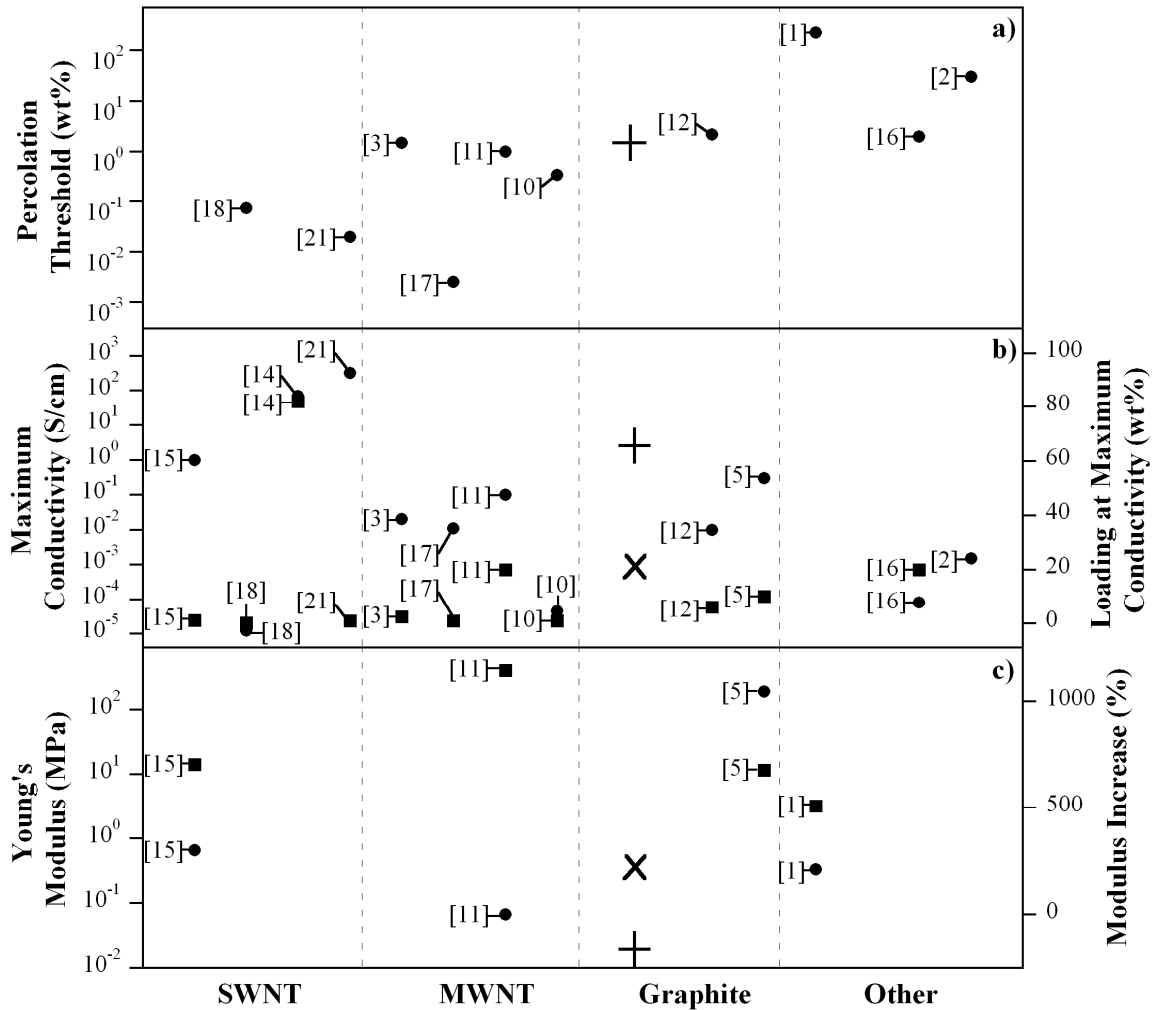


Figure 23. Research results by others showing, versus filler material, a) the percolation threshold, b) the maximum conductivity (circles) and the loading at maximum conductivity (squares), and c) the Young's modulus (circles) and the modulus increase (squares). The + symbols show the values for PDMS/EG of the percolation threshold, maximum conductivity, and Young's modulus, while the x symbols show the values of loading at maximum conductivity and the modulus increase. (Reference numbers pertain to the original publication.)

Table 3. Modulus and conductivity of 15 wt% PDMS/EG and results from prior work on elastomers with conductive fillers.

Conductive Filler	Host Polymer	Loading	Modulus (MPa) / Increase (%)	Conductivity (S/cm)	Reference
This Work					
EG	PDMS	15 wt%	1 / 220	10-1	
Prior Work					
SWCNTs	PDMS	1.2 wt%	14 / 300	100	[117]
EG	nitrile-butadiene rubber	10 wt%	11.5 / 1040	10-1	[131]
Ag particles	PDMS	17 vol%	2.7 / 210	unreported	[137]

3.4.3 Modulus and strain versus EG loading

As mentioned previously, composites having low percolation thresholds are desirable because they retain the low modulus of the host material. Parameters affecting the percolation threshold include filler shape, filler size and distribution, particle-matrix and particle-particle interactions, and processing method [112, 138].

The conductivity of the PDMS/EG is shown in Figure 24a as a function of loading. The highest conductivities were reached between 15 and 30% strain for all the PDMS/EG samples. The onset of percolation was observed at 3 wt% for unstrained samples and at 4 wt% for strained samples. Below that, the resistance was too great to measure in our system (higher than 10 M Ω). These thresholds are comparable to those found previously for EG [124, 131] and MWCNT [113, 139] composites, but are higher than the percolation

thresholds reported for SWCNTs (> 0.1 wt%)^[118, 121]. The cost benefits of using EG may, however, be more important. Above the onset of percolation, the conductivity increased with loading, as expected. (The conductivity vs. loading data are fit with a power law model in the Chapter 3 Appendix, giving critical exponents of 3.0 and 3.5 for strained and unstrained samples, respectively.) Measurements at loadings higher than 25% could not be obtained because the samples became too brittle.

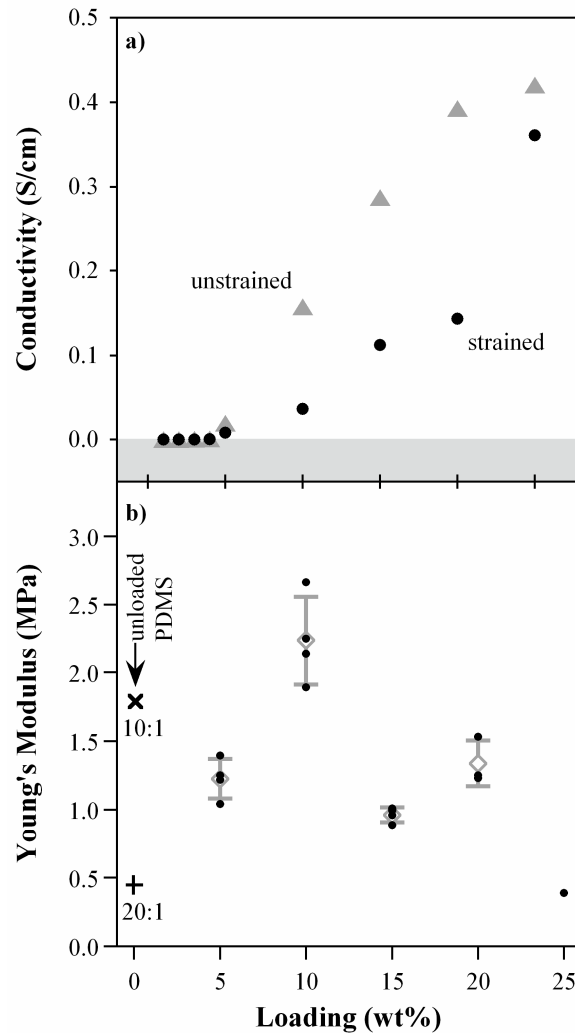


Figure 24. a) Conductivity and b) Young's modulus vs. loading of EG in 20:1 PDMS. For the modulus, 4 points were taken for 5, 10, and 15 wt%, three points for 20 wt%, and one for 25 wt%. The average and standard deviation are also indicated in gray in (b).

Figure 24b shows the Young's modulus as a function of loading; there was no discernable dependence. The average for all samples was 1.44 MPa, corresponding to a three-fold increase compared to the unloaded host 20:1 PDMS, which has a modulus of 0.44 MPa at 10% strain based on our measurements.

3.4.4 Strain to failure

Another desirable feature of compliant electrodes is an ability to undergo large deformations without breaking. This is important for applications such as flexible displays, strain gauges, and dielectric elastomers. To determine the ultimate tensile strain, samples with loadings from 2 to 20 wt% were fixed at one end, clamped to a moving stage at the other, and stretched until they failed mechanically. The results are shown in Figure 25. Even samples with loadings as high as 15 and 20 wt% were capable of undergoing 30% strain, and at loadings of 5 wt% they achieved 150%. (Results for loadings from 2-5 wt% are averaged from 4 samples, and loadings from 10-20 wt% are averaged from 2 samples.) This compares with 240% ultimate tensile strain for unloaded 20:1 PDMS and 110% for unloaded 10:1 PDMS*.

Two 5 wt% samples were subjected to repeated strain cycles between 0 and 30% strain, one for 10^5 cycles (27 hrs) and one for 10^6 cycles (11.5 days). They were then strained to failure. Surprisingly, these samples showed ultimate strains of 230% and 250%,

* R. Gray (personal correspondence, Technical Information Center, Dow Corning. Midland, MI 2008.

respectively (shown as the triangular point in Figure 25), which is the same result as for unloaded 20:1 PDMS and a substantial increase compared to the other samples.

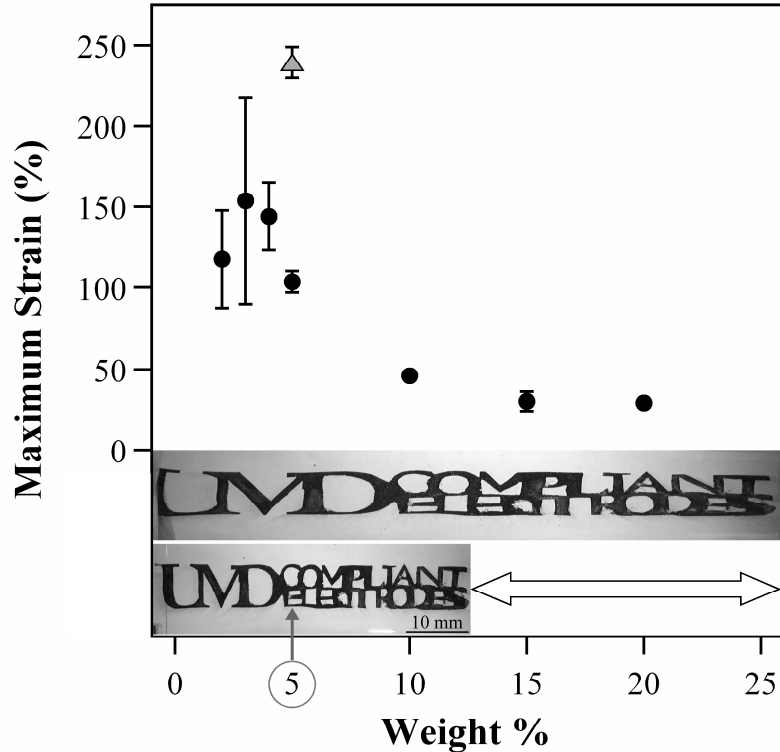


Figure 25. Ultimate tensile strain for PDMS/EG samples as a function of loading. A 5 wt% 20:1 PDMS/EG film spin coated onto a 10:1 PDMS film and patterned with “UMD compliant electrodes” is shown at rest and at 100% strain.

To demonstrate the patternability and stretchability of the composite electrode, a film of PDMS/EG was spin coated onto a base film of 100 μm thick 10:1 PDMS topped by a stencil with the phrase “UMD Compliant Electrodes”. Upon removing the stencil, the desired composite pattern, 7 mm wide and 50 mm long, was left on the base film. The thickness of the PDMS/EG layer was 50 μm . This sample can be seen at rest and at 100% strain in Figure 25.

3.4.5 SEM images of composites

SEM images were obtained for PDMS with and without EG loading (Figure 26). The samples were cleaved after immersion in liquid nitrogen and the cross-sections examined. The sample in Figure 26b had a 15 wt% loading, although it appears to be composed entirely of EG owing to the high surface area of the particles. The images revealed voids in the composites, but no voids in unloaded PDMS. The voids are the likely reason for the retention of the low Young's modulus by the composites even at relatively high loading. The formation of voids and pores is not uncommon in two-phase composites [119, 123, 130]

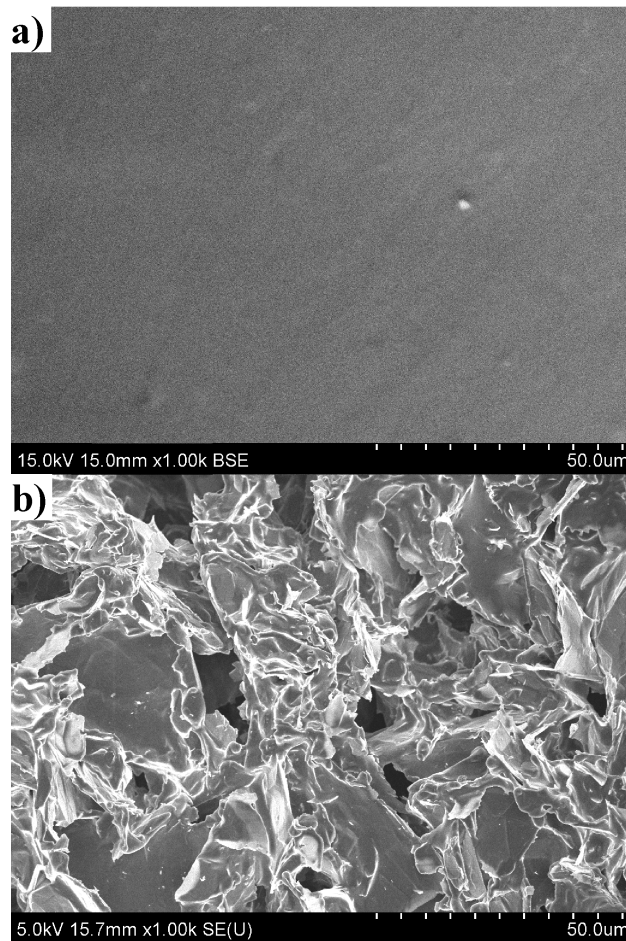


Figure 26. SEM images of a) PDMS without EG and b) PDMS with 15 wt% EG.

3.5 Discussion

The 1 MPa modulus is the lowest on record for a conductive two-phase composite material. Nevertheless, it is our hypothesis that electrical conductivity can be achieved at even lower loadings, which could reduce the modulus of the electrodes even further, by using alternative processing to produce more fully exfoliated graphite. This hypothesis is supported by the theoretical work of Guth^[140], Halpin^[141], and Celzard^[142]. Therefore, future work will focus on the production of exfoliated graphite with higher fractions of single sheet graphene and its incorporation into elastomers for compliant electrodes. To produce single sheet graphene, mechanical^[143], chemical^[125, 127, 144, 145], and solution^[135, 146] exfoliation are the preferred methods.

Surprisingly few publications on compliant electrode materials (less than 14% of the articles on this topic) have measured conductivity under strain^[112, 147-152], despite the materials being labeled as flexible, stretchable, or bendable. Since conductivity under deformation is one of the most important performance metrics for a compliant electrode, future research in this field should include such testing.

For the advancement of the field of compliant electrodes, it is necessary to compare results with those from previous work. Currently, this is difficult because no consensus has been reached on which units should be employed (resistance, resistivity, sheet resistance, conductance, or conductivity), and the sample dimensions are frequently not provided to allow readers to convert between them. We suggest the use of conductivity or resistivity when reporting on material properties.

Although this research focused solely on PDMS, other elastomers could also be used. However, this will require addressing issues relating to solvent compatibility, viscoelasticity, creep, processing and fabrication techniques, and cost.

3.6 Conclusions

A compliant electrode material has been formed by mixing exfoliated graphite into PDMS. The composite exhibited a low percolation threshold (3 wt%), moderate conductivity (0.4 S/cm at 25 wt%), and low stiffness (average Young's modulus of 1.44 MPa). It was also capable of undergoing large deformations (ultimate strains as large as 250% after extended cycling), and it was durable (5 wt% samples were capable of 10^6 cycles to 30% strain without failure).

3.7 Acknowledgements

This research was supported by the US Army Research Laboratory under the MAST CTA program. We would like to thank Dr. Michael Fuhrer and Alexandra Curtin from the Physics Department at the University of Maryland for assistance with materials development, Zach Cummins from the Department of Aerospace Engineering at the University of Maryland for fabrication of stencils, and Michael Hnatow from HiTechTrader (www.HiTechTrader.com) for donating a tube furnace used in the materials development process for this research. We would also like to thank Santa Fe

Science and Technology, Inc. for their kind donation of the force-strain transducer and the custom Labview software.

3.8 Chapter 3 Appendix

3.8.1 Alternative electrodes

The first alternative compliant electrode material we experimented with, as a replacement for carbon grease, was patterned metals. Gold was chosen for its high conductivity; however, gold alone does not adhere well to PDMS when thermally evaporated, therefore a base layer of chromium was required. To maximize the stretchability of the electrode material, Cr/Au layers were thermally evaporated having thicknesses on the order of 100 nm. As shown in Figure 27a, to prevent the wires (used to connect the DEA to the high voltage power supply) from interfering with the actuation strain, both top and bottom contact pads were patterned on the same side of the DEA. This meant that one contact pad was patterned on the top of the PDMS (PDMS was glued to the glass slide) and the other contact pad was patterned on the bottom of the glass slide. This configuration did not work because the Cr/Au would not cover the step from the PDMS, around the thickness of the glass slide, and then to the face of the glass slide. Carbon grease had to be used to help cover this step (Figure 27a).

Next, we tried patterning the contact pads on opposite sides of the DEA to eliminate the un-coatable step from PDMS to the glass surface (Figure 27b). Now, a method to make electrical connection to the gold coated free end of the DEA was required that still would not interfere with the DEA actuation.

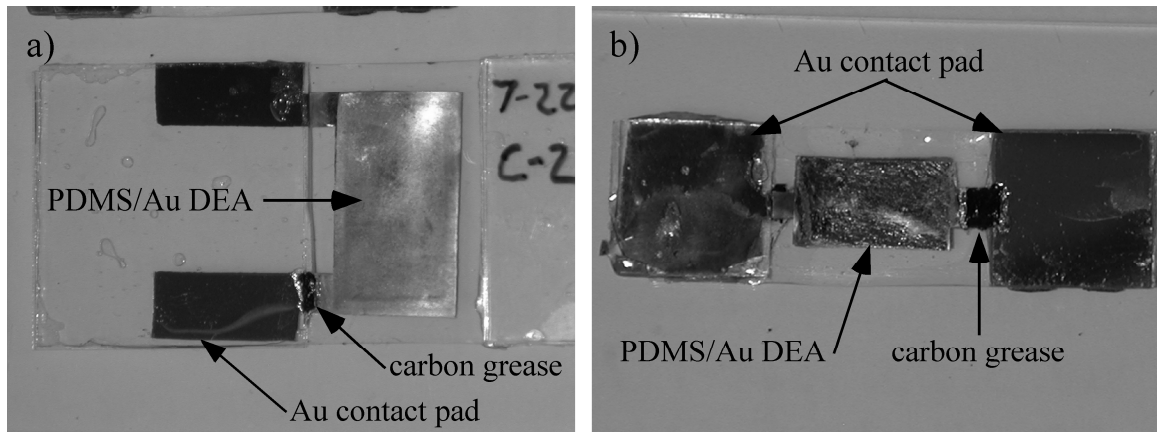


Figure 27. Images of PDMS DEAs with a) gold electrodes with the contact pads patterned on the same-side of the DEA, and b) gold electrodes with the contact pads patterned on the opposite-sides of the DEA.

Three experimental electrical connection methods were attempted for the gold patterned electrodes. The first method was a spring that was mounted to the head of a screw and soldered to a wire that was connected to the high voltage power supply (Figure 28a).

When the DEA was actuated, the gold contact pad would move back and forth and remain in physical contact with the spring (Figure 28b). The spring was chosen to reduce friction, however positioning of the device was critical to maintain contact during actuation.

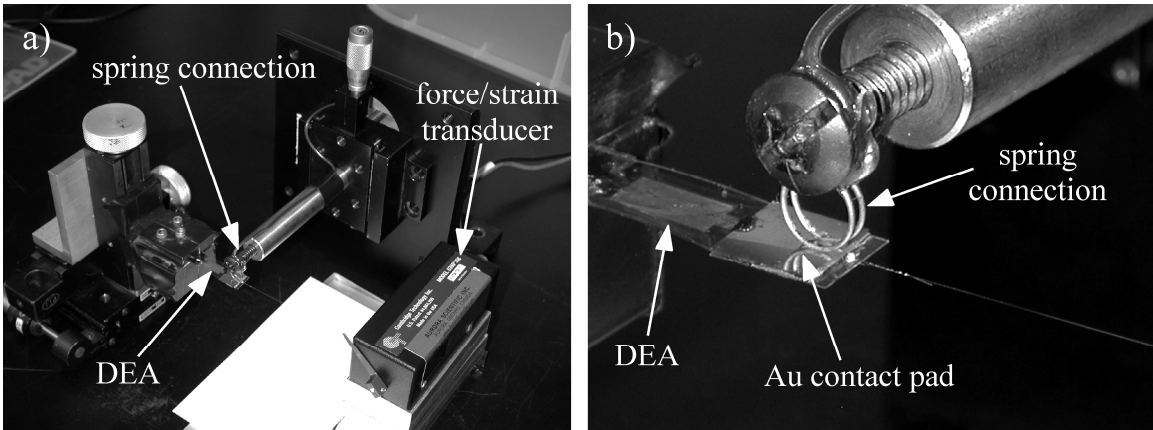


Figure 28. Images of a) the spring connection for DEAs with patterned gold electrodes, and b) close up of the spring making contact with the top gold contact pad.

The second experimental electrical connection used a flat ski that would make physical contact with the gold contact pads (Figure 29a). The ski was soldered to a wire that was connected to the high voltage power supply that ran through the center of a spring. The spring allowed a small force to be applied to the ski to ensure physical connection during actuation. This design worked better than the ski design, but was still difficult to connect and did not make continuous contact with the DEA contact pad when actuated.

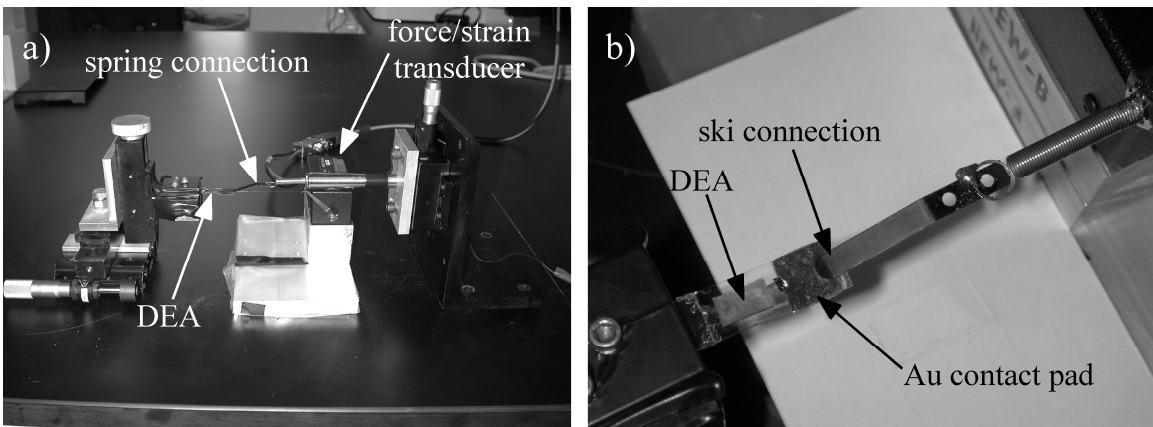


Figure 29. Images of a) the ski connection for DEAs with patterned gold electrodes, and b) close up of the ski making contact with the top gold contact pad.

The third experimental electrical connection used magnets soldered to wires that were then connected to the high voltage power supply (Figure 30a). Two magnets were used for each electrode. The magnets were placed over one of the two contact pads (Figure 30b) to make electrical connection to the DEA. This method worked well, but was still not a long-term solution to the electrode issue.

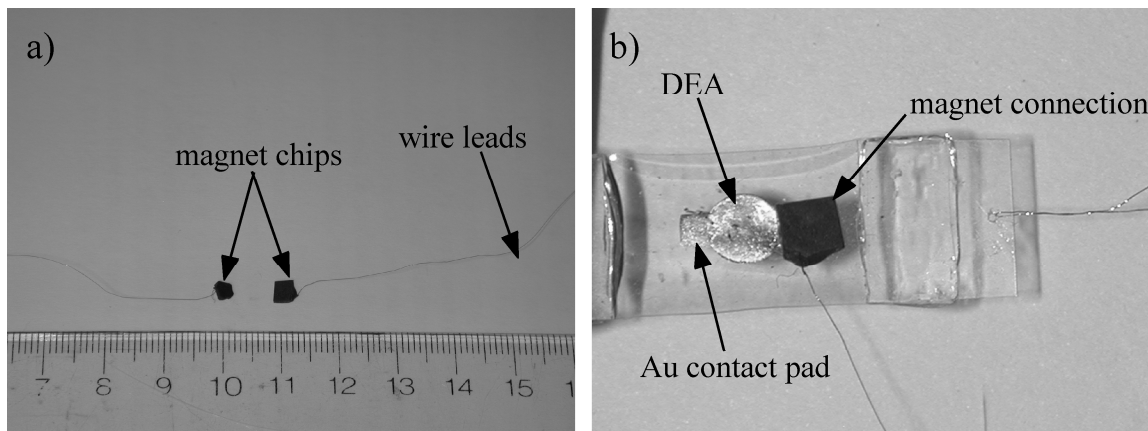


Figure 30. Images of a) the magnet type connection used for DEAs with patterned gold electrodes, and b) close up of the magnet making contact with the top gold contact pad.

A completely new approach was used as an alternative compliant electrode to replace carbon grease that provided the patternability of the thermally evaporated metals, but eliminated the need for bulky electrical connections. This approach was a composite of electrically conductive graphite filler particles blended with PDMS. Hexane was used to dilute the composite and assist in mixing of the two phases. An example of the PDMS/graphite composite is shown in Figure 31. This composite was flexible and conductive, but there was certainly room for improvement. The patternability of the composite was poor, and often resulted in wrinkles, cracks, and delamination from substrates (Figure 32a-b). The size of the graphite particles was determined to be the

cause of the poor mechanical and electrical properties, and for the poor patternability. Therefore, to lower the filler particle loading and improve electrical conductivity, we began to experiment with reducing the particle size by exfoliation.

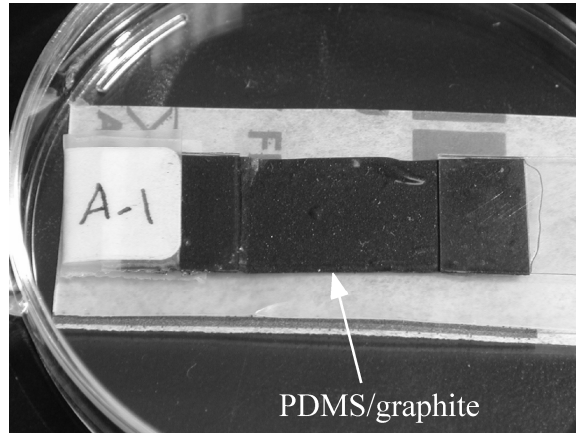


Figure 31. Image of a PDMS/graphite composite material.

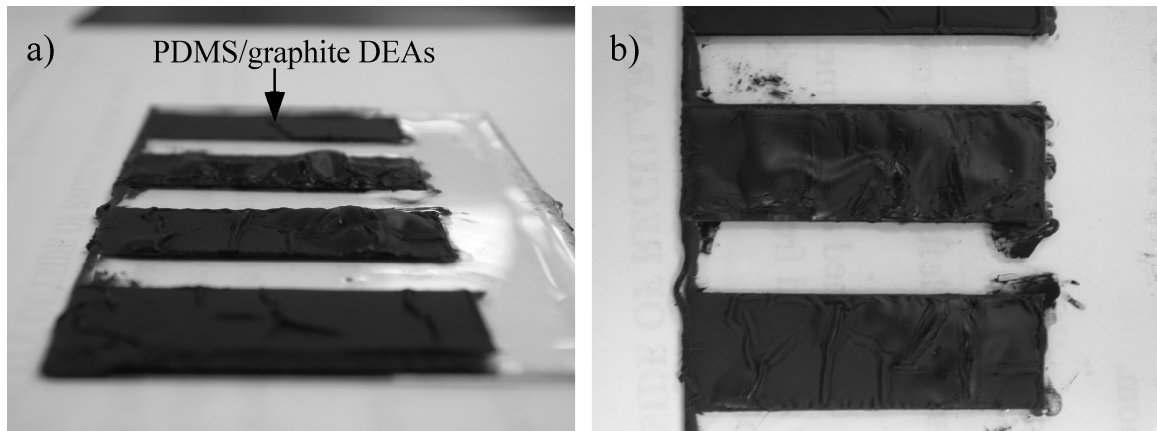


Figure 32. Images of DEAs fabricated with PDMS/graphite electrodes.

The final compliant electrode material was PDMS/EG, which had good electrical conductivity and mechanical properties (Figure 33). The patternability of the composite allowed the electrical connections to be patterned outside of the active area and on the

fixed end of the DEA. This prevented the electrical connections from interfering with the actuation strains.

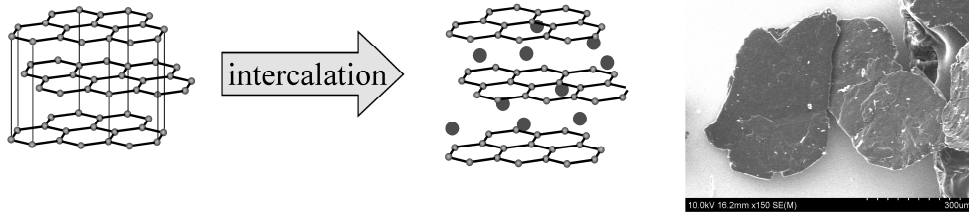


Figure 33. Image of a patterned PDMS/EG DEA showing the silver epoxy contact pads applied over non-overlapping areas of the top and bottom electrode layers.

Graphite is composed of single atom thick sheets of sp^2 hybridized carbon atoms arranged in a hexagonal close packed (HCP) crystal structure. The individual sheets are called graphene and are bound together by van der Waals interactions produced by delocalized π -orbitals^[153]. The HCP unit cell of graphite has an in-plane bond-length spacing of 1.42 Å between neighboring carbon atoms and 3.35 Å between sheets^[153]. The spacing between sheets allows atoms and molecules, such as acids, to be intercalated. Graphite soaked with sulfuric and nitric acids (4:1 wt%) is exfoliated by rapidly heating the acids, causing them to vaporize and generate enough force to overcome the van der Waals binding, and results in c-axis expansion. EG particles are then broken down via sonication in solvents and added to the host elastomer, forming the compliant electrode composite. The processing and fabrication is shown schematically in Figure 34.

1) start with graphite flake

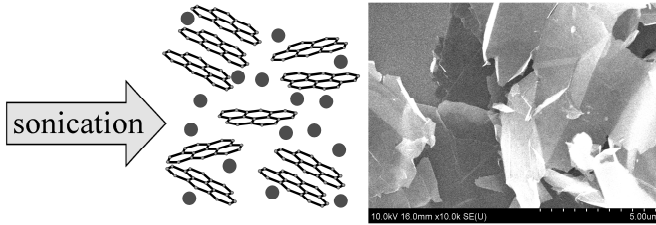
2) soak with sulfuric and nitric acids (4:1 w/w ratio)



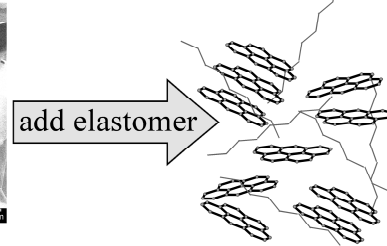
3) rapidly heat the acid-soaked graphite in a microwave or in a tube furnace at 1000 °C



4) break down worm-like structures via sonication



5) mix with elastomer



6) apply stencil and pattern the compliant electrode material



Strain = 0%

Strain = 100%

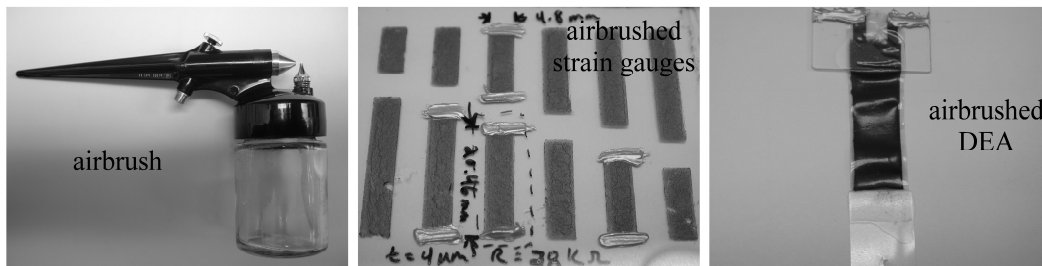


Figure 34. Processing and fabrication sequence for elastomer/EG compliant electrodes.

The third alternative electrode material was also exfoliated graphite; however, the exfoliation of the graphite was chemically obtained from graphite oxide. Oxidized EG particles were prepared using a modified version of the Hummer's method ^[154] in which a water free mixture of concentrated sulfuric acid, sodium nitrate, and potassium permanganate is used to oxidize the particles.

The oxidization procedure was as follows:

In a fume hood, 20 g sp1 graphite (Bay Carbon Inc.) was added to a solution containing 30 mL concentrated sulfuric acid (Sigma Aldrich), 10 g potassium persulfate (Sigma Aldrich), and 10 g phosphorous pentoxide at 80 °C. The solution turned from black, to brown, to yellow, to purple. The solution was thermally isolated and allowed to cool to room temperature over 6 hrs. Water was slowly added to the solution, and the solution was vacuum filtered through a 300 mL sintered glass funnel with medium porosity over paper filter (Whatman #2). Water was added until the rinse water became pH neutral as determined via litmus paper. This process was repeated five times before continuing on to the next steps.

In a fume hood, 20 g of the chemically treated graphite was added slowly into a 1000 mL triple neck flask containing 50 g sodium nitrate (Sigma Aldrich) and 460 mL concentrated sulfuric acid heated to 66 °C using a digital hotplate. A glass thermometer was placed in one of the necks of the flask with a through-hole rubber plug and the other two necks were sealed with glass stoppers. The solution was then cooled to 0 °C in an ice bath. A Teflon coated 1" magnetic stir bar was then placed into the flask and

vigorously agitated at 1000 rpm throughout the following steps. When the solution reached 0 °C, 60 g potassium permanganate (Sigma Aldrich) was slowly added while carefully monitoring the temperature so that it did not exceed 20 °C. The solution was then removed from the ice bath and the temperature was increased to 35 ± 3 °C.

After 30 min the solution was then divided into two 1000 mL beakers and 460 ml H₂O was slowly added to each of the solutions causing violent effervescence. The temperature rose to 98 °C during this step. After 15 min, the effervescence diminished and the solution turned into a thick paste. The paste solutions (each beaker) were then further diluted with 1.4 L H₂O that was warmed to 30 °C on a hotplate. Next, the solutions were treated with 0.315 mL of a 30% solution of hydrogen peroxide (Sigma Aldrich) to reduce the residual permanganate and manganese dioxide into colorless and soluble manganese sulfate. This addition rendered the solution yellow-brown and was filtered using a vacuum assisted filtration system.

After drying the oxidized graphite for 24 hrs at room temperature, 0.1 g of the particles were placed in a 23 mL glass vial and suspended in 6 g hexane. The solution was bath sonicated for 9 hrs and 3.17 g PDMS resin was added to the solution, followed by sonication for 30 min. Next, 0.185 g of the PDMS crosslinking agent was added to produce a 10:1 ratio by weight (resin to crosslinker) and the solution was sonicated for 10 min. The filler particle loading in the PDMS composite was 3 wt% (the percolation threshold for PDMS/EG composites determined in Chapter 3). The composite solution

was then spin coated on a cleaned glass slide at 1000 rpm, vacuum desiccated to remove air bubbles for 30 min, and cured on a hotplate at 90 °C overnight.

The following protocol was developed by Stankovich et al ^[155]. The rinsed, filtered, and dried graphite oxide was placed over phosphorous pentoxide in vacuum and left undisturbed for one week. Next, 500 mg dried graphite oxide was suspended in 50 mL anhydrous dimethylformamide (DMF) (Sigma Aldrich). Then, 20 mmol phenyl isocyanate (Sigma Aldrich) was added to the solution, and the solution was isolated for 24 hrs at room temperature. The solution was filtered through the sintered glass funnel and the filter cake was dried overnight on a hotplate at 110 °C. The dried graphite oxide particles (now ~ 40 mg batches) were re-suspended in 40 mL DMF and bath sonicated for three hrs.

At this stage, the graphite oxide is reduced to exfoliated graphite by adding 0.4 mL dimethylhydrazine (Sigma Aldrich) to the solution containing 10 mL DMF and 40 mg graphite oxide. The DMF/dimethylhydrazine/graphite oxide solution was heated to 80 °C on a hotplate for 24 hrs, then added one drop at a time (~1 ml/drop/sec) to 1000 mL of vigorously stirred methanol. The coagulations were filtered from the suspension using the vacuum assisted sintered glass funnel, washed with methanol to remove remaining solvents, and left to dry under vacuum for 10 hrs.

The chemically exfoliated graphite was now able to be re-suspended in hexane and blended with PDMS. Unfortunately, this process produced composites with poor

conductivities (< 0.001 S/cm). It is believed that the concentrated sulfuric acid was not concentrated enough. The most concentrated sulfuric acid available is fuming sulfuric acid (Sigma Aldrich), or oleum. Oleum was purchased, however; there was an 8 month backlog. By the time the oleum arrived, the project had shifted gears and this method was not attempted again due to time constraints. SEM images of a PDMS composite containing 15 wt% of the chemical exfoliated graphite are shown in Figure 35.

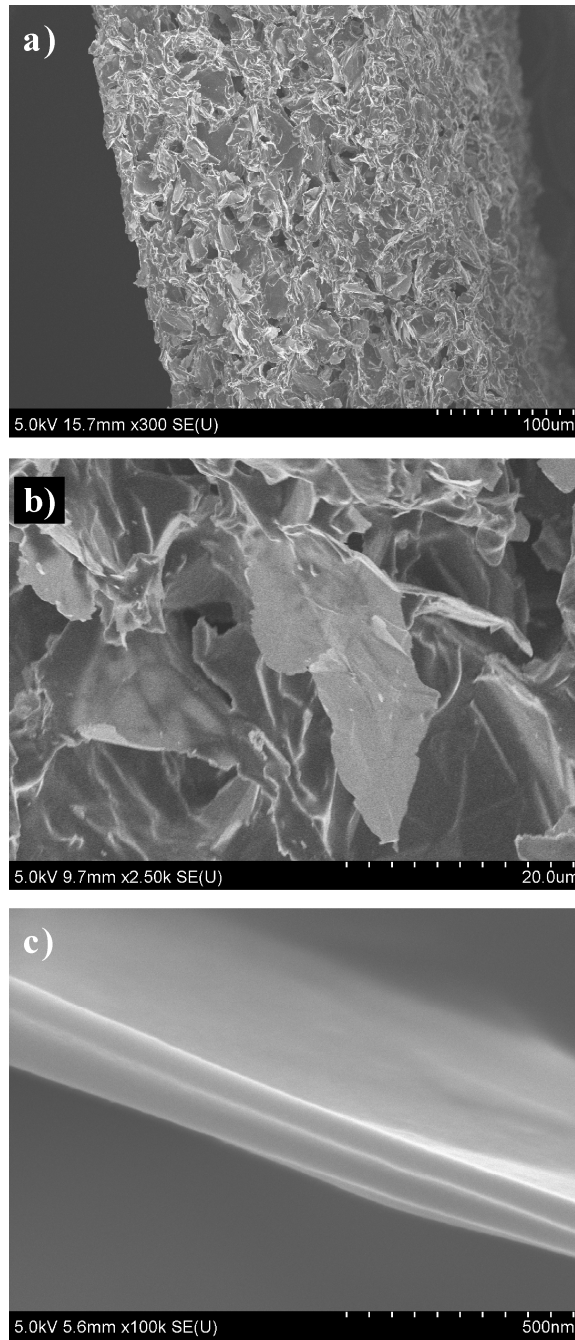


Figure 35. SEM images of chemically exfoliated graphite a) in a 15 wt% composite with PDMS at 300 times magnification, b) at 2,500 times magnification, and c) at 100,000 times magnification.

3.8.2 Surfactants

To improve the exfoliation and dispersion of the EG particles in hydrophilic elastomer hosts, various surfactants were explored. Surfactants were used to blend the hydrophobic EG particles with the hydrophilic elastomers. Generally, compliant electrode samples were fabricated with a constant weight of 0.1 g EG into a 20 mL glass vial with 3g of the surfactant solutions.

3.8.2.1 *Triton X-100 and DSPE-mPEG 5000*

EG particles were suspended in a solution of 95.6 wt% deionized water, 4 wt% Triton X-100 surfactant, and 0.4 wt% DSPE-mPEG 5000 (Laysan Bio, Inc.) phospholipids. Liquid latex resin was added to the solution. The resulting latex/EG composite was 10 times more conductive than the PDMS/EG composites where the EG particles were sonicated in hexane without surfactants.

3.8.2.2 *Triton X-100*

Triton X-100 is commonly used to suspend carbon nanomaterials (e.g. graphite and nanotubes). Using the critical micelle concentration (CMC) of Triton X-100 (0.25 mmol) as a starting point, the optimal surfactant concentration was determined to be 0.75 wt% through a process of trial and error with higher and lower concentrations. The average conductivity is plotted as a function of surfactant concentration in Figure 36.

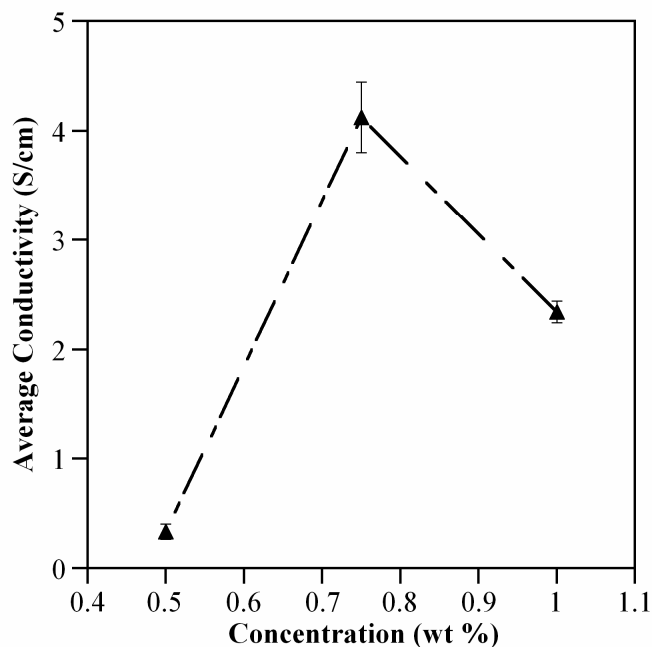


Figure 36. Average conductivity as a function of surfactant concentration (wt% in DI water) for latex/EG composites fabricated with Triton X-100 surfactants.

3.8.2.3 Triton X- 45

Triton X-45 (linear formula: $t\text{-Oct-C}_6\text{H}_4\text{-(OCH}_2\text{CH}_2)_x\text{OH}$, $x = \sim 5$) surfactant has the same chemical structure as X-100 (linear formula: $t\text{-Oct-C}_6\text{H}_4\text{-(OCH}_2\text{CH}_2)_x\text{OH}$, $x = 9\text{-}10$), with a shorter alkyl chain; however, this particular surfactant was insoluble in DI water. When added to DI water, the surfactant resulted in a milky color, which became more apparent as concentration increased above 0.1 wt%. Samples fabricated with these solutions, despite the insolubility, resulted in conductivities nearly an order of magnitude less than that of the Triton X-100.

3.8.2.4 *Sodium cholate hydrate*

Sodium cholate hydrate was also tested as a surfactant for suspending EG particles in hydrophilic solutions. Using the CMC (9-15mmol) as a starting point, the optimal concentration was determined to be ~ 4.75 wt% in DI water. Fabricated samples had conductivities on the order of 1 S/cm. This is compared to the conductivity of 4-5 S/cm for samples fabricated with Triton X-100. The samples were also more brittle than X-100 samples; therefore, it was concluded that Triton X-100 was the ideal surfactant at a concentration of 0.75 wt% in DI water.

3.8.3 Comparison of PDMS/EG to similar compliant electrode materials

Table 4 specifies the host material and provides the references for the data in Figure 23 in the main text of Chapter 3.

Table 4. Host materials and references for Figure 5 in the main text. Reference numbers are those used in the main text.

Filler material	Host material	Reference
SWNT	PDMS	[117]
SWNT	epoxy	[118]
SWNT	polystyrene	[119]
SWNT	PEDOT-PSS	[121]
MWNT	PDMS	[114]
MWNT	epoxy	[115]
MWNT	polystyrene	[116]
MWNT	polyurethane-urea	[147]
EG	polystyrene	[124]
EG	NBR	[131]
silver particles	PDMS	[137]
CB	polystyrene	[111]
CB	polyurethane	[156]

3.8.4 Basis of Using EG for Conductive Composites with Low Modulus

There has been theoretical work on predicting the mechanical and electrical properties of composites. Starting with the mechanical properties, the Guth equation ^[140] predicts a strong increase in the modulus of the composite with increasing aspect ratio and volume fraction of the filler material:

$$\text{Eq. 7} \quad E = E_0 (1 + 0.67f\phi + 1.62f^2\phi^2),$$

where f is the filler aspect ratio, φ is the filler volume fraction, E_0 is the modulus of the unfilled polymer, and E is the modulus of the composite. Similarly, the Halpin-Tsai model ^[141] predicts that the modulus of composites with fiber-shaped fillers will be much higher than that of the host polymer:

$$\text{Eq. 8} \quad E = E_0 (1 + 2f\varphi) / (1 - \varphi).$$

The dependences of the two models on aspect ratio are shown in Figure 37. From (Eq. 7) and (Eq. 8), it would not appear to be promising to use EG, which has a high aspect ratio. This conclusion has been supported in systems such as polymer/fiber composites and elastomers filled with carbon nanotubes.

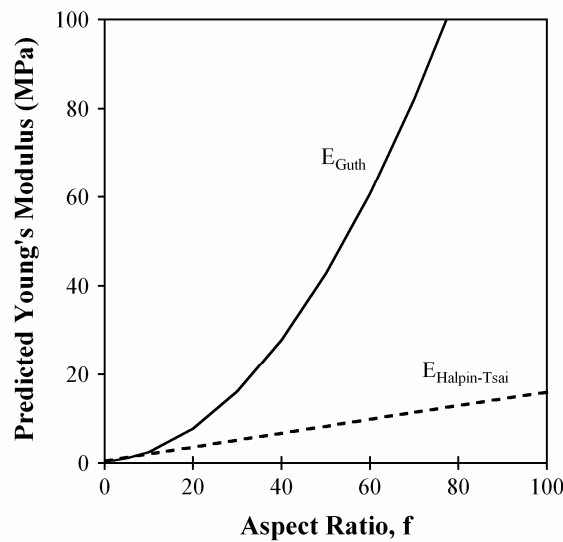


Figure 37. Guth and Halpin-Tsai model predictions for the Young's modulus as a function of aspect ratio f for $E_0 = 0.44$ MPa and $\varphi = 0.15$.

Turning to the electrical properties, Celzard *et al.* ^[142] developed a model to predict the percolation threshold for composites with randomly-oriented, disk-shaped particles in an

insulating matrix. They concluded that there would be a linear relationship between the percolation threshold and the aspect ratio:

$$\text{Eq. 9} \quad \varphi_C \propto t/r,$$

where φ_C is the critical concentration at which a conductive pathway is formed (in vol%), t is the particle thickness, and r is the particle radius. This equation shows that a percolative network is formed at lower loadings for particles with higher aspect ratios, with a factor of 10 reduction in loading for each factor of 10 reduction in particle thickness. Thus, graphene should form a conductive material at much lower loadings than graphite. Based on these relationships, the question is, then, does the material become conductive before the modulus rises significantly?

Figure 38 shows the conductivity and Young's modulus in our composites as a function of EG loading. Surprisingly, their stiffness did not increase significantly with loading, deviating from both the Guth and Halpin-Tsai equations. This is most likely due to the formation of voids in our material (Figure 26b), which neither model takes into account.

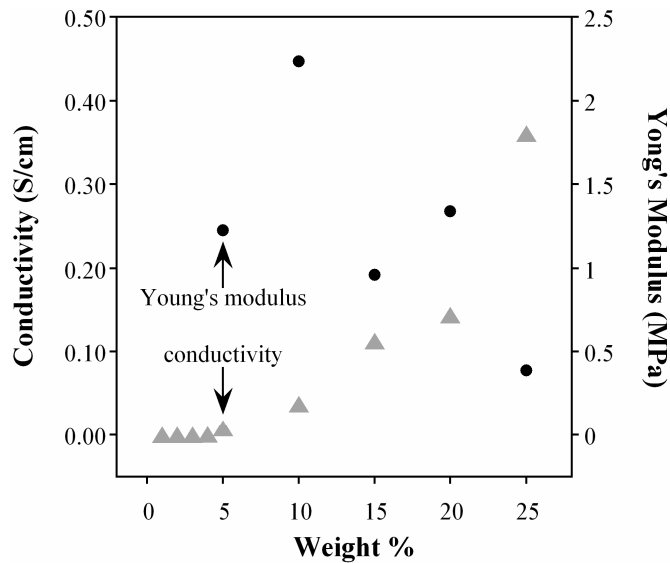


Figure 38. Conductivity and Young's modulus as a function of weight% of EG for PDMS/EG composites.

3.8.5 Effects of voids on the tangent moduli

As shown in Figure 26, voids were present in the elastomer composites. We hypothesize that the voids may have contributed to the low tangent modulus. From the SEM image, we estimate that the PDMS/EG composite contained between 5% and 20% voids by volume. To test this hypothesis, the tangent moduli were recalculated for a 15 wt% PDMS/EG composite assuming 5 vol% and 20 vol% voids. For simplicity, the voids were assumed to be cubic; therefore, the L , W , and t of the composite were multiplied by $(1-(0.05)^{1/3})$ for 5 vol% voids and by $(1-(0.2)^{1/3})$ for 20 vol% voids, the stress and strains were recalculated, and the results are shown in Figure 39. Accounting for the loss of volume resulted in a 7% increase in the tangent modulus of the composite for 20 vol% voids. This does not account for the lower modulus in our composites compared to other composites (the increase in the modulus of our composites was 64% lower than similar composites^[131]).

Adjusting the sample geometry to account for the loss of volume due to the presence of voids does not take into account the additional crosslinking sites that may be formed between the host elastomer molecules if the voids were not present. The additional crosslinking sites would also be expected to increase the tangent modulus of the composite.

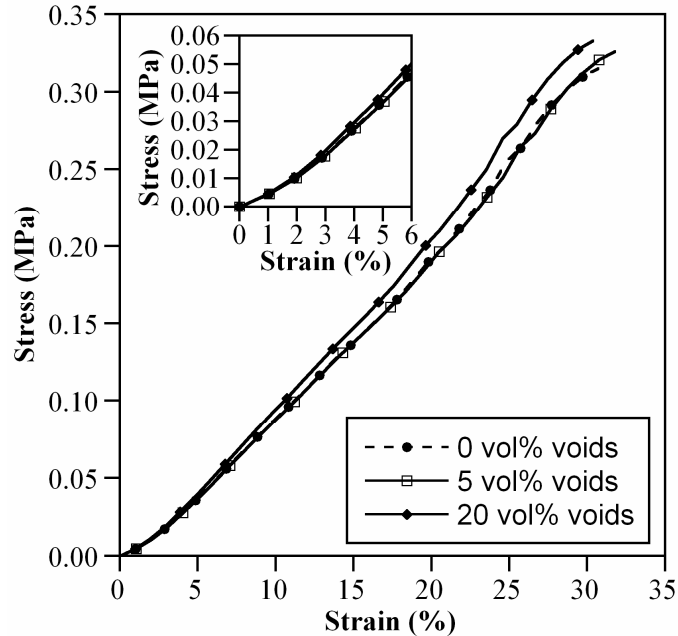


Figure 39. Stress as a function of strain for 15 wt% PDMS/EG composite calculated using the measured sample geometry (circles) compared to the stress strain curves for the same sample that were calculated using adjusted geometries to account for 5 vol% voids (squares) and 20 vol% voids (diamonds).

3.8.6 Uncertainty calculations for conductivity

3.8.7 Uncertainty calculations for conductivity

The measurement equipment used to determine sample conductivity (i.e. multimeter, micrometer, and surface profiler) have an associated uncertainty that result in some error in the calculations. To determine the impact of instrument uncertainties on conductivity

calculations, the error was determined for five 6 wt% latex/EG samples. The sample dimensions, resistance, uncertainty, calculated conductivity, and calculated error are provided in Table 5.

Table 5. Measured length, width, thickness, and resistance of five 6 wt% latex/EG samples and the calculated averages and standard deviations.

	<i>L</i> (cm)	<i>W</i> (cm)	<i>t</i> (cm)	<i>R</i> (Ohm)	Conductivity (S/cm)	Uncertainty (S/cm)
	1.913	0.525	1.60x10 ⁻³	1.00x10 ⁶	2.28x10 ⁻³	1.49x10 ⁻⁵
	1.900	0.510	1.36x10 ⁻³	1.20x10 ⁶	2.27x10 ⁻³	1.74x10 ⁻⁵
	1.380	0.526	1.68x10 ⁻³	0.89x10 ⁶	1.75x10 ⁻³	1.10x10 ⁻⁵
	1.550	0.500	1.38x10 ⁻³	1.11x10 ⁶	2.02x10 ⁻³	1.52x10 ⁻⁵
	1.770	0.499	1.72x10 ⁻³	1.15x10 ⁶	1.78x10 ⁻³	1.10x10 ⁻⁵
Uncertainty	0.001	0.001	0.01x10 ⁻³	0.0001x10 ⁶		

Sample conductivity $\sigma_{conductivity}$ was calculated using

$$\text{Eq. 10} \quad \sigma_{conductivity} = L/WtR,$$

where L is the length, W is the width, t is the thickness, R is the resistance. The uncertainties associated with the conductivities U_{σ} due to the measurement errors were determined using ^[157]

$$\text{Eq. 11} \quad U_{\sigma} = \sqrt{[(U_L \cdot \sigma_L)^2 + (U_W \cdot \sigma_W)^2 + (U_t \cdot \sigma_t)^2 + (U_R \cdot \sigma_R)^2]},$$

where $U_{L,W,t,R}$ are the uncertainties for the measured length L , width W , thickness t , and resistance R , respectively, and $\sigma_{L,W,t,R}$ are the calculated errors for the length L , width W , thickness t , and resistance R , respectively. The errors $\sigma_{L,W,t,R}$ were calculated using ^[109]

$$\text{Eq. 12} \quad \sigma_L = d\sigma/dL = 1/(WtR),$$

$$\text{Eq. 13} \quad \sigma_W = d\sigma/dW = -L/(tRW^2),$$

$$\text{Eq. 14} \quad \sigma_t = d\sigma/dt = -L/(WRt^2), \text{ and}$$

$$\text{Eq. 15} \quad \sigma_R = d\sigma/dR = -L/(WtR^2).$$

Using the above equations, it was determined that the uncertainties in the calculated conductivities (1.10×10^{-5} S/cm to 1.74×10^{-5} S/cm) due to the measurement uncertainties were two orders of magnitude smaller than the variation in the conductivities (1.75×10^{-3} S/cm to 2.28×10^{-3} S/cm) observed from sample to sample. Therefore, the measurement uncertainties are not responsible for the variation in sample conductivities. Rather, the variation may be due to either to variations in sample properties or preparation (i.e., EG loading, sonication time, extent of particle settling, contact of the epoxy with the composite) or variability in the measurement method (such as placement or pressure of the probes).

3.8.8 Dynamic stress-strain characterization of the composites

To probe the elastic behavior and determine the Young's moduli of the composite samples, stress-strain tests were performed. The Young's moduli reached a steady state after the first few strain cycles for loadings below 15 wt%, as shown in Figure 40a for a 5 wt% PDMS/EG sample. However, for samples containing 20 and 25 wt%, the modulus kept decreasing with increasing strain cycle number, as shown in Figure 40b.

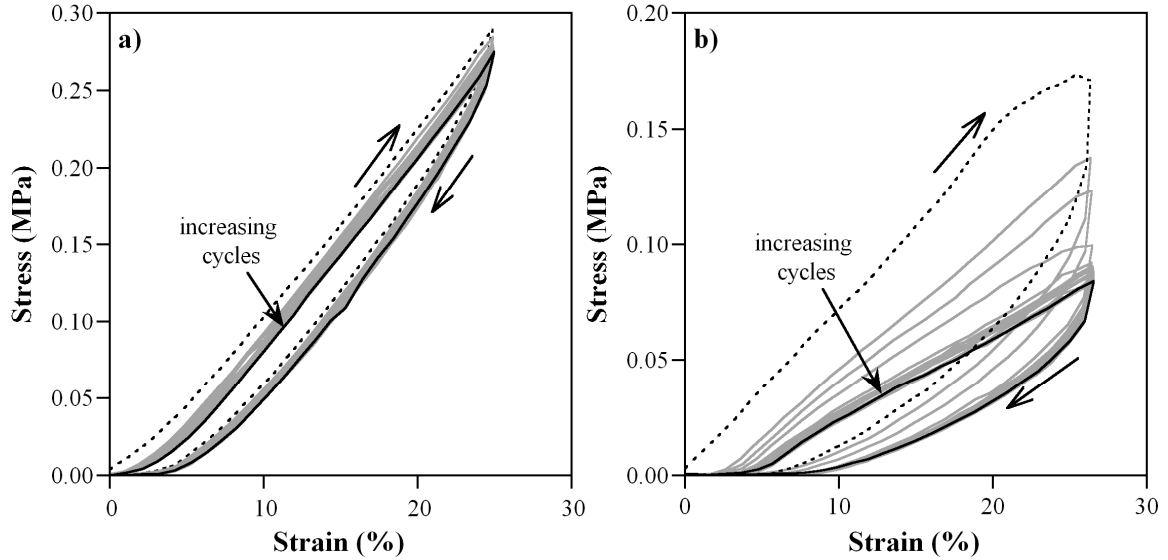


Figure 40. a) Stress as a function of strain for a sample with 5 wt% loading. b) Stress as a function of strain for 25 wt% loading.

3.8.9 Sample fabrication

The fabrication process for forming an individual PDMS/EG sample was as follows:

- In a 23 mL glass vial, combine 0.05 g of the filtered/dried EG with 6.0 g hexane.
- Sonicate the solution until the worm-like structures have broken apart (3+ hrs).
- Evaporate off 4.5 g of the hexane in the mixture on a hot plate at 150 °C.
- Add the desired amount of PDMS resin and sonicate for 30 min.
- Add the corresponding amount of PDMS curing agent and sonicate for 10 min.
- Cast the solution in a polyethylene dish and vacuum desiccate for 2 hrs.
- Bake on a hot plate at 75 °C overnight.
- Cut the sample into strips 38 mm long and 10 mm wide.

- Attach a 14 mm length of the sample to 1" x 3" x 1.2 mm glass slides using a photo-curable adhesive (such as Loctite 3108) leaving 24 mm of the sample unattached. This is the fixed end of the sample.
- Glue a 16 mm long, 12 mm wide transparency sheet to the unattached end of the sample so that 2 mm of the transparency sheet remains unattached and there are 1 mm edges on either side of the 10 mm wide sample. This will leave a 10 mm wide, 10 mm long section of the PDMS/EG sample (active area) between the glass slide and the transparency sheet. This is the free end of the sample.
- Punch a small hole in the center of the 2 mm unattached area of the transparency sheet. Thread this hole with one end of a piece of suture thread and tie off with a knot. Connect the other end of the thread to the hole in the force/strain transducer arm the same way.
- Add 4 electrical connections for 4-point probe resistance measurements by painting conductive silver epoxy (Chemtronics, CircuitWorks CW2400) across the surface of the PDMS/EG sample. The contact pads should be 2 mm wide and have a 10 mm spacing between them. Before the epoxy sets, place 10 mm of a 200 mm length of fine stainless steel wire (43 gauge, California fine Wire co.) into each of the pads; 200 mm is long enough not to impede the stress/strain tests. Allow the silver epoxy to cure for 24 hrs.

3.8.10 Power law model for conductivity as a function of EG loading

Conductivity as a function of loading data are often fit with a power law model [25, 112, 119, 125, 138, 158, 159].

$$\text{Eq. 16} \quad \sigma = ((V - V_c)/(1 - V_c))^t,$$

where V is the volume fraction of the filler, V_c is the percolation threshold, and t is the critical exponent. Figure 41 shows such power law fits for both the strained and unstrained samples, giving $t = 3.0$ and 3.5 , respectively.

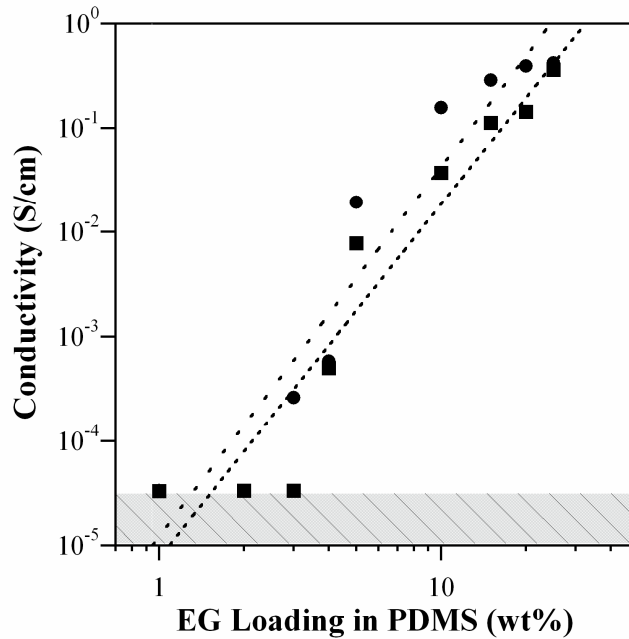


Figure 41. Power law fit to the conductivity as a function of loading data, with the dotted line representing the fit for unstrained samples (squares) and the dashed line representing the fit for strained samples (circles). Each point represents one sample.

The exponent t has been postulated to depend on the dimensionality of the conductive network, with values ranging from 1.30 to 1.43 for two dimensional systems [115, 160] and

1.5 to 2.0 for three dimensional systems ^[112, 115, 158, 160-162]. Values of $t > 2$ (so called non-universal values) have also frequently been reported ^[112, 119, 123, 124, 158, 161]. Non-universal values of t have been attributed to high aspect ratio filler particle geometries (i.e. as found in CNTs and graphene) ^[158], the formation of voids in the material ^[119], and tunneling through insulating coatings on the particles ^[158, 161-164].

Some experimentally obtained values of t from prior work are compared to the results from this research in Table 5. The exponents range from 1.2 to 3.8 and appear to be uncorrelated with performance parameters such as conductivity and modulus. The merit of the critical exponent is therefore unclear. The values of t obtained in this investigation are similar to those reported for PS/EG, PMMA/EG, and PS/graphite composites.

Table 6. Critical exponents t for PDMS/EG compared with results from prior work on unstrained elastomers with conductive fillers.

Filler Material	Host Polymer	t	Reference
This Work			
EG	PDMS	3.50 3.00 (strained)	
Prior Work			
MWNT	epoxy	1.20	[115]
SWNT	epoxy	1.30	[118]
MWNT	polyvinylalcohol	1.33	[160]
graphite powder	PMMA	1.82	[158]
MWNT	polyurethane-urea	1.98 1.60 (strained)	[147]
SWNT	PS	2.20	[119]
EG	epoxy	2.50	[123]
EG	PS	3.07	[124]
EG	PMMA	3.47	[158]
graphite particles	PS	3.50	[161]
CB	ethylene-octene	3.80	[112]

The decrease in the exponent t after straining shown in Figure 41 was also observed in MWNT/polyurethane-urea elastomer composites^[147]. In that work, the decrease was attributed to either a change in the dimensionality of the system or to a decrease in the

width of the distribution of tunneling resistances ^[147]. Also, as mentioned earlier, the voids shown in Figure 26b may contribute to the high values of the exponent t found in the power law fit.

Chapter 4: PDMS/graphite stretchable electrodes for dielectric elastomer actuators

Proceedings of IEEE Electroactive Polymer Actuators and Devices (EAPAD),
San Diego, CA, 7642(24), (2010).

Reproduced by permission of SPIE-IEEE.

M. Kujawski¹, J. D. Pearse², and E. Smela^{2*}

¹Dept. of Materials Science and Engineering, University of Maryland, College Park, MD
20742

²Dept. of Mechanical Engineering, University of Maryland, College Park, MD 20742

*smela@eng.umd.edu; tel: 301-405-5265; fax: 301-314-9477

4.1 Abstract

Dielectric elastomer actuators (DEAs) consist of an elastomer sandwiched between two electrodes, and they undergo a large in-plane expansion upon the application of an electric field. They therefore require compliant electrodes that can stretch tens of percent. The most commonly used electrode material is carbon grease, which smears easily and is difficult to pattern. This paper outlines the fabrication and performance of a novel polydimethylsiloxane (PDMS) composite having a 15 wt% loading of exfoliated graphite (EG). This new material has a Young's modulus of only 0.9 MPa and a conductivity of 0.15 S/cm. Unlike other composite electrode materials, the Young's modulus of the PDMS/EG increases only slightly, by a factor of two, upon addition of the EG. Furthermore, the PDMS/EG composite is patternable and will not rub off. DEAs were fabricated with 20:1 PDMS as the elastomer using this new electrode material. The actuation strains were equal to those of 10:1 PDMS DEAs with carbon grease electrodes

under the same electric field. Elastomer/EG composites may also find applications in areas such as flexible electronics, robotics, strain gauges, and sensors.

4.2 Introduction

Compliant electrodes for dielectric elastomer actuators (DEAs) should ideally be less stiff than the dielectric elastomer so that they do not impede the actuation of the devices.

These materials must also remain conductive while undergoing large deformations.

Carbon grease (CG) is one of the most widely used electrode materials for DEAs because it meets the above criteria and is easy to apply; however, it smears and rubs off, is difficult to pattern, dries out, and its solvents diffuse into the elastomer over time, which reduces the dielectric breakdown strength. Thus, a new compliant electrode material is required.

Over the past decade, a great deal of research on compliant electrode materials has focused on two-phase composites comprising insulating polymer matrices with embedded conductive filler particles ^[111-114, 116, 117, 119, 124, 125, 131, 137, 147, 156, 158, 165, 166].

Some of the more commonly used conductive filler materials include carbon black (CB) ^[111, 112], carbon fibers ^[112], multi-wall carbon nanotubes (MWNTs) ^[113-116, 147, 166], and single wall carbon nanotubes (SWNTs) ^[117-121, 134]. Most of these composites suffer from a dramatic increase in stiffness with the addition of the filler particles ^[33, 119, 147]. Using lower concentrations of the filler particles can minimize the increase in the stiffness;

however, the filler particle loading must be above the percolation threshold, at which the material becomes conductive.

Graphite is a promising alternative filler particle because it is electrically conductive, easily obtained, and relatively inexpensive^[123-125, 131, 158]. Graphite is composed of stacks of graphene, which are single sheets of hexagonally arranged carbon atoms. These individual sheets are stacked along the c-axis and bound together by van der Waals forces. These weak secondary forces allow small molecules, such as acids, to readily enter the graphite (intercalate) between the layers. Rapid heating of acid-intercalated graphite will vaporize the acids, generating enough force to break the van der Waals forces and separate the graphite into graphene^[124, 127-129]. Separation of the layers is known as exfoliation, and is commonly performed in a furnace^[130] or by using microwave irradiation^[124, 128, 129, 131]. The exfoliated graphite (EG) structures can then be sonicated in solvents and further separated. Production of pure single-sheet graphene remains difficult with these methods because the exfoliation is generally incomplete, which results in a combination of graphite and graphene.

In this paper we demonstrate that EG can be used to create a compliant electrode material having a low stiffness and moderate conductivity at low loadings. By combining the EG particles with a polydimethylsiloxane (PDMS) elastomer, we have produced a material that can be cast, spin-coated, and patterned. DEAs with PDMS/EG electrodes were fabricated in a simple three step process that can be repeated in virtually any lab.

4.3 Experimental

4.3.1 Microwave exfoliation

Exfoliation of the acid-intercalated graphite flake (Asbury Graphite Mills, Inc.) used in this work was conducted by a microwave irradiation method presented by Falcao *et al.*^[128] and Wei *et al.*^[129]. An 1100 W microwave oven (Kenmore) with an operating frequency of 2.45 GHz was used. Exfoliation was conducted under an inert atmosphere of forming gas (97% nitrogen, 3% hydrogen) by fitting a flexible silicone tube (MasterFlex® HV-96410-18) through the vent in the back of the microwave and into the cooking chamber. The forming gas was turned on for 10 min at a flow rate of 1 L/min prior to applying full power for 60 sec. The graphite flake (2 g) was placed into an 18 mL glass vial in the center of the microwave. The particles must be in close proximity to one another for exfoliation to occur. Large sparks were generated between the particles during exfoliation, and the expanded material glowed orange-red. Exfoliation was complete after only a few sec, and a 200-300 fold increase in volume was observed (Figure 42a-b). The resulting worm-like particles (Figure 42c-d) were separated from any remaining unexfoliated particles by stirring them into hexane. The more dense (unexfoliated) particles would sink and the less dense ^ξ (exfoliated) particles would float.

^ξ Exfoliated graphite particles have the same density as unexfoliated graphite particles; however, they probably contained trapped air which allows them to float on the surface of hexane.

The exfoliated particles were collected from the surface and dried on a hot plate overnight at 150 °C.

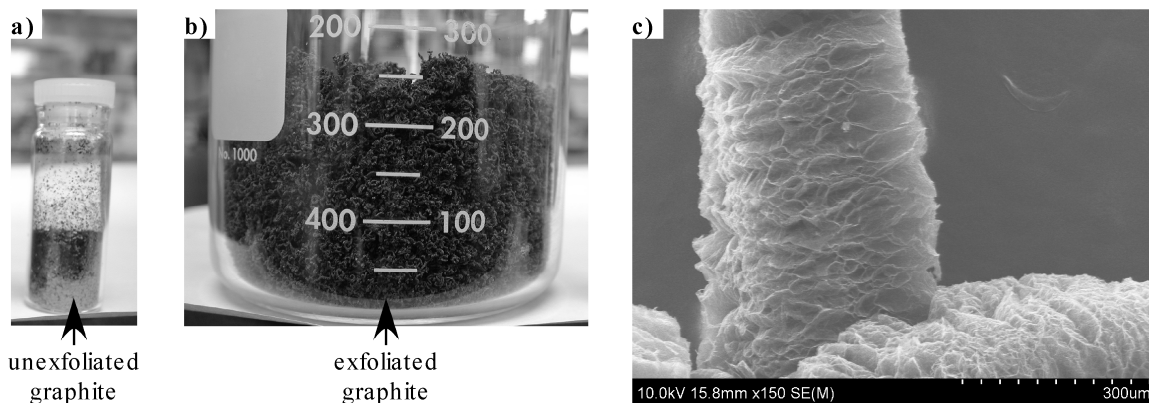


Figure 42. a) Acid-washed graphite flakes before microwave exfoliation, b) acid-washed graphite flakes after microwave exfoliation, c) SEM image of worm-like EG particles at 30 times magnification, and d) SEM image of worm-like EG particles at 150 times magnification.

4.3.2 Characterization

SEM images of composite samples were obtained with a Hitachi SU-70 SEM at an acceleration voltage of 10 kV and a working distance of 15 mm. Unloaded PDMS samples were imaged using a Hitachi S-3400N variable pressure SEM at an acceleration voltage of 15 kV, a working distance of 15 mm, and a pressure of 100 Pa. No conductive coatings were used in either case.

4.3.3 Sample fabrication

The PDMS used in this investigation was Sylgard 184 (Dow Corning). DEAs were fabricated with PDMS/EG compliant electrodes containing 15 wt% EG particles and PDMS with a 20:1 ratio of resin to cross-linking agent, giving a Young's modulus of 0.44 MPa. Standard PDMS is made with a ratio of 10:1, and has thus approximately twice the

modulus (1.1 MPa). For comparison purposes, DEAs were also fabricated with carbon grease electrodes (MG Chemicals) and PDMS with the 10:1 ratio of resin to cross-linking agent.

To break apart the worm-like EG structures, Figure 42c-d, the EG particles were added to hexane at a 1:30 ratio (w/w), and the solution was sonicated (Branson 1510) at a frequency of 40 kHz. Hexane was chosen as the solvent because it dissolved both the EG and the PDMS, and it did not prevent the elastomer from curing. After 3 hrs, the PDMS resin was added to the solution and sonicated for 30 min. The solution was then heated to 95 °C on a hot plate, driving off excess hexane until a 1:7.5 ratio (w/w) of EG to hexane was reached. Next, the curing agent was added and the solution was vigorously shaken by hand for 60 sec and sonicated for another 10 min. These solutions would remain stable for 10+ hrs without curing and were viscous enough to produce uniform films during spin-coating.

To fabricate the DEAs, a protective layer of PDMS was first spin-coated on cleaned glass slide at 1500 rpm for 120 sec, followed by vacuum desiccation for 10 min to remove air bubbles and baking on a hot-plate at 95 °C for 10 min. Without the protective layers, during later actuation of the device the current sparked across the electrode surfaces when the voltage was applied. The first electrode layer was deposited by spin-coating the PDMS/EG solution, over a stencil applied to the cured PDMS, at 1000 rpm for 120 sec. The stencil, which was cut from Scotch tape (3M) with the pattern shown in Figure 43, was then removed and the electrode layer cured at 95 °C for 6 hrs. The middle dielectric

layer was applied in two coats ^ξ, each of which were applied by spin-coating the PDMS at 1000 rpm for 60 sec, vacuum desiccating for 5 min, and baking at 95 °C for 10 min. The top electrode layers and the top protective coatings were applied in the same method as the first.

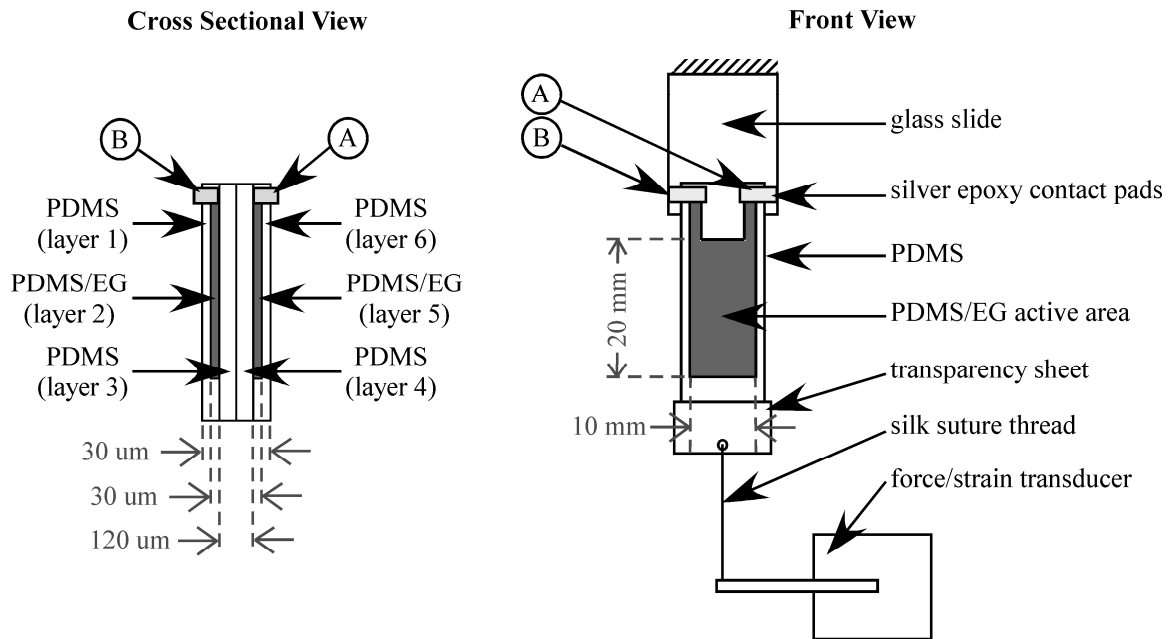


Figure 43. Schematic of a cross sectional view of a DEA sample and the DEA testing configuration.

The active area of the DEA (i.e. the area covered by PDMS/EG) was 10 mm wide and 20 mm long. The dielectric elastomer was 120 μm thick, the electrodes were each 30 μm thick, and the protective PDMS layers were also 30 μm thick. A schematic of a cross sectional view of the DEAs and the testing configuration used in this investigation are

^ξ PDMS was applied in two coats to assist the removal of trapped air during vacuum treatment.

shown in Figure 43. Electrical contact was made to the DEA by patterning two non-overlapping segments above the active electrode areas (labeled A and B in Figure 43). The DEAs were fully encapsulated, having a 1 mm edge of PDMS on either side of the active area to prevent sparking. One end of the sample (the fixed end) was glued to a 3" x 1" x 1.2 mm glass microscope slide (VWR, Cat No. 16004-424) using a photo-curable adhesive (Loctite® 3108). The other end (the moving end) was glued to a 16 mm long, 14 mm wide section of transparency sheet (3M CG3300). The glass slide was clamped, and the DEA was held vertically. Silk suture thread (CP Medical, 675S) was used to connect the sample to a force/strain transducer arm via a small hole drilled into the transparency sheet and a small hole at the tip of the arm.

Electrical connections to the devices were made by cutting through all 6 layers of the spin-coated DEA, across the non-overlapping areas discussed above, and then painting a conductive silver epoxy (Chemtronics, CircuitWorks CW2400) over the exposed electrode layers. The epoxy was then given 24 hrs to cure. Alligator clips were used to attach a high voltage power supply (UltraVolt, Inc.) to the devices.

A sample demonstrating the patternability of the PDMS/EG electrode material is shown in Figure 44. The PDMS/EG material was prepared in the same method described above using a stencil cut by hand from tape^ξ. The stencil was placed on the surface of a film of

^ξ Cutting stencils with a laser cutter or similar system would be easier and would allow smaller patterns to be realized.

cured PDMS, the PDMS/EG material was spin-coated over the stencil, and the stencil was removed. It can be seen that fairly complex shapes can be attained with relative ease, making this new material an excellent candidate as a replacement for CG electrodes.



Figure 44. PDMS/EG material patterned with “UMD compliant electrodes” showed at rest (left) and at 100% strain (right).

4.4 Electrical and mechanical characterization

The PDMS/EG compliant electrode material was mechanically and electrically characterized. Mechanical characterization of PDMS/EG samples was performed by applying a known strain, measuring the resulting stress, and calculating the Young’s modulus at 10% strain. Electrical characterization was carried out by applying a known strain, measuring the resulting change in resistance, and calculating the conductivity as a function of strain. DEAs were characterized by applying an electric field between the electrodes and measuring the resultant actuation strain.

Mechanical testing was performed using a force/strain transducer (Aurora Scientific Inc., model 3000LR) with a custom LabView program. A pre-stress of 75 kPa and a constant strain-rate of 0.1 mm/s were applied to all samples. Samples were strained from 0 to 30%, and back to 0%, 15 times, and the resulting stress was measured. For creep strain, a

pre-stress of 75 kPa was applied to the samples, and the resulting strain was recorded over a 10 hr period.

Electrical characterization was conducted using the 4-point probe technique in order to eliminate contact resistance. Four 2 mm wide strips of silver epoxy were patterned over PDMS/EG samples leaving 10 mm of spacing between the strips. An Autolab potentiostat/galvanostat (Eco Chemie, PGSTAT30) was used to apply a current of 0.001 A to the outermost electrodes, while a digital multimeter (Craftsman Professional, model no. 82324) simultaneously measured the voltage drop across the two innermost electrodes. Using Ohm's law, the recorded voltage drop was then converted to conductivity using measured sample geometries and the applied current.

Electro-mechanical characterization of DEAs was conducted by applying electric fields between 15 and 65 V/ μm , in 2.5 V/ μm intervals, and measuring the resulting actuation strain. All actuation strains were corrected by removing the creep strains. Electric fields were applied to the DEAs in frequencies of 0.011, 0.016, 0.025, 0.085, 0.11, 0.16, 0.25, 0.5, 1.0, 2.5, 5.0, and 10.0 Hz. Rise/relaxation times were calculated as the time required for the devices to reach 90% of their maximum/minimum actuation strains.

4.5 Results and discussion

4.5.1 Mechanical characterization of PDMS/EG composites

The Young's modulus, defined as the slope of the stress-strain curve at a particular externally applied strain, is an important material property for DEAs since it ultimately affects actuation strain and force: stiffer devices (high modulus) will have lower strains and higher forces; softer devices (low modulus) will have higher strains and lower forces. Example of stress-strain curves, from which the Young's moduli were derived, are shown in Figure 45a for the 15th strain cycle. A 20:1 PDMS/ 15wt% EG sample is compared to an unloaded 10:1 PDMS sample. The slope ξ for the PDMS/EG was somewhat smaller, corresponding to a modulus of 0.9 MPa, than that of the 10:1 PDMS, which had a modulus of 1.1 MPa. The low modulus of the composite is partially due to the greater 20:1 ratio of PDMS resin to cross-linking agent, and also to the formation of voids, which can be observed in Figure 46. The up-ramps (0 \rightarrow 30% strain) and the down-ramps (30 \rightarrow 0% strain) are indicated by the unfilled arrows. There was a greater separation between the curves, or hysteresis, for the PDMS/EG material.

For high performance applications, such as in micro-autonomous air vehicles (MAVs), actuators are required to provide reproducible driving and steering without loss of power or strain over time. Therefore, understanding the long-term strain behavior, or creep, of

ξ Modulus was measured as the slope of the stress-strain curve at 5% strain by fitting a linear line between 4% and 6% strain.

DEA elastomers is critical for such applications. Creep strains of the PDMS/EG material and of unloaded PDMS are shown in Figure 45b. Large creep strains are undesirable for DEAs because they result in non-repeatable actuation. The creep strain at 10 hrs for the PDMS/EG material is 3.6%, nearly double that of plain PDMS. However, compared to elastomers like VHB tape (3M), which can exhibit 100-300% strain over the same duration, the PDMS/EG material has almost no creep strain.

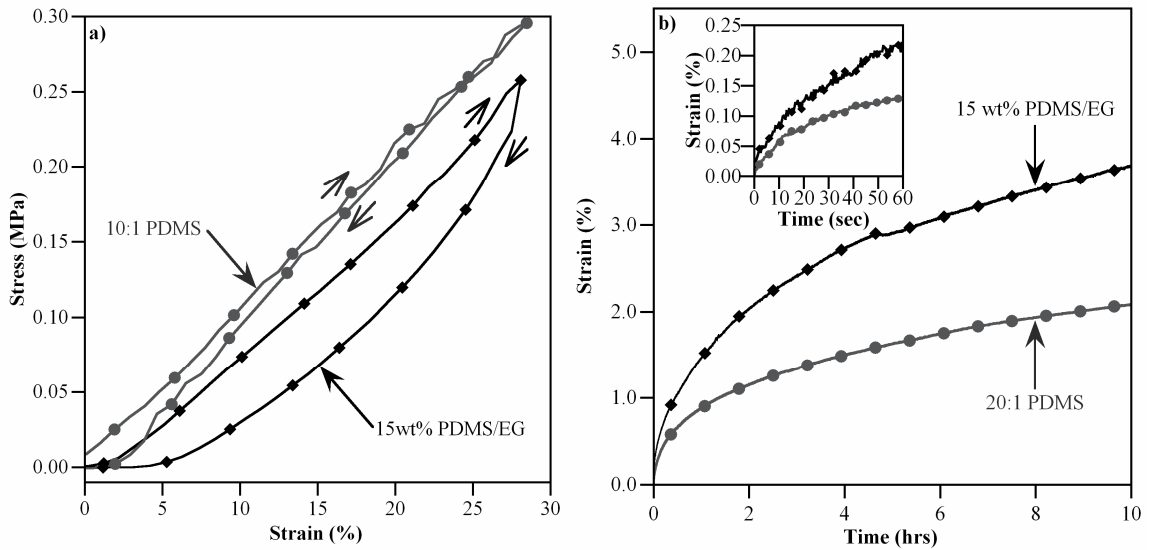


Figure 45. PDMS/EG compliant electrode material (black diamonds) compared to 10:1 PDMS (gray circles) in terms of a) stress vs. applied strain and b) creep strain vs. time.

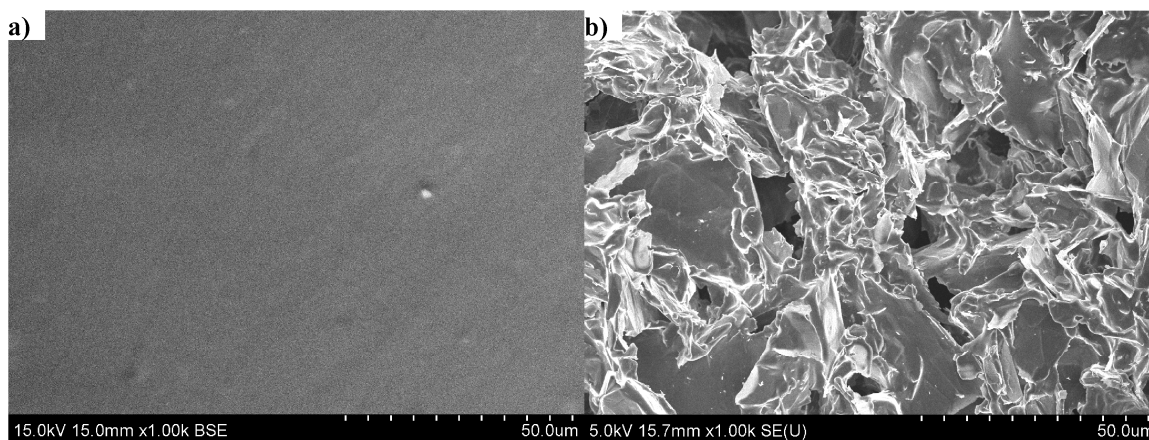


Figure 46. SEM images at 1000 times magnification of a) unloaded PDMS, and b) 15 wt% PDMS/EG with voids present.

4.5.2 Electro-mechanical characterization of PDMS/EG composites

For high performance DEAs, it is also important that the compliant electrode remains both elastomeric and conductive when subjected to repeated strain cycles. The conductivity and Young's modulus of the PDMS/EG composite is plotted in Figure 47 as a function of strain cycle number. The conductivity (lower curve) was on the order of 0.15 S/cm and increased a little with increasing strain cycle number. (Conductivities as high as 0.44 S/cm were obtained with samples containing 25 wt% EG. However, these samples were brittle, having a low ultimate tensile strain, and were therefore not used in this investigation.) The conductivity was actually higher under strain than fully relaxed, reaching a maximum between 20% and 30% strain for all samples ^ξ.

^ξ Conductivity results as a function of strain can be found for additional EG loadings in [167].

The Young's modulus (upper curve) of the PDMS/EG was 1 MPa in the first strain cycle and dropped slightly to 0.9 MPa by the 15th strain cycle, indicating a softening of the material. In our experience, unlike CG, the PDMS/EG electrode properties improved over time, further promoting the replacement of conventional CG electrodes with this new material.

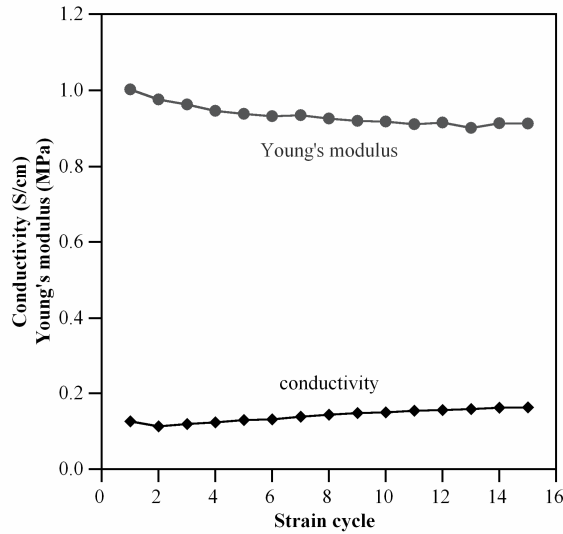


Figure 47. Conductivity (black diamonds) and Young's modulus (gray circles) vs. strain cycle for the PDMS/EG electrode material.

Increasing conductivity during repeated strain cycling has been reported previously for a variety of conductive-filler/insulating-host composites [112, 134, 137, 165]. It has been hypothesized that the formation of additional conductive pathways through the material, by removal of matrix material between the EG particles, may be the cause for such behavior [112].

4.5.3 Electro-mechanical characterization of DEAs

The achievable actuation strains determine which applications are possible. The actuation strains for a DEA with PDMS/EG electrodes are shown in Figure 48a at electric fields of 15, 17.5, and 20 V/ μm . Recall that these actuators were not pre-strained, so the data cannot be directly compared with results for pre-strained PDMS devices. The raw actuation strain (upper gray line) was corrected by removing the creep strain (middle black line) to produce the actuation strain (lower black line).

Corrected actuation strains are plotted in Figure 48b as a function of applied electric field for DEAs with PDMS/EG electrodes and a 20:1 PDMS dielectric layer and for DEAs with CG electrodes and a 10:1 PDMS dielectric layer ^ξ. It can be seen from the data in Figure 48b that the actuation strains were identical for both electrode materials and followed the expected quadratic dependence on field. At 50 V/ μm , the strain reached 1.2%. However, the DEAs with PDMS/EG electrodes could be encapsulated in PDMS, which allowed higher electric fields to be applied before device failure: 65 V/ μm versus 50 V/ μm . Because the actuation strain in DEAs depends on the square of the electric field, this 30% increase in voltage led to a three-fold increase in strain, which reached 3.5% at 65 V/ μm . These findings further support the replacement of CG with the PDMS/EG composite for DEA electrodes.

^ξ Measured dielectric constants of the 10:1 and 20:1 PDMS elastomers were similar, ranging between 2.3 and 2.8, and were assumed to have a small impact on the actuation of the DEAs.

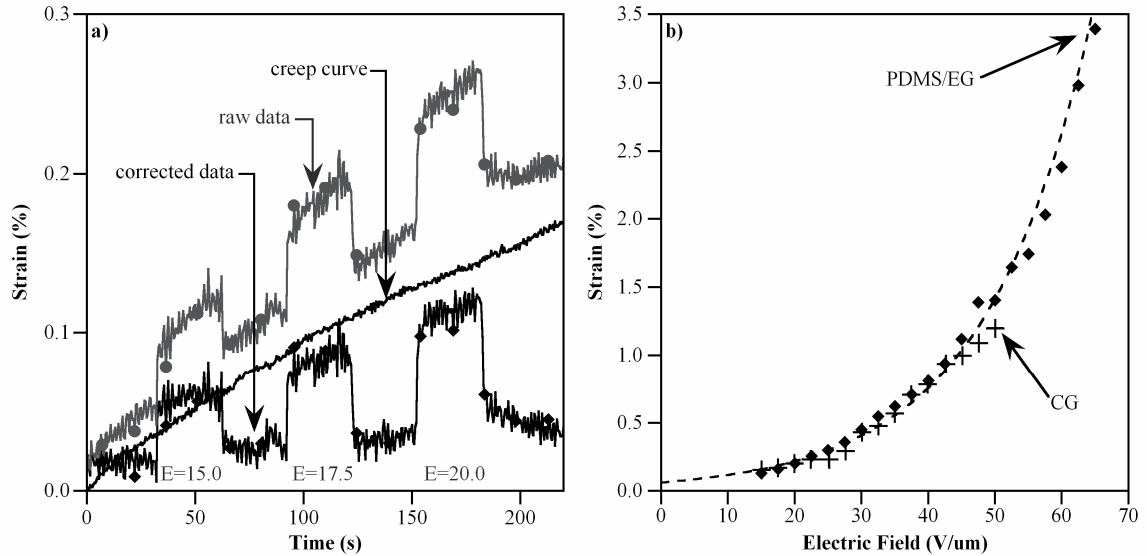


Figure 48. a) Actuation strains of a DEA made with PDMS/EG electrodes (black line marked by diamonds) vs. time under applied electric fields of 15, 17.5, and 20 V/ μm . The actuation strain was found by removing the creep strain from Figure 45b (middle solid line) from the raw data (gray line marked by circles). b) Actuation strain vs. electric field of PDMS/EG (diamonds) compared to the strain in a DEA with CG electrodes (crosses). The dashed line is a guide for the eye.

Aside from large actuation strains, the ability of a DEA to quickly respond to the application or removal of an applied electric field is important for applications like flapping-wing MAVs. The actuation strains of DEAs with PDMS/EG electrodes and CG electrodes are shown in Figure 49a under an electric field of 50 V/ μm over a 30 sec duration. The corresponding rise and relaxation times were calculated to be 0.49 and 1.04 sec for DEAs with PDMS/EG electrodes and 0.48 and 1.09 sec for DEAs with CG electrodes. The softer DEAs with PDMS/EG electrodes achieved greater actuation strains at this electric field, as expected, with rise/relaxation times that were nearly identical to DEAs with CG electrodes. One can therefore conclude that the PDMS/EG electrodes do not slow down the response times.

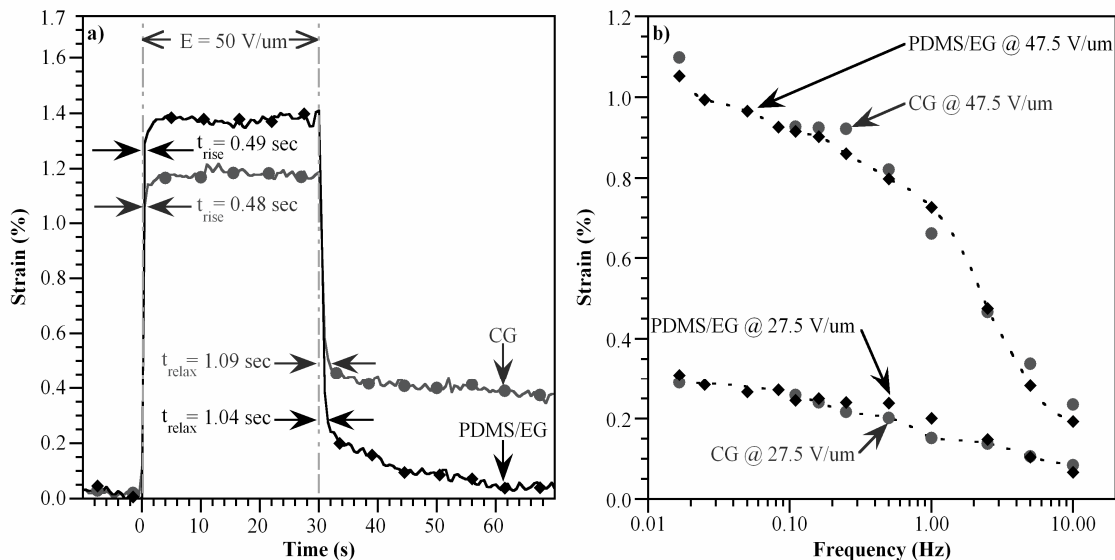


Figure 49. a) Actuation strains of DEAs made with PDMS/EG electrodes (diamonds) and CG electrodes (circles) vs. time under an electric field of 50 V/ μ m showing the corresponding rise and relaxation times. b) Actuation strains vs. frequency under electric fields of 27.5 and 47.5 V/ μ m showing the fall-off of the actuation strains with increasing frequency. The dotted lines are guides for the eye.

The actuation strains for DEAs with PDMS/EG electrodes and DEAs with CG electrodes are shown in Figure 49b as a function of frequency. Electric fields of 27.5 and 47.5 V/ μ m were applied at frequencies between 0.01 and 10 Hz. Similar to the results in Figure 48b, the actuation strains were nearly identical for both electrode materials, and for both the actuation strains begin to decline at a frequency of 1 Hz.

4.6 Conclusion

A novel compliant electrode material was developed composed of PDMS loaded with EG produced by microwave irradiation. At a 15 wt% loading of EG, the compliant electrode exhibited a conductivity of 0.15 S/cm and a Young's modulus of only 0.9 MPa. This

modulus is the lowest reported for two-phase composites consisting of a conductive filler and an insulating polymer matrix. Un-prestrained DEAs fabricated with PDMS/EG electrodes exhibited actuation strains as high as 3.45% at 65 V/ μm . Results from this investigation have demonstrated that PDMS/EG is superior to CG in the following ways: 1) during fabrication, it has the benefit of being castable, spin-coatable, and patternable; 2) it will not smear or rub off; 3) because it does not dry out over time like CG, its conductivity and modulus are steady over time; and 4) because it can be completely encapsulated in additional protective PDMS layers, higher electric fields can be used, which yields larger actuation strains.

4.7 Acknowledgements

This research was supported by the US Army Research Laboratory under the MAST CTA program. We would like to thank Dr. Michael Fuhrer and Alexandra Curtin from the Physics Department at the University of Maryland for assistance with materials development, and Michael Hnatow from HiTechTrader (www.HiTechTrader.com) for donating a tube furnace used in the materials development process for this research. We would also like to thank Santa Fe Science and Technology, Inc. for their kind donation of the force-strain transducer and the custom Labview software.

Chapter 5: Paintable elastomeric strain sensors: Characterization and application

Sensors and Actuators, full article, draft

M. Kujawski¹, K. Miller³, T. Neumann³, C. Elder², O. Dear², and E. Smela^{3*}

¹Dept. of Materials Science and Engineering, University of Maryland, College Park, MD 20742

²Dept. of Civil Engineering, Lawrence Technological University, Southfield, MI 48075

³Dept. of Mechanical Engineering, University of Maryland, College Park, MD 20742

*smela@eng.umd.edu; tel: 301-405-5265; fax: 301-314-9477

5.1 Abstract

This paper characterizes the performance of electrically conductive and mechanically compliant composites as strain sensors and demonstrates their application in structural health monitoring and tactile sensing. The composites were fabricated by blending exfoliated graphite (EG) into either polyisoprene (latex) or polychloroprene (neoprene) host rubbers, and they were applied to various surfaces by either brush painting or airbrushing. Their electrical and mechanical properties were determined as functions of strain, temperature, humidity, and EG loading. Composites had conductivities between 0.004 and 0.03 S/cm and tangent moduli of less than 5 MPa at 5% strain for EG loadings up to 10 wt%. Compared to carbon black filled composites, the conductivities are orders of magnitude higher^[111, 156] and the percolation threshold is lower^[156]. The dependence of resistance on temperature was small between -50 °C and +50 °C ($-6 \times 10^{-3}/^{\circ}\text{C}$ or lower), and the resistance increased 10-20% between 30% and 70% RH. These effects were dwarfed by the increase of resistance with strain. At strains $< 0.2\%$ the gauge factor was

linear. The composites were applied to measure the deformation of a ½ scale concrete bridge beam as it was loaded to failure and as contact sensors on a glove.

5.2 Introduction

A variety of strain gauge materials and devices are commercially available, the most common of which are the metallic foil types. Metallic foil strain gauges are limited to measuring strains smaller than 5% ^[168], have gauge factors (GFs) less than 5.5 ^[1], and are unable to conform to non-flat surfaces. Other strain sensors, such as the piezoelectric and piezoresistive types, have been reported having GFs as high as 1000 ^[1, 3], but they are typically limited to strains of less than 1% ^[1, 3, 4]. Furthermore, commercial sensors typically have dimensions on the order of 50 mm²; such a small sensor size leads to the requirement for numerous sensors when monitoring large areas. Therefore, a need exists for an alternative strain gauge that is easily applied and that can be patterned into custom shapes and sizes.

Nano-composites consisting of host polymers blended with conductive filler particles like carbon nanotubes (CNTs) are an attractive alternative to commercial sensors and have previously been used for strain gauge applications ^[80, 169]. Host materials are typically rigid polymers, such as epoxies, which cannot withstand large strains. Use of elastomeric hosts allows larger strains ^[117, 151, 170]. Previously, we have demonstrated PDMS blended with exfoliated graphite (EG) having high conductivity and low moduli as compliant electrodes ^[167]; however, these composites were not paintable. Following up on our

previous work, latex elastomers were used as the host material, producing elastomeric composites for sensing applications that are paintable.

In the present work, changes in elastomer/EG composite resistance is investigated for strain gauge applications as a function of strain, temperature, and filler particle loading. Both mechanical and electrical properties of the composites are characterized. We show that the advantages of these composites include higher GFs (ranging from 2 to 27,000), ease of application (by brush painting or spray painting), and ability to produce a range wide of desired shapes and sizes.

5.3 Experimental

5.3.1 Composite formulation

Nanocomposites were prepared by blending electrically conductive EG particles with an electrically insulating host elastomer. Acid-washed graphite particles (Asbury Graphite Mills, Inc.) were exfoliated using microwave irradiation (Kenmore, $P = 1100$ W, $f = 2.45$ GHz) in an atmosphere of forming gas (97% nitrogen, 3% hydrogen). Any remaining unexfoliated graphite was removed by stirring the irradiated powder into hexane, in which the lighter EG particles floated and could be skimmed off. The filtered EG particles were added to fresh hexane (1:120 w/w) and bath-sonicated (Branson 1510, 40 kHz) for 3 hours to further exfoliate them; during this process they became suspended in the solvent. The hexane was removed by placing the solution on a hotplate at 150 °C overnight. (See ^[167] for more details on the exfoliation process.)

Liquid suspensions of the strain gauge material were prepared by adding together in a 20 mL glass vial 0.1 g of EG, 3 g of a solution containing 0.75 wt% Triton® X-100 (Sigma Aldrich), and 6 mL of deionized (DI) water. The surfactant was required to blend the hydrophobic EG with the hydrophilic elastomer. (In our prior work, surfactants were not required because PDMS is hydrophobic.) To neutralize acid remaining in the EG and to prevent the elastomer from forming clumps, 0.4 g of NaOH (1 N) was then added to the solution. Finally, 0.4 g Antifoam SE-15 (Sigma Aldrich) was added. The solution was vortex-mixed (Fischer Scientific) at 3000 rpm for 20 sec, followed by bath-sonication for 1.5 hrs. Either liquid latex (Environmolds, RD-407 Mask Making Latex) or polychloroprene (neoprene) rubber (Critical Coatings, LLC., CC1103F Mask Making Neoprene) was then added to the vial to produce latex/EG composites at the desired loading. The solution was vortex mixed for 30 sec prior to use.

5.3.2 Sample fabrication

Mechanical and electrical characterization were conducted using the latex composites with EG loadings of 6, 7, 8, 9, and 10 wt%. The percolation threshold, or lowest EG loading rendering the composites electrically conductive, was 4 w%; however, 4 and 5 wt% composites were omitted from this investigation because their resistance went above 40 M Ω when they were strained. At loadings above 10% the strain sensitivity decreased, and above 30% the films became brittle.

Samples for characterization were fabricated by airbrushing (Badger Air-Brush Co., Model # 250-4), at an air pressure of 25 psi and a working distance of 200 mm, an

average of 5 thin layers of the latex/EG suspension over a glass slide that had been cleaned with acetone. Each layer was dried on a hotplate at 80 °C for 2 minutes before applying the next layer. Samples were cut into strips 20 mm long and 5 mm wide. When removed to be mounted to substrates for measurements and sample fabrications, the samples readily peeled off of the glass slides. Sample thicknesses (average of three points across one sample) were 60, 30, 15, 30, and 95 μm for the 6, 7, 8, 9, and 10 wt% samples, respectively, determined using mechanical profilometry (Dektak³ ST). Since the airbrushing was done by hand and since the viscosity of the suspension depended on loading, the film thicknesses varied. (The amount of EG in the water/surfactant solution was held constant at 0.1g, so suspensions with lower EG loadings had a greater concentration of elastomer). The conductivities ranged from 0.004 S/cm for 6 wt% composites to 0.03 S/cm for 10 wt%; these values are similar to those of PDMS/EG composites. (We have made 20 wt% latex/EG composites with conductivities > 12.5 S/cm by processing 15 g EG with 900 ml of a DI water solution containing 0.75 wt% Triton X-100 for 30 min using a horn sonicator (Q-sonica Inc., model #S-4000-001) with a 1" probe tip and booster.) The conductivity σ was determined from the sample resistance R and dimensions using $\sigma = L/(Rwt)$, where L is the sample length, w the width, and t the thickness. Conductive silver epoxy (Chemtronics, CircuitWorks CW2400) having a volume resistivity < 0.001 Ohm-cm^[171] was used to form contact pads for the placement of the multi-meter probe tips.

For stress-strain measurements, the latex/EG samples were peeled off of the glass slide and attached at one end onto another glass slide (75 mm x 25 mm x 1.2 mm, VWR, Cat

No. 16004-424) using a photo-curable adhesive (Loctite 3108). The other end of the sample was similarly attached to a 10 mm x 10 mm x 110 μ m piece of a transparency sheet (3M, CG3300). This configuration left a 10 mm long, 5 mm wide section in the center of the sample that was free to stretch. The glass was clamped vertically to allow the latex/EG and the transparency to hang downward. The transparency sheet was attached to the transducer using a silk suture threaded through a small hole at the bottom of the transparency and another small hole at the tip of the transducer arm. Testing was performed at room temperature, approximately 20 °C, unless otherwise stated.

5.3.3 Temperature-resistance measurements

Samples were prepared by cutting airbrushed latex/EG sheets into 10 mm long and 5 mm wide strips. One end only of each strip was attached to a 75 mm x 50 mm x 1.2 mm glass slide using silver epoxy, and the epoxy was cured. The free ends of the strips were then strained manually and fixed to the glass slide using silver epoxy, locking them in place at the desired strains. For each EG loading, seven strips with strains ranging from 0-30 % in 5% increments were prepared, as shown in Figure 50.

The temperatures of +50 and -50 °C were achieved using a hotplate oven (Thermolyne Co., model 0V-10600) and an ultra-low freezer (So-Low, model CH 43-5), respectively. Temperatures of 0 and -20 °C were achieved using a refrigerator/freezer (Kenmore, model 183.93972). To prevent ice formation from the condensation of moisture upon inserting the samples from the freezers, a glass slide was placed on top of the samples, the sandwich was vacuum desiccated for 30 min, and the edges were sealed using photo-

curing adhesive (Loctite 4108). (Ice would otherwise form under the samples, causing them to bulge and imposing a small additional strain, and the moisture from the freeze/thaw cycles would also cause the epoxy to release from the glass substrate.)

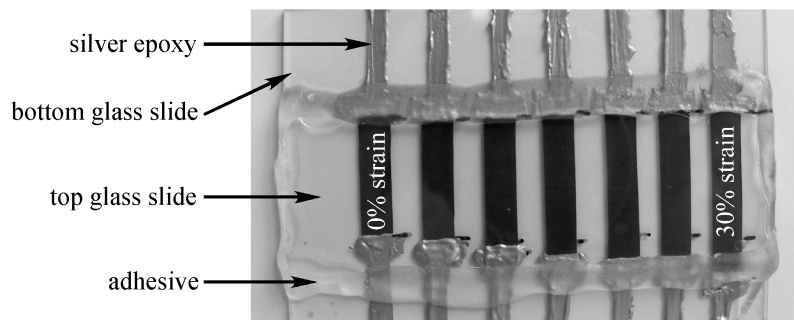


Figure 50. Sample configuration for temperature dependence measurements.

5.3.4 Temperature-humidity measurements

The relationship between humidity and elastomer conductivity was investigated by resistance measurements in an atmosphere of controlled relative humidity (RH) at a temperature of 22 ± 1 °C. RH levels ($30 \pm 2\%$, $50 \pm 2\%$, and $70 \pm 2\%$) were measured with a digital temperature/humidity indicator (Envirocaire, model # E10). Samples were given a minimum of 1 hour to equilibrate at each RH. The RHs were achieved by a bubbling compressed air through a beaker of water. Desired RHs were reached by controlling the compressed air flow rate.

Samples were prepared by cutting airbrushed latex/EG sheets into 10 mm long and 5 mm wide strips. One end only of each strip was attached to a 75 mm x 50 mm x 1.2 mm glass slide using silver epoxy, and the epoxy was cured. The free ends of the strips were then strained manually and fixed to the glass slide using silver epoxy, locking them in place at

the desired strains. For EG loadings of 8 and 10 wt%, strips with strains of 0 and 30% were prepared in triplicate for each loading.

5.4 Results and Discussion

5.4.1 Characterization of latex composites

Because the resistance of elastomeric/conductive filler composites changes with strain, these materials can be used for strain sensing. For applications such as structural health monitoring, these sensing elements may be exposed to a wide range of temperatures, and little information on the temperature sensitivity has been published. For applications in robotics, high sensitivity may be required, and for smart textiles or small autonomous vehicles, compliance may be critical. To determine the suitability of the elastomer/EG composites for various applications, their stiffness at strains up to 30% (tangent modulus) and sensitivity (gauge factor) were determined as functions of EG loading in latex. (The Young's modulus is the slope of the stress-strain curve in the range of strain for which Hook's law is valid, and represents the elastomer stiffness. For larger strains, Hook's law is no longer valid, as evidenced by a nonlinear stress-strain curve, and the slope of the stress-strain curve at a particular strain is defined as the tangent modulus.) Also, resistance was measured at temperatures between -50 °C to +50 °C at strains between 0 and 30%.

5.4.2 Young's modulus as a function of EG loading

If the strain sensor has a low stiffness, it will not interfere with the deformations being monitored. This can be useful when making measurements on thin films and structures, such as the wings of micro-air vehicles. Dynamic stress-strain measurements were conducted using a force/strain transducer (Aurora Scientific Inc., model 3000LR) to apply strains of up to 30% at a rate of 0.01 mm/s, and to measure the resulting forces, which were converted to stress based on the sample dimensions and the strain. Tangent moduli were obtained from the slopes of the stress-strain curves at 5% strain by fitting a line to the data between 4% and 6% strain and calculating the slope.

The tangent moduli of latex/EG composites are plotted in Figure 51a as a function of EG loading. As predicted by the Guth^[140] equation (see below) the composite stiffness increased with EG loading. The moduli increased from 2 MPa for the 6 wt% samples up to 5 MPa for the 10 wt% samples. Despite the increase in stiffness, the moduli remained low in all cases, so the elastomeric properties of the host were maintained. A typical stress-strain curve for unloaded latex is compared to those for 6 and 10 wt% latex/EG composites in Figure 51c.

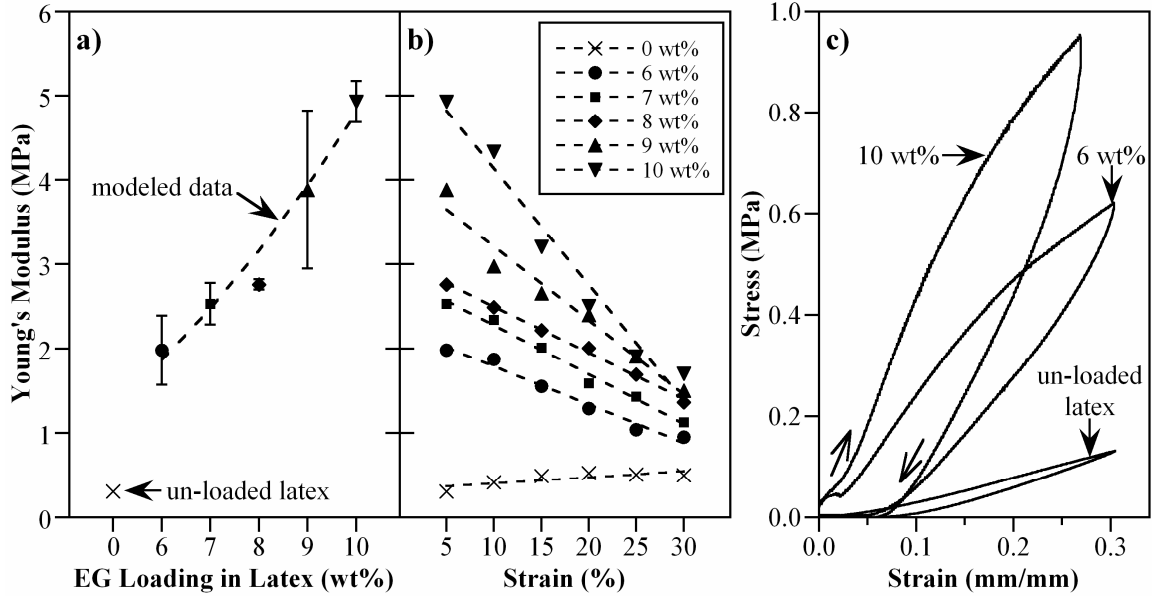


Figure 51. a) Young's moduli of latex/EG as a function of EG loading. Each point represents an average of two samples, and the standard deviations are indicated. The dashed line shows the Guth model. b) Young's moduli as a function of strain (dashed lines are linear guides for the eye). c) Stress-strain curves for latex and for 6 and 10 wt% latex/EG composites.

The well known Guth^[140] equation relates composite stiffness to filler particle aspect ratio and loading:

$$\text{Eq. 17} \quad E = E_0(1 + 0.67fc + 1.62f^2c^2),$$

where E is the modulus of the composite, E_0 is the modulus of the unloaded elastomer, f is the filler particle aspect ratio (diameter/thickness), and c is the filler concentration (vol%). Values from the Guth^[140] equation Eq. 17 are represented by the dashed line in Figure 51a. The best fit (smallest least squares error) between experimental and calculated values was obtained using an EG aspect ratio of 65, which is within the range of 20^[172] to 300^[173] reported for EG, and assuming densities of 2.2^[174] and 0.94 g/cm³^[175] for EG and latex, respectively. The average particle diameter (Figure 52) and

thickness were determined from SEM images. Because the diameter and thickness of the particles could not both be obtained for the same particle, the EG particle aspect ratio was calculated as the ratio of the particle diameter to the particle thickness, using a particle diameter of $2.9 \mu\text{m} \pm 3.5 \mu\text{m}$ (average of 58 particles) and thickness of $46.7 \text{ nm} \pm 78.5 \text{ nm}$ (average of 12 particles).

The stress-strain curves of elastomers are nonlinear^[101]. Figure 51b plots the tangent moduli of the composites at increasing strains. Whereas the modulus of unloaded latex increased from 0.3 MPa at 5% strain to 0.6 MPa at 30% strain (strain hardening), the modulus of the composites instead dropped. Decreasing stiffness with strain has been observed previously in similar composite systems^[176].

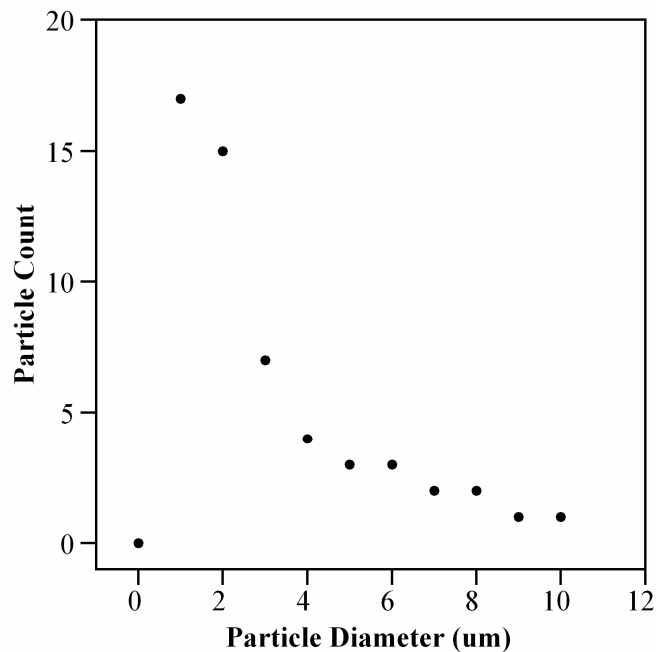


Figure 52. Particle count as a function of particle diameter for EG particles.

5.4.3 Resistance as a function of strain

In some applications it may be beneficial having sensors capable of measuring small displacements ($\leq 2\%$) with a high resolution ($\geq 0.0001\%$), such as the daily thermal expansions and contractions of a bridge deck. In other applications it may be beneficial to measure large displacements ($\geq 2\%$) with lower resolution ($\geq 0.1\%$), such as roadway crack propagation over time. The sensitivity is characterized by the gauge factor, GF [177].

$$\text{Eq. 18} \quad \text{GF} = (\Delta R/R_0)/\varepsilon,$$

where ΔR is the change in resistance, R_0 is the initial resistance, and ε is the strain. The force/strain transducer was used to apply strains up to 30% at a rate of 0.01 mm/s while the resistance was measured with the two-point probe technique (Craftsman Professional digital multi-meter model no. 82324, 1 Hz sampling rate).

The $\Delta R/R_0$ of 6, 8 and 10 wt% latex/EG composites are plotted as a function of strain in Figure 53. The $\Delta R/R_0$ increased with strain, as determined by least squares fitting. At 30% strain, the GFs were 1040, 570, and 160 for the 6, 8, and 10 wt% samples, respectively.

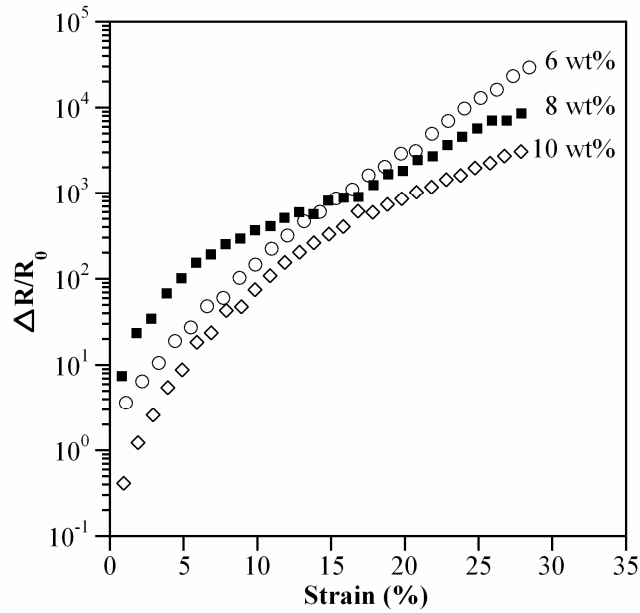


Figure 53. Gauge factor as a function of strain for latex/EG composites with three EG loadings strained at a rate of 0.1 mm/s.

The increase in resistance with strain is expected based on percolation theory ^[17, 18].

Insulating host/conductive filler composites become conductive when the filler concentration reaches the percolation threshold, at which conductive pathways are formed through the composite. Thereafter, the conductivity increases exponentially with increasing filler particle concentration until it begins to saturate ^[178]. Under strain, the distance between filler particles increases ^[179, 180] and conductive pathways are lost, resulting in an exponential decrease in the conductivity (or exponential increase in resistivity, similar to the data in Figure 53).

At strains below 15%, the 8 wt% samples exhibited an anomalously higher GF than the other loadings: the GF at 1% strain for the 6, 8, and 10 wt% samples were 0.8, 9.3, and 0.4, respectively. However, GFs are calculated using resistance, not resistivity.

Therefore, they are sample-specific numbers, not material properties, and higher GFs are obtained for smaller cross-sectional areas or greater lengths. (The anomalously high values at low strain for the 8 wt% composites are currently under investigation.) Thus, one 10 wt% sample, having an initial resistance of 24 k Ω , was strained to 105% and allowed to equilibrate for 10 min, after which its resistance was 680 M Ω , an increase of 28,000. (This corresponds to a gauge factor of 27,000 using Eq. 0, to our knowledge the highest ever reported, although it must be borne in mind that GFs are geometry-dependent.)

Many sensor applications are cyclic, such as those found on robotic end effectors, and require repeatable feedback with little deviation from cycle to cycle. Figure 54a plots the resistance as a function of time for a 6 wt% latex/EG composite subjected to 5 strain cycles from 0 to 5% at a strain rate of 0.01 mm/s. (Switching the transducer direction from the forward cycle to the reverse cycle was performed by hand, and therefore the cycle durations are not exactly 45 sec.) One sample at each loading was tested for this experiment, and the results for the 6 wt% loading are presented; results for the other samples were similar. The baseline resistance at 0% strain was 0.39 M Ω and was consistent throughout the test. When the sample was strained to 5%, the peak resistance was higher for the first (1.14 M Ω) and second (0.94 M Ω) cycles, after which it remained stable at 0.85 M Ω . The nonlinear, asymmetric resistance data are attributed to the composite hysteresis observed in Figure 51. The GF of this particular sample was 23. This repeatability of the resistance response is sufficient for many strain gauge applications ^[181].

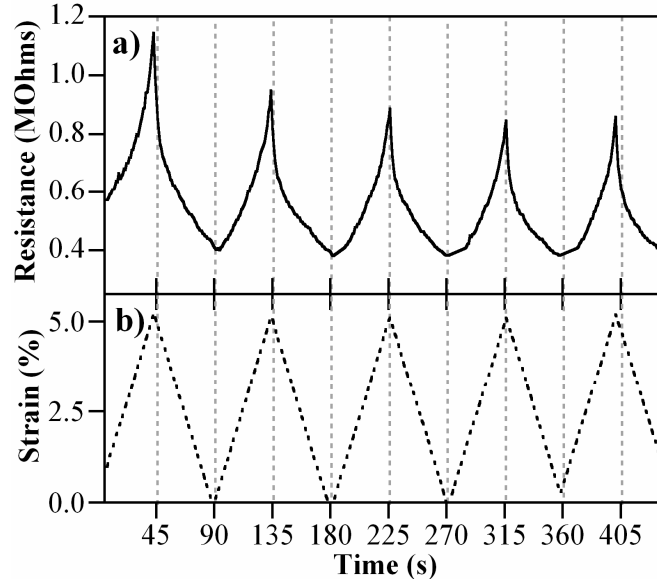


Figure 54. a) Resistance (solid line) vs. time for a 6 wt% latex/EG composite cycled 5 times b) from 0 to 5% strain (triangle wave).

5.4.4 Resistance as a function of temperature

Environmental effects on new strain gauge materials are often unreported. The resistance of the latex/EG composites was measured at temperatures of -50, -20, 0, +20, and +50 °C via the two-point probe technique (digital multi-meter Tektronix DMM 4050). Samples were allowed to equilibrate at each temperature for ten minutes before measurements were taken, and a minimum of three samples at each loading and strain (see section 5.3.3) were tested. Above 20% strain, the resistance of the most lightly loaded 6 wt% composites, which had the greatest strain sensitivity, exceeded 1.2 GΩ and could no longer be measured.

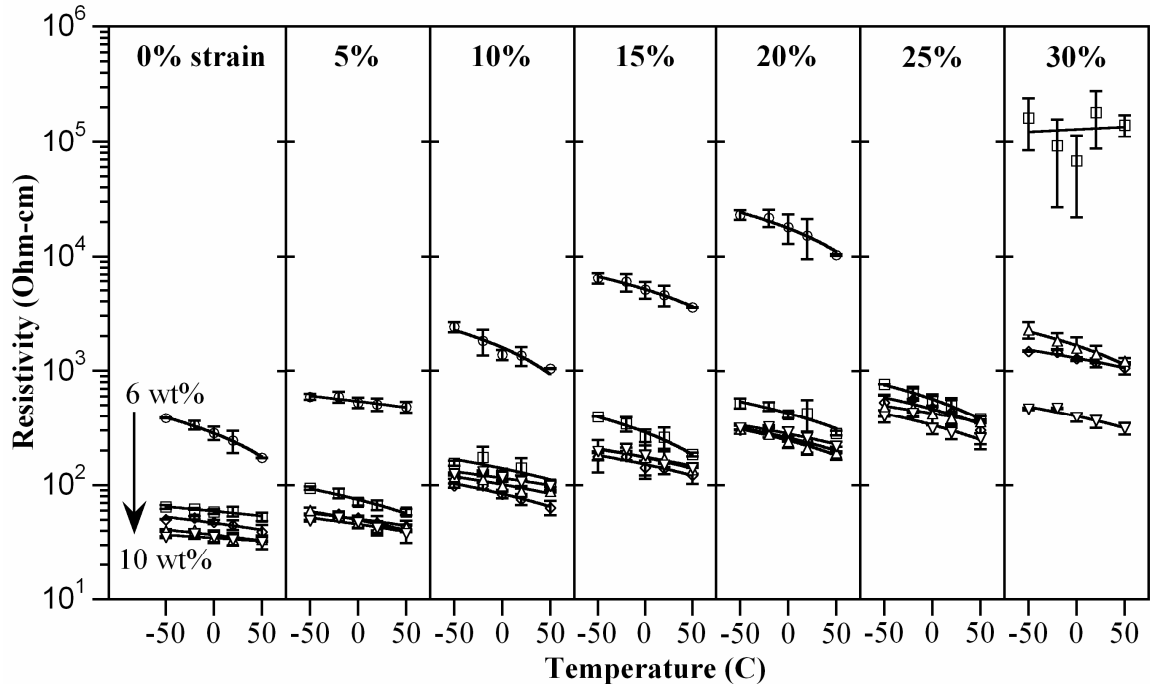


Figure 55. Resistivity vs. temperature for latex/EG composites at increasing strains. Each point represents the average of 3 samples. EG loadings were 6 wt% (circles), 7 wt% (squares), 8 wt% (diamonds), 9 wt% (triangles-up), and 10 wt% (triangles-down).

The resistivity of the composites decreased somewhat with temperature, by at most a factor of 2 over the 100°C range. There was a jump from the 6 wt% sample, which decreased by a factor of $-5.5 * 10^{-3}/^{\circ}\text{C}$, to the higher loadings, which decreased by smaller factors, between $-1 * 10^{-3}/^{\circ}\text{C}$ and $-2 * 10^{-3}/^{\circ}\text{C}$. Although the magnitude of the decrease in resistance with temperature is of the same order as for metallic foil strain sensors ^[1], the resistance of the foil sensors typically increases with temperature ^[182-184]. While rare, decreasing resistance with temperature has been reported in resin, cement, and elastomer composites with carbon fillers ^[185, 186].

5.4.5 Resistance as a function of humidity

Understanding how humidity affects the strain gauge conductivity is important because these sensors must function in changing environmental conditions. The resistance of the latex/EG composites was measured at humidities of 30%, 50%, and 70% via the two-point probe technique (digital multi-meter Tektronix DMM 4050). The resistances of the composites were normalized to their values at 30% RH (166 k Ω for 8 wt% at 0% strain, 425 k Ω for 8 wt% at 5% strain, 23 k Ω for 10 wt% at 0% strain, 34 k Ω for 10 wt% at 5% strain) and the results are plotted in Figure 56.

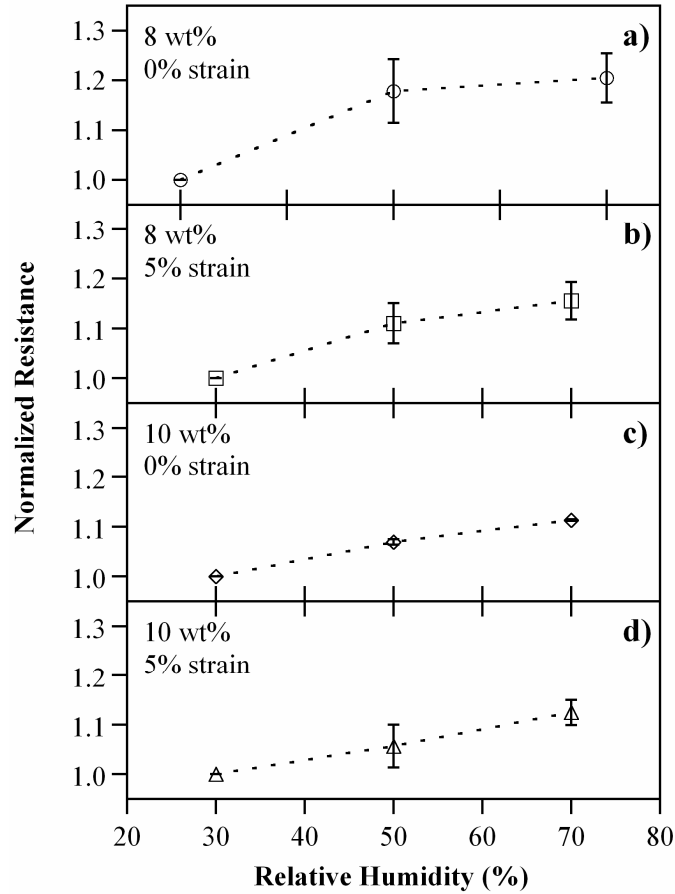


Figure 56. Normalized resistance as a function of relative humidity for a) 8 wt% latex/EG composites at 0% strain, b) 8 wt% latex/EG composites at 5% strain, c) 10 wt% latex/EG composites at 0% strain, and d) 10 wt% latex/EG composites at 5% strain. The dotted lines are guides for the eye.

The resistance of the composites increased 10% - 20% with humidity. This increase has been observed in other polymer composites^[187-189], but the mechanism for it is still not fully understood. The sensitivity of the composites was unaffected, but accurate measurements of strain would require calibration with an unstrained reference sensor.

5.5 Applications of the composites as sensors

5.5.1 Tactile sensor application

For prosthetics and robot grippers, tactile sensors can provide feedback on when contact has been made, as well as on the gripping force. To determine the effectiveness of the composites as tactile sensors, meandering traces were patterned onto the fingertips of a nitrile glove, shown in Figure 57. A 20 wt% neoprene solution was airbrushed in a single layer onto the glove through a masking tape stencil, which was removed after airbrushing, to produce the serpentine geometry. The thickness of the sensor was approximately $30 \pm 10 \mu\text{m}$ measured by profilometry (Dektak³ ST). Neoprene was chosen as the host elastomer instead of latex because it is tougher and has good resistance to wear. Silver epoxy was used to form electrical connections. Before the epoxy cured, 200 mm long strips of fine stainless steel wire (43 gauge, California fine Wire Co.) were pressed into the epoxy. After curing the epoxy for 24 hrs at room temperature, the free ends of the wire leads were connected to a multi-meter (Craftsman Professional digital multi-meter model no. 82324) using alligator clips. Electrical tape was used to secure the wire leads to the back of the glove, preventing them from being torn out of the silver epoxy during testing. The fabrication process took approximately 10 minutes for each sensor, excluding drying times (samples were cured overnight at room temperature before testing).

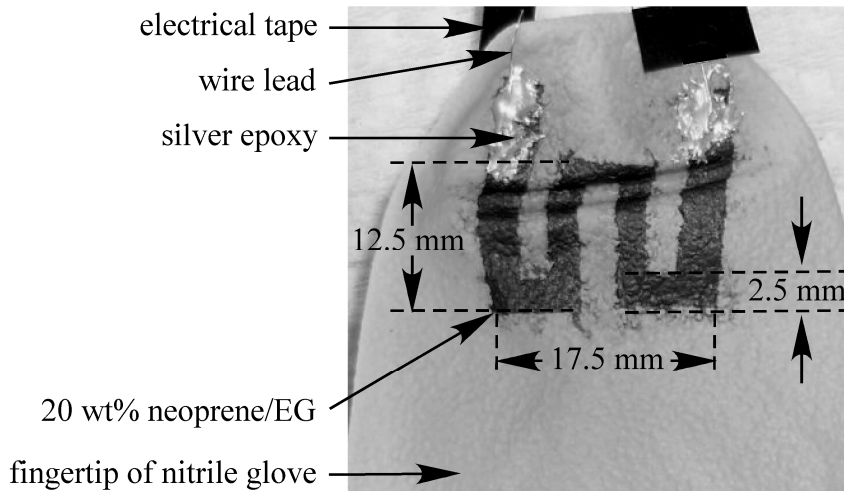


Figure 57. Image of a 20 wt% neoprene/EG tactile sensor patterned via airbrushing onto a nitrile glove.

Upon gripping an object with the glove, the sensor resistance increased as shown in Figure 58a-b. While it might be assumed that the pressure would reduce the interparticle separation in the out-of-plane direction and produce a decrease in the resistivity, the material instead behaved in the same way as when it was stretched. One can speculate that this is because a compression out of plane results in an inplane expansion, raising the inplane resistance, which was the direction in which it was measured. Increasing resistance with pressure has been observed for composites with carbon filler particles^[190, 191], but further experimentation is required to understand the mechanism.

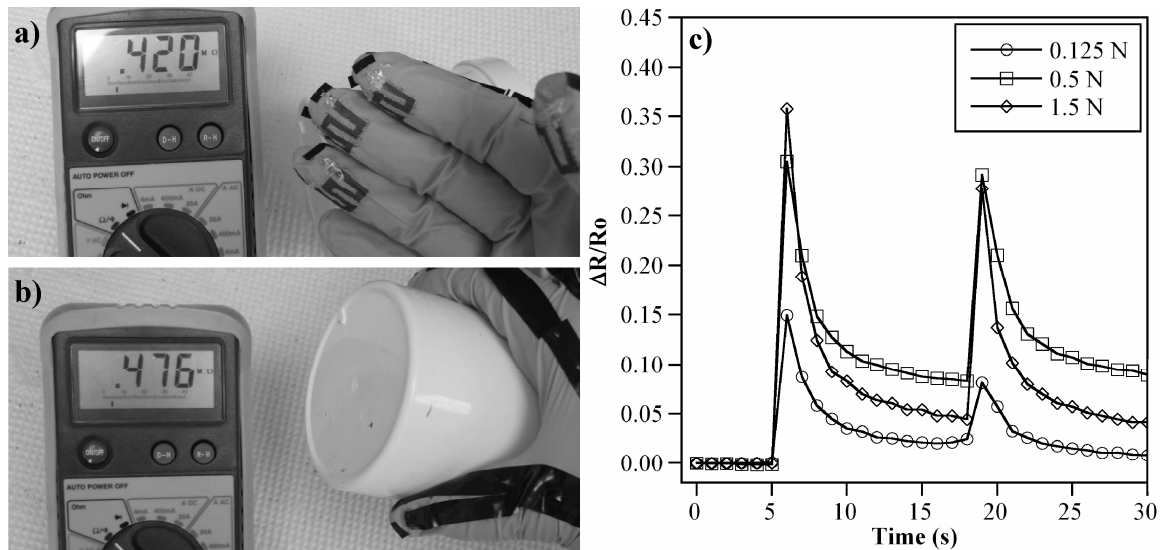


Figure 58. Neoprene/EG tactile glove sensor. a) Resistance at rest. b) Resistance when gripping an object. c) Normalized resistance $\Delta R/R_0$ vs. time under applied forces.

With the glove lying flat on the benchtop, forces of 0.125, 0.5, and 1.5 N were applied for one second by placing weights on the sensor areas; the time between applying the weights was 12 sec. Changes in resistance were measured via the two point probe technique (Craftsman Professional digital multi-meter model 82324; 1 Hz data collection rate). The normalized resistance $\Delta R/R_0$ is plotted in Figure 58c. The normalized resistance increased with load, but nonlinearly; only qualitative feedback on the force was obtained. The peak resistance for the first cycle was higher than in subsequent tests, similar to the cyclic strain data in Figure 54 and not unexpected for an elastomer. This experiment was simply for proof of concept purposes, and further investigation is required to fully characterize the composite sensors for this particular application, including optimization of the composite formulation and the application method in order to improve the force-resistance properties.

These results demonstrate that the composites can be used to determine contact with an object. The simplicity and ease of fabrication of these sensors is attractive, particularly for prototyping robots with tactile feedback.

5.5.2 Structural health monitoring application

As mentioned above, one application for paintable strain gauges is non-destructive health-monitoring of large structures. To ascertain whether the elastomer/EG composites would be appropriate for this, a single coat of an 8 wt% latex/EG composite was brush painted into a 1.22 m long x 12.7 mm wide rectangular pattern on the top surface of a ½ scale (9.385 m long, 0.425 m wide, 0.349 m high, Michigan Bridge Design Guide 6.65.10) reinforced concrete bridge beam at Lawrence Technological University in Southfield, MI (Figure 59) to monitor deformations in the plane of the beam. The composite was applied in 10 minutes and dried for 60 minutes, with an estimated cost of materials of \$0.01 (~\$0.08/ft², single coat, brush painted). One of the advantages of the composite is that it can be painted over corners, cracks, joints, and rolled edges (Figure 60). The composite solution was painted over 20 mm long, 5 mm wide strips of aluminum tape (Nashua, 324A) that were attached to the bridge beam at the ends of the sensor area. Electrical connections were made by attaching wire leads to the exposed ends of the aluminum tape strips using conductive silver epoxy, as shown in Figure 60a.

3 hrs per sensor. For comparison, data were collected from a foil sensor (Vishay Intertechnology, Inc.) located on the other side of the ram, 0.26 m from the latex/EG sensor.

The box beam was strained to failure using a hydraulic ram (Figure 59) at various strain rates (Table 7). Changes in the resistance of the latex/EG were measured with a digital multi-meter (Tektronix DMM 4050) and LabView Signal Express software. Strain was calculated with Eq. 18 using a GF of 13, found by comparing the data with that from the commercial strain gauge.

Table 7. Bridge beam deformation rate and duration.

Time (sec)	0 - 30	30 - 105	105 - 272	272 - 875	875 - 1475
Rate (mm/s)	0.0211	0.0423	0.211	0.338	0.423

Figure 61 shows the load applied to the beam measured using a high capacity force transducer (MTS, model 661. 31B-01), the strain measured with a commercial strain gauge, and the resistance measured from the latex/EG sensor. The bridge beam began to crack after 1000 μ -strain and started to break apart after 1250 μ -strain. At approximately 900 sec, the commercial force transducer and strain gauge exhibited a reduction in load and sudden increase in strain from 1250 to 2250 μ -strain, likely due to crack formation as the bridge began to crumble. Cracking of the beam resulted in the sudden decrease in the applied load; therefore, the applied load does not necessarily correspond to the local strains that were measured. Several of the commercial strain gauges failed prematurely due to cracks forming beneath them during testing. One of the main benefits of the

composite sensor was that it continued to function and provide useful information despite the formation of cracks beneath the sensor area, as determined by visual inspection, whereas the commercial gauges were prone to detach.

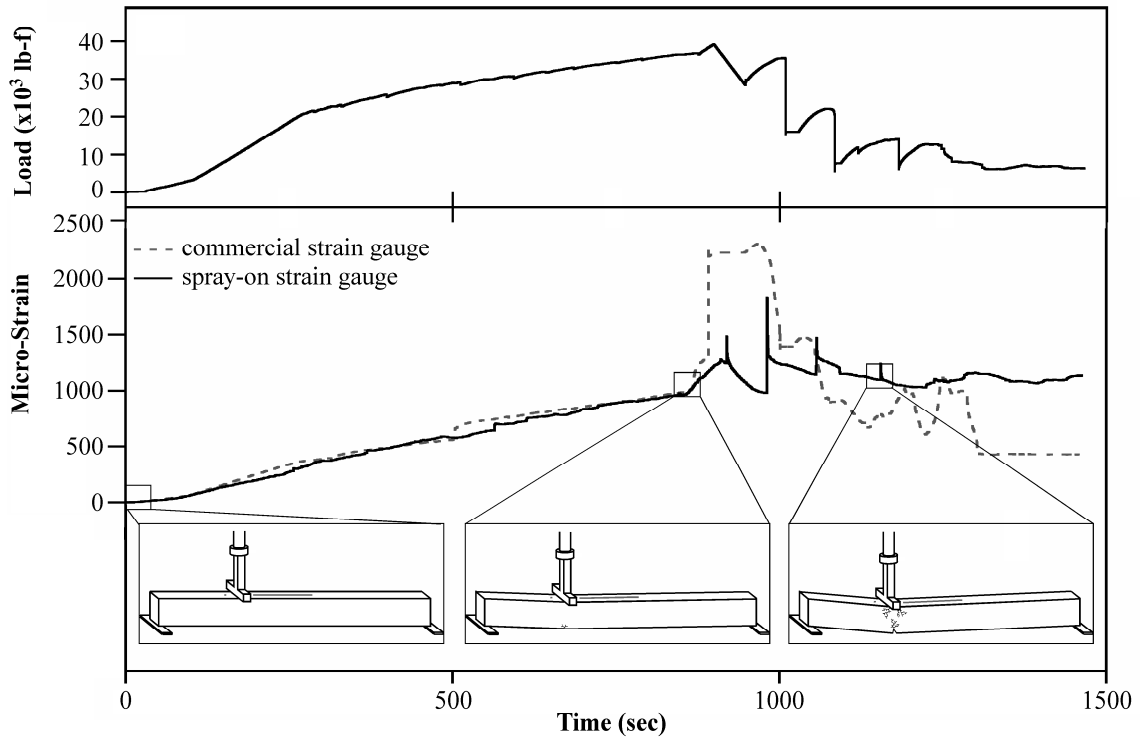


Figure 61. a) Load applied by the hydraulic ram. b) Strain measured with a commercial strain gauge and the 8 wt% latex/EG strain gauge applied to a $\frac{1}{2}$ scale concrete composite bridge beam strained to failure.

The resistance of the latex/EG sensor is compared to the strain recorded by the commercial strain gauge in Figure 61. The two gave nearly identical results up to ~ 1000 μ -strain, at which the bridge beam began to crack and deteriorate. The composite strain gauge had, however, the benefits of reduced preparation time, lower cost, and application on non-flat surfaces. The resistance of the latex/EG sensor changed 15 seconds after the onset of beam deformation, corresponding to a load of 170 lbs. With this degree of

sensitivity, it is possible that a composite sensor could even be used to monitor pedestrian traffic across similar structures.

5.6 Conclusions

A composite material comprising exfoliated graphite in latex or neoprene rubbers has been characterized and demonstrated as a strain gauge. These composites can be applied to surfaces via brushing or airbrushing, and so can cover large or small areas. Patterns can be produced using stencils to generate the desired shape. By varying the EG loading, sample thickness, and sample geometry, the sensitivity and stiffness can be tailored (with GFs up to 27,000). The versatility of the composites allows the same base materials to be used for a wide range of strain measurement applications.

The sensing materials were demonstrated in tactile sensors and for structural monitoring. Neoprene/EG tactile sensors were capable of determining when contact was made, and the latex/EG bridge sensors provided the same quality of data as commercial sensors long after the commercial sensors had come off due to the formation of cracks. The speed and ease of application, the conformability, and the unrestricted geometries of these sensors are advantageous. Furthermore, the composite sensors exhibited little dependence on temperature, a benefit for outdoor use.

5.7 Acknowledgments

This research was supported by the US Army Research Laboratory under the MAST CTA program in the Center for Microsystem Mechanics. We would like to thank Professor Grace, Charles Elder, Omkar Dear, and Steve Downing from Lawrence Technological University in Southfield, MI for graciously providing the resources and facilities necessary to conduct the bridge beam tests.

5.8 Chapter 5 Appendix

5.8.1 Electron tunneling and activation energy of latex/EG composites

Graphite is a zero band gap semiconductor with an intrinsic NTC ^[153]. An energy barrier, or activation energy, is created when electrons traverse from one conductive particle (EG), through an insulator (latex), to another conductive particle ^[185, 192, 193]. If the available thermal energy is higher than the activation energy then composites fabricated with graphite may exhibit increasing electrical conductivity with increasing temperature (e.g. an NTC). To determine if the conduction mechanism in the latex/EG composites is a thermally activated process, and to gain insight into the observed NTC, conductivity was expressed using the Arrhenius equation ^[185, 192, 193]:

$$\text{Eq. 19} \quad \sigma = \sigma_o \exp(-E_a / k_B T),$$

where σ is the DC conductivity, σ_o is a material constant depending on the mobility of charge carriers, k_B is Boltzmann constant, T is absolute temperature, and E_a is the activation energy. The material constant σ_o is the σ as $T \rightarrow \infty$ and was determined as the y-intercept of the $\ln\sigma/T^{-1}$ plot for each EG loading (Figure 62).

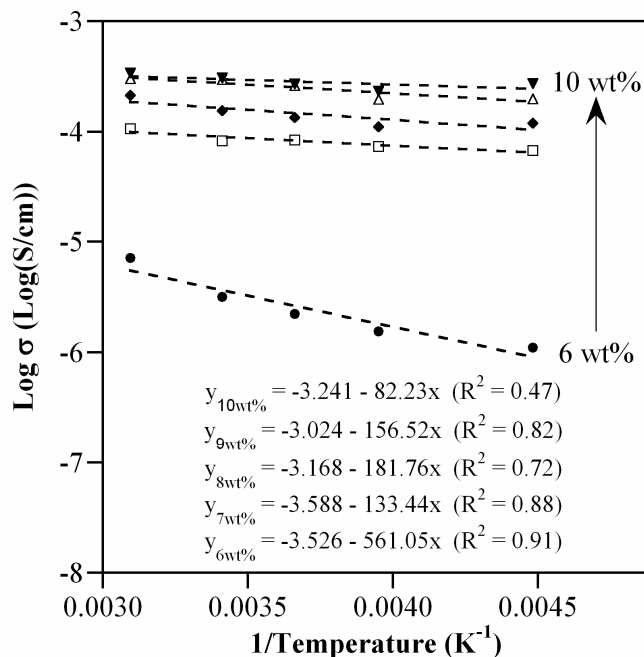


Figure 62. The natural logarithm of conductivity as a function of inverse absolute temperature for latex/EG composites with EG loadings of 6 (circles), 7 (squares), 8 (diamonds), 9 (triangles - up), and 10 wt% (triangles - down).

The calculated activation energies (using Eq. 19 and the values of σ_0 obtained from Figure 62) for the latex/EG composites are shown in Figure 63. The Activation energies for each composite loading were independent of temperature, as represented by the standard deviations, and dependent on EG loading. 6 wt% composites exhibited higher activation energies (0.046 eV), compared to 7 - 10 wt% composites, and is believed to be due to the composite microstructure. Activation energies are a reflection of composite microstructures and are a function of both particle size and interparticle separation^[193, 194]. It is also understood by percolation modeling that, near the percolation threshold, particles begin to form conductive pathways by a reduction in particle-particle separation distance as a result of the increasing filler particle concentration. The increased activation energy of the 6 wt% composites is postulated to be attributed to larger

separation distances at lower EG loadings, and hence larger energy barriers for electron transport. The calculated activation energies for the latex/EG composites are similar to those reported in the literature for other NTC composites, such as for carbon fiber/epoxy (0.0015 - 0.018 eV) ^[185] and for carbon fibers in latex (0.018 eV) ^[186]

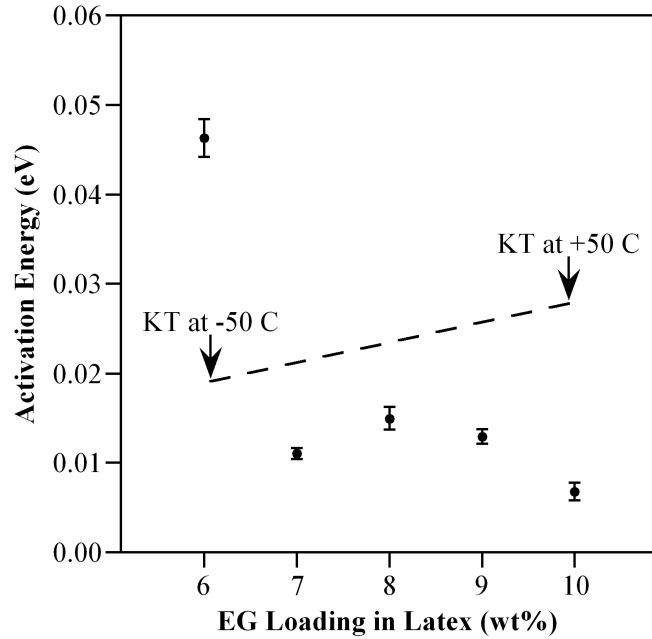


Figure 63. Activation energy of latex/EG composites as a function of EG loading.

From the above analysis, it was concluded that the conduction mechanism for latex/EG composites with EG loadings ≥ 7 wt% were indeed thermally activated processes; however, the calculated activation energy for 6 wt% composites (0.046 eV) was higher than the calculated thermal energy in the -50 to +50 °C range (0.019 - 0.027 eV) indicating that the conduction mechanism for this loading is due, at least in part, to some other non-thermally activated process. Further analysis is required to fully understand this phenomenon.

Chapter 6: Concluding remarks and suggestions for future work

6.1 Concluding remarks

New elastomer composites have been fabricated, characterized, and implemented as mechanical sensors and polymer actuators. The composites were comprised a relatively unexplored filler particle, exfoliated graphite, blended with one of several host elastomers. Processing of the particles was improved, resulting in higher degrees of exfoliation and reduced processing time. The improved processing conditions provided the fabrication of composites with lower percolation thresholds and higher conductivities. The objective of maintaining the mechanical properties of the host elastomers while rendering the composite electrically conductive was accomplished.

6.2 Future work

Despite the best efforts of many researchers over the past decade, DEAs are still limited by the mechanical and electrical properties of the elastomer dielectrics and compliant electrodes being used, particularly the low dielectric constants. Low dielectric constants result in high voltages (10kV +) required for actuation. Such high voltages restrict the number of possible applications. For DEAs to reach their full potential and become widely used in consumer products, new elastomers and/or elastomer composites are required that increase the dielectric constant without greatly increasing the associated loss. Composites with metallic filler particles with insulating coatings are one potential solution. Future work should focus on maintaining the mechanical properties of the

elastomeric hosts, minimizing dielectric loss, and increasing the dielectric constant of the composites. It is also important that the resistance of the composite remains high to reduce current leakage through the dielectric and to minimize power consumption. Future work should also focus on providing a physical explanation for the critical exponent t in percolation modeling of conductive composites.

The mechanical properties of the elastomer dielectrics are another issue requiring further research to ensure the continued use of DEAs. DEA elastomers should ideally exhibit little creep strain when pre-stressed, actuate at high frequencies, be able to be processed in to various shapes and sized, and have high efficiency. Synthesis of new elastomers, engineered for DEA applications are one possible solution. Another possible solution is to explore bio-polymers, such as resilin. Resilin is the elastomeric protein found in insect cuticle and is gives insects like fleas the ability to jump many times their body length and cicadas the ability to generate loud noises used for attracting mates. Resilin is the most energy efficient polymer known to man; over 98% of elastic strain energy is returned from cycle to cycle, losing less than 2% to heat ^[195].

Sensors have and will continue to benefit from the development of new composite materials. Current limitations such as lengthy installation times and small monitoring areas can be alleviated using composites that can be painted onto surfaces. Future work should explore new materials, such as graphene and carbon nanotubes, and take advantage of their unique properties for the development of advanced sensors.

Conductive elastomer composites should also be more extensively studied to determine i)

the mechanisms for increasing resistance with increasing humidity, and ii) the mechanisms for electron tunneling and additional thermally activated processes responsible for the observed negative temperature coefficients of resistance that were observed.

Chapter 7: Intellectual contributions

There were a number of intellectual contributions made during the completion of this dissertation.

- 1) Improved the degree of exfoliation, resulting in elastomer composites with higher conductivity, lower percolation thresholds, and improved mechanical properties.
 - Replacing bath sonication with horn sonication increased the degree of exfoliation, decreased sonication time from 9 hours down to 20 minutes, increased the processing volume from 20 ml to 300 ml, and increased the composite conductivities from 0.5 S/cm to 12.5 S/cm. Improved exfoliation resulted in lower percolation thresholds and higher conductivities.
 - Compared three methods of exfoliation: chemical, thermal, and microwave irradiation. Developed a one-step microwave procedure that was safer and less complicated than published methods. Optimization of this protocol reduced the processing time down to 60 sec, compared to 20 min for thermal exfoliation and 2 weeks for chemical exfoliation.

- 2) Developed new methods of fabrication for improving elastomer composite properties.
 - Tailored selection of solvents and surfactants and optimized their concentrations based on particular host/particle combinations. This allowed immiscible mixtures to be blended and resulted in improved conductivity and processability.

- Introduced shear mixing to blend the EG into the elastomeric precursor. This was required to prevent airbrushes from clogging due to partial curing of the elastomer precursors caused by the heat generated during bath sonication.
 - Added a desiccation step to the fabrication protocol to removed trapped air in the uncured composites and increase conductivity.
- 3) Developed new methods of fabricating multi-layer DEAs with compliant electrodes.
- Optimized composite solution viscosity to improve layer thickness, cure time, and surface roughness and to allow layered structures to be fabricated.
 - Developed spin coating methods that preventing the liquid composites from penetrating under the stencils and preventing wrinkling due to the solvents swelling underlying cured layers.
 - Identified compatible organic solvents and optimized concentrations to allow EG to be mixed into elastomers without phase separation upon curing.
 - Optimized the size and shape of DEA electrode stencils to prevent sparking between electrodes when actuated.
- 4) Developed paintable composites.
- In order to air brush composite solutions without clogging the nozzle, the pH of the uncured composites was adjusted using sodium hydroxide to prevent premature crosslinking due to remaining acids from the exfoliation process.

- 5) Demonstrated real world applications of the new materials.
- Produced compliant electrodes with high conductivities (12.5 S/cm) and the lowest modulus ever reported for conductive filler composites (1.4 MPa).
 - Fabricated and characterized DEAs with patterned compliant electrodes.
 - Created tactile sensors for robotic and prosthetic applications.
 - Developed paintable strain gauges for structural health monitoring having performance equal to those of commercial gauges while having the additional benefits of providing data even after the structure began cracking, larger monitoring areas, and reduced installation time. Developed a strain gauge with the highest gauge factor ever reported (27,000).
 - Implemented strain gauges for structural health monitoring.
- 6) For the first time, detailed comparisons were conducted on the actuation performance of three elastomers for DEAs, including strain, stress, and speed.
- 7) For the first time, measured changes in material properties for paintable composite strain gauges as functions of temperature and humidity.

References

- [1] Rajanna, K. and Nayak, M. M., "Strain sensitivity and temperature behavior of invar alloy films," *Mater. Sci. Eng., B*, 3(77), 288-292 (2000).
- [2] Zhao, Q., Wang, C., Liu, Y., and Wang, S., "Bacterial adhesion on the metal-polymer composite coatings," *Int. J. Adhes. Adhes.*, 2(27), 85-91 (2007).
- [3] Thayer, A. M., "Advanced polymer composites tailored for aerospace use," *Chem. Eng. News*, 30(68), 37-58 (1990).
- [4] Kofod, G., "The static actuation of dielectric elastomer actuators: how does pre-stretch improve actuation?," *Journal of Physics D-Applied Physics*, 21(41), 11 (2008).
- [5] Balakrisnan, B., Kujawski, M., Pearse, J. D., and Smela, E., "Dielectric Elastomer Actuators: Review of Performance," (in preparation).
- [6] Pelrine, R., Kornbluh, R., Joseph, J., and Chiba, S., "Electrostriction of polymer films for microactuators," in *Proc., IEEE MEMS*, 238-243 (1997).
- [7] Pelrine, R., Kornbluh, R., and Joseph, J., "Electrostriction of polymer dielectrics with compliant electrodes as a means of actuation," *Sens. Actuators, A*, 1(64), 77-85 (1998).
- [8] Pelrine, R., Kornbluh, R., and Chiba, S., "Artificial muscle for small robots and other micromechanical devices," *Transactions of the Institute of Electrical Engineering of Japan*, 2(122), 97-102 (2002).
- [9] Pelrine, R., Kornbluh, R., Pei, Q., and Joseph, J., "High-speed electrically actuated elastomers with strain greater than 100%," *Science*, 5454(287), 836-839 (2000).
- [10] Kwak, J. W., Chi, H. J., Jung, K. M., Koo, J. C., Jeon, J. W., Lee, Y., Nam, J. D., Ryew, Y., and Choi, H. R., "A face robot actuated with artificial muscle based on dielectric elastomer," *Journal of Mechanical Science and Technology*, 2(19), 578-588 (2005).
- [11] Kim, H. S., Park, J., Chuc, N. H., Choi, H. R., Nam, J. D., Lee, Y., Jung, H. S., and Koo, J. C., "Development of dielectric elastomer driven micro-optical zoom lens system," in *Smart Structures and Materials & Nondestructive Evaluation and Health Monitoring 2007: Electroactive Polymer Actuators and Devices (EAPAD)* San Diego, CA, USA 65241V (2007).
- [12] Heydt, R., Kornbluh, R., Eckerle, J., and Pelrine, R., "Sound radiation properties of dielectric elastomer electroactive polymer loudspeakers," in *Proc., IEEE EAPAD*, 61681M (2006).
- [13] Lee, S., Jung, K., Koo, J., Lee, S., Choi, H., Jeon, J., Nam, J. D., and Choi, H. R., "Braille display device using soft actuator," in *Smart Structures and Materials 2004: Electroactive Polymer Actuators and Devices (EAPAD)*, San Diego, CA, USA 368-379 (2004).
- [14] Pelrine, R., Kornbluh, R., Pei, Q., Stanford, S., Oh, S., Eckerle, J., Full, R., Rosenthal, M., and Meijer, K., "Dielectric elastomer artificial muscle actuators: Toward biomimetic motion," in *IEEE Smart Structures and Materials: Electroactive Polymer Actuators and Devices*, 126-137 (2002).

- [15] Intelligent robotics and mechatronics systems laboratory, <<http://mecha.skku.ac.kr/source/MicroMoving/inchworm.jpg>>, Accessed on 02/12, (2011).
- [16] Dielectric-elastomer-driven airship uses fish-like propulsion <<http://spie.org/x39863.xml?ArticleID=x39863>>, Accessed on 02/12, (2011).
- [17] Trujillo, R., Mou, J., Phelan, P. E., and Chau, D. S., "Investigation of electrostrictive polymers as actuators for mesoscale devices," *Int. J. Adv. Manuf. Technol.*, 3-4(23), 176-182 (2004).
- [18] Plante, J. S. and Dubowsky, S., "Large-scale failure modes of dielectric elastomer actuators," *International Journal of Solids and Structures*, 25-26(43), 7727-7751 (2006).
- [19] Di Spigna, N., Chakraborti, P., Yang, P., Ghosh, T., and Franzon, P., "Application of EAP materials toward a refreshable Braille display," in *Smart Structures and Materials & Nondestructive Evaluation and Health Monitoring: Electroactive Polymer Actuators and Devices (EAPAD)*, San Diego, CA, USA, 72871K-9 (2009).
- [20] Kofod, G., Sommer-Larsen, P., Kronbluh, R., and Pelrine, R., "Actuation response of polyacrylate dielectric elastomers," *J. Intell. Mater. Syst. Struct.*, 12(14), 787-793 (2003).
- [21] Gere, J. M. and Goodno, B. J., *Mechanics of materials*, 7th ed. Toronto, ON: Cengage Learning (2009).
- [22] Gonzalez, M., Axisa, F., BuIcke, M. V., Brosteaux, D., Vandeveld, B., and Vanfleteren, J., "Design of metal interconnects for stretchable electronic circuits," *Microelectronics Reliability*, 48), 825-832 (2008).
- [23] Rosset, S., Niklaus, M., Dubois, P., and Shea, H., "Metal ion implantation for the fabrication of stretchable electrodes on elastomers," *Adv. Funct. Mater.*, 3(19), 470-478 (2009).
- [24] Yuan, W., Hu, L., Ha, S., Lam, T., Gruner, G., and Pei, Q., "Self-clearable carbon nanotube electrodes for improved performance of dielectric elastomer actuators," in *Smart Structures/Nondestructive Evaluation for Health Monitoring + Diagnostics 2008: Electroactive Polymer Actuators and Devices (EAPAD)* San Diego, CA, USA 69270P (2008).
- [25] Kirkpatrick, S., "Percolation and Conduction," *Rev. Mod. Phys.*, 4(45), 574 (1973).
- [26] Konagaya, S., Abe, K., and Ishihara, H., "Conductive polymer composite PET film with excellent antistatic properties," *Plastics, Rubber and Composites*, 5(31), 201-204 (2002).
- [27] Jung, Y. J., Kar, S., Talapatra, S., Soldano, C., Viswanathan, G., Li, X., Yao, Z., Ou, F. S., Avadhanula, A., Vajtai, R., Curran, S., Nalamasu, O., and Ajayan, P. M., "Aligned carbon Nanotube-polymer hybrid architectures for diverse flexible electronic applications," *Nano Lett.*, 3(6), 413-418 (2006).
- [28] Huang, C., Zhang, Q. M., and Su, J., "High-dielectric-constant all-polymer percolative composites," *Applied Physics Letters*, 20(82), 3502-3504 (2003).
- [29] Szabo, J. P., Hiltz, J. A., Cameron, C. G., Underhill, R. S., Massey, J., White, B., and Leidner, J., "Elastomeric composites with high dielectric constant for use in

- Maxwell stress actuators," in *Smart Structures and Materials: Electroactive Polymer Actuators and Devices (EAPAD)*, San Diego, CA, USA, 180-190 (2003).
- [30] Rajamani, A., Grissom, M. D., Rahn, C. D., and Zhang, Q. M., "Wound roll dielectric elastomer actuators: Fabrication, analysis, and experiments," *IEEE-ASME Transactions on Mechatronics*, 1(13), 117-124 (2008).
- [31] Wissler, M., Mazza, E., and Kovacs, G., "Electromechanical coupling in cylindrical dielectric elastomer actuators," in *Smart Structures and Materials & Nondestructive Evaluation and Health Monitoring 2007: Electroactive Polymer Actuators and Devices (EAPAD)* San Diego, CA, USA 652409 (2007).
- [32] Tanaka, T., Sato, M., and Kozako, M., "Voltage-strain characteristics of cylindrical polymer actuators," in *Proceedings of 2005 International Symposium on Electrical Insulating Materials (ISEIM 2005)*, Kitakyushu, Japan, 780-783 (2005).
- [33] Arora, S., Ghosh, T., and Muth, J., "Dielectric elastomer based prototype fiber actuators," *Sensors and Actuators A-Physical*, 1(136), 321-328 (2007).
- [34] Cameron, C. G., Szabo, J. P., Johnstone, S., Massey, J., and Leidner, J., "Linear actuation in coextruded dielectric elastomer tubes," *Sens. Actuators, A*, 1(147), 286-291 (2008).
- [35] Carpi, F. and Rossi, D. D., "Improvement of electromechanical actuating performances of a silicone dielectric elastomer by dispersion of titanium dioxide powder," *IEEE Transactions on Dielectrics and Electrical Insulation*, 4(12), 835-843 (2005).
- [36] Mazzoldi, A., Carpi, F., and De Rossi, D., "Polymers responding to electrical or electrochemical stimuli for linear actuators," *Annales De Chimie-Science Des Materiaux*, 6(29), 55-64 (2004).
- [37] Ren, K. L., Liu, S., Lin, M. R., Wang, Y., and Zhang, Q. M., "A compact electroactive polymer actuator suitable for refreshable braille display," *Sensors and Actuators A-Physical*, 2(143), 335-342 (2008).
- [38] Shankar, R., Ghosh, T. K., and Spontak, R. J., "Electromechanical response of nanostructured polymer systems with no mechanical pre-strain," *Macromolecular Rapid Communications*, 10(28), 1142-1147 (2007).
- [39] Tanaka, T., Sato, M., and Kozako, M., "High field Maxwell stress-strain characteristics of conventional polymers as actuators," in *2004 Annual Report Conference on Electrical Insulation and Dielectric Phenomena (CEIDP '04)*, 364-367 (2004).
- [40] Wissler, M. and Mazza, E., "Mechanical behavior of an acrylic elastomer used in dielectric elastomer actuators," *Sensors and Actuators A-Physical*, 2(134), 494-504 (2007).
- [41] Carpi, F., Chiarelli, P., Mazzoldi, A., and De Rossi, D., "Electromechanical characterisation of dielectric elastomer planar actuators: comparative evaluation of different electrode materials and different counterloads," *Sensors and Actuators A-Physical*, 1(107), 85-95 (2003).

- [42] Carpi, F. and De Rossi, D., "Dielectric elastomer cylindrical actuators: electromechanical modelling and experimental evaluation," *Materials Science & Engineering C-Biomimetic and Supramolecular Systems*, 4(24), 555-562 (2004).
- [43] Carpi, F., Gallone, G., Galantini, F., and De Rossi, D., "Silicone-poly(hexylthiophene) blends as elastomers with enhanced electromechanical transduction properties," *Advanced Functional Materials*, 2(18), 235-241 (2008).
- [44] Carpi, F., Migliore, A., Serra, G., and De Rossi, D., "Helical dielectric elastomer actuators," *Smart Materials & Structures*, 6(14), 1210-1216 (2005).
- [45] Carpi, F., Salaris, C., and De Rossi, D., "Folded dielectric elastomer actuators," *Smart Materials & Structures*, 2(16), S300-S305 (2007).
- [46] Galler, N., Ditzbacher, H., Steinberger, B., Hohenau, A., Dansachmüller, M., Camacho-Gonzales, F., Bauer, S., Krenn, J. R., Leitner, A., and Aussenegg, F. R., "Electrically actuated elastomers for electro-optical modulators," *Applied Physics B-Lasers and Optics*, 1(85), 7-10 (2006).
- [47] Carpi, F., Khanicheh, A., Mavroidis, C., and De Rossi, D., "Silicone made contractile dielectric elastomer actuators inside 3-Tesla MRI environment," in *IEEE/RSJ International Conference on Intelligent Robots and Systems (IROS 2008)*, Nice, France 137-142 (2008).
- [48] Shankar, R., Ghosh, T. K., and Spontak, R. J., "Electroactive nanostructured polymers as tunable actuators," *Advanced Materials*, 17(19), 2218-2223 (2007).
- [49] Zhang, X., Löwe, C., Wissler, M., Jähne, B., and Kovacs, G., "Dielectric elastomers in actuator technology," *Advanced Engineering Materials*, 5(7), 361-367 (2005).
- [50] Carpi, F., Frediani, G., Mannini, A., and DeRossi, D., "Contractile and buckling actuators based on dielectric elastomers: Devices and applications," *Advances in Science and Technology*, (61), 186-191 (2008).
- [51] Liu, Y. J., Liu, L. W., Zhang, Z., and Leng, J. S., "Dielectric elastomer film actuators: Characterization, experiment and analysis," *Smart Mater. Struct.*, (18), 095024 (2009).
- [52] Carpi, F. and Rossi, D. D., "Contractile folded dielectric elastomer actuators," in *Smart Structures and Materials & Nondestructive Evaluation and Health Monitoring 2007: Electroactive Polymer Actuators and Devices (EAPAD)* San Diego, CA, USA 65240D (2007).
- [53] Chuc, N. H., Park, J., Thuy, D. V., Kim, H. S., Koo, J., Lee, Y., Nam, J. D., and Choi, H. R., "Linear artificial muscle actuator based on synthetic elastomer," in *Smart Structures and Materials & Nondestructive Evaluation and Health Monitoring 2007: Electroactive Polymer Actuators and Devices (EAPAD)* San Diego, CA, USA 65240J (2007).
- [54] Yuan, W., Lam, T., Biggs, J., Hu, L., Yu, Z., Ha, S. M., Xi, D., Senesky, M. K., Gruner, G., and Pei, Q., "New electrode materials for dielectric elastomer actuators," in *Smart Structures and Materials & Nondestructive Evaluation and Health Monitoring 2007: Electroactive Polymer Actuators and Devices (EAPAD)* San Diego, CA, USA 65240N (2007).
- [55] Aschwanden, M. and Stemmer, A., "Low voltage, highly tunable diffraction grating based on dielectric elastomer actuators," in *Smart Structures and Materials*

- & Nondestructive Evaluation and Health Monitoring 2007: Electroactive Polymer Actuators and Devices (EAPAD) San Diego, CA, USA 65241N (2007).
- [56] Bolzmacher, C., Biggs, J., and Srinivasan, M., "Flexible dielectric elastomer actuators for wearable human-machine interfaces," in Smart Structures and Materials 2006: Electroactive Polymer Actuators and Devices (EAPAD), San Diego, CA, USA 616804 (2006).
 - [57] Zhang, R., Lochmatter, P., Kunz, A., and Kovacs, G., "Spring roll dielectric elastomer actuators for a portable force feedback glove," in Smart Structures and Materials 2006: Electroactive Polymer Actuators and Devices (EAPAD), San Diego, CA, USA 61681T (2006).
 - [58] Schlaak, H. F., Jungmann, M., Matysek, M., and Lotz, P., "Novel multilayer electrostatic solid state actuators with elastic dielectric (Invited Paper)," in Smart Structures and Materials 2005: Electroactive Polymer Actuators and Devices (EAPAD), San Diego, CA, USA, 121-133 (2005).
 - [59] Cameron, C. G., Underhill, R. S., Rawji, M., and Szabo, J. P., "Conductive filler-elastomer composites for Maxwell stress actuator applications," in Smart Structures and Materials: Electroactive Polymer Actuators and Devices (EAPAD), San Diego, CA, USA 51-59 (2004).
 - [60] Carpi, F., Mazzoldi, A., and Rossi, D. D., "High-strain dielectric elastomer for actuation," in Proc. IEEE EAPAD, San Diego, CA., 419-422 (2003).
 - [61] Lorussi, F., Tognetti, A., Carpi, F., Mazzoldi, A., and Rossi, D. D., "Recruited dielectric elastomer motor units as pseudomuscular actuator," in Smart Structures and Materials 2003: Electroactive Polymer Actuators and Devices (EAPAD), San Diego, CA, USA 464-467 (2003).
 - [62] Sommer-Larsen, P., Hooker, J. C., Kofod, G., West, K., Benslimane, M., and Gravesen, P., "Response of dielectric elastomer actuators," in Smart Structures and Materials 2001: Electroactive Polymer Actuators and Devices, Newport Beach, CA, USA 157-163 (2001).
 - [63] Kornbluh, R., Pelrine, R., Pei, Q., Oh, S., and Joseph, J., "Ultrahigh strain response of field-actuated elastomeric polymers," in Proc. IEEE EAPAD, Newport Beach, CA., 51-64 (2000).
 - [64] Li, Z. and Cheng, Z.-Y., "Partially ordered region: a new mechanism for electromechanical response of EAPs," in Smart Structures and Materials 2005: Electroactive Polymer Actuators and Devices (EAPAD), San Diego, CA, USA, 252-259 (2005).
 - [65] Cai, Z., Chen, Y., and Kim, J., "Cellulose-chitosan blended electroactive paper actuator," in Smart Structures and Materials & Nondestructive Evaluation and Health Monitoring: Electroactive Polymer Actuators and Devices (EAPAD), San Diego, California, USA, 69271H-7 (2008).
 - [66] Kovacs, G., Ha, S. M., Michel, S., Pelrine, R., and Pei, Q., "Study on core free rolled actuator based on soft dielectric EAP," in Smart Structures and Materials & Nondestructive Evaluation and Health Monitoring: Electroactive Polymer Actuators and Devices (EAPAD), San Diego, California, USA, 69270X-15 (2008).

- [67] Kovacs, G. and During, L., "Contractive tension force stack actuator based on soft dielectric EAP," in Smart Structures and Materials & Nondestructive Evaluation and Health Monitoring: Electroactive Polymer Actuators and Devices (EAPAD), San Diego, CA, USA, 72870A-15 (2009).
- [68] Walder, C., Molberg, M., Opris, D. M., Nuesch, F. A., Lowe, C., Plummer, C. J. G., Leterrier, Y., and Manson, J. A. E., "High k dielectric elastomeric materials for low voltage applications," in Smart Structures and Materials & Nondestructive Evaluation and Health Monitoring: Electroactive Polymer Actuators and Devices (EAPAD), San Diego, CA, USA, 72870Q-9 (2009).
- [69] Tryson, M., Kiil, H.-E., and Benslimane, M., "Powerful tubular core free dielectric electro activate polymer (DEAP) push actuator," in Electroactive Polymer Actuators and Devices (EAPAD) 2009, San Diego, CA, USA, 72871F-11 (2009).
- [70] Carpi, F., Migliore, A., and Rossi, D. D., "A new contractile linear actuator made of dielectric elastomers (Invited Paper)," in Smart Structures and Materials 2005: Electroactive Polymer Actuators and Devices (EAPAD), San Diego, CA, USA, 64-74 (2005).
- [71] Danfoss PolyPower A/S, Technical information listed on company webpage (www.polypower.com), Accessed on 02/01 (2011),
- [72] Rosset, S., Niklaus, M., Dubois, P., and Shea, H. R., "Performance characterization of miniaturized dielectric elastomer actuators fabricated using metal ion implantation," in IEEE 21st International Conference on Micro Electro Mechanical System (MEMS 2008), Tucson, AZ 503-506 (2008).
- [73] Rosset, S., Niklaus, M., Dubois, P., and Shea, H., "Mechanical characterization of a dielectric elastomer microactuator with ion-implanted electrodes," *Sensors and Actuators A-Physical*, 1(144), 185-193 (2008).
- [74] Kovacs, G. and During, L., "Contractive tension force stack actuator based on soft dielectric EAP," in Smart Structures and Materials & Nondestructive Evaluation and Health Monitoring 2009: Electroactive Polymer Actuators and Devices (EAPAD), San Diego, CA, USA 72870A (2009).
- [75] Choi, H. R., Jung, K., Ryew, S., Nam, J. D., Jeon, J., Koo, J. C., and Tanie, K., "Biomimetic soft actuator: Design, modeling, control, and applications," *IEEE-ASME Transaction on Mechatronics*, 5(10), 581-593 (2005).
- [76] Ohlckers, P. and Jakobsen, H., "High volume production of silicon sensor microsystems for automotive applications," in IEEE Colloquium on Assembly and Connections in Microsystems (Digest No. 1997/004) 8/1-8/7 (1997).
- [77] Russell, R. A., "A thermal sensor array to provide tactile feedback for robots," *The International Journal of Robotics Research*, 3(4), 35-39 (1985).
- [78] Jin, Z., Su, Y., and Duan, Y., "Development of a polyaniline-based optical ammonia sensor," *Sens. Actuators, B*, 1(72), 75-79 (2001).
- [79] Liu, H., Kameoka, J., Czaplowski, D. A., and Craighead, H. G., "Polymeric Nanowire Chemical Sensor," *Nano Lett.*, 4(4), 671-675 (2004).
- [80] Kang, I., Schulz, M. J., Kim, J. H., Shanov, V., and Shi, D., "A carbon nanotube strain sensor for structural health monitoring," *Smart Mater. Struct.*, 3(15), 737-748 (2006).

- [81] Kujawski, M., Miller, K., Neumann, T., Elder, C., Dear, O., and Smela, E., "Paintable elastomeric strain sensors: Characterization and application," *Sens. Actuator A-Phys.*, (in preparation).
- [82] Khodaparast, P., Ghaffarian, S. R., Khosrosham, M. R., Yousefimehr, N., and Zamani, D., "Electrode structures in high strain actuator technology," *Journal of Optoelectronics and Advanced Materials*, 11(9), 3585-3591 (2007).
- [83] Gharavi, N., Kashani, M. R., and Moradi, A., "Effect of organo-clay on actuation response of silicone rubber actuators," in *Smart Structures and Materials & Nondestructive Evaluation and Health Monitoring: Electroactive Polymer Actuators and Devices (EAPAD)*, San Diego, CA, USA, 72871W-6 (2009).
- [84] Tryson, M., Kiil, H., and Benslimane, M., "Powerful tubular core free dielectric electro activate polymer (DEAP) push actuator," in *Smart Structures and Materials & Nondestructive Evaluation and Health Monitoring: Electroactive Polymer Actuators and Devices (EAPAD)*, San Diego, CA, USA, 72871F-11 (2009).
- [85] Lochmatter, P. and Kovacs, G., "Design and characterization of an active hinge segment based on soft dielectric EAPs," *Sens. Actuators, A*, 2(141), 577-587 (2008).
- [86] Plante, J. S. and Dubowsky, S., "On the properties of dielectric elastomer actuators and their design implications," *Smart Materials & Structures*, 2(16), S227-S236 (2007).
- [87] Cho, S., Ryew, S., Jeon, J., Kim, H., Nam, J., and Choi, H., "Development of micro inchworm robot actuated by electrostrictive polymer actuator," in *Smart Structures and Materials 2001: Electroactive Polymer Actuators and Devices*, Newport Beach, CA, USA 466-474 (2001).
- [88] Wingert, A., Lichter, M. D., and Dubowsky, S., "On the design of large degree-of-freedom digital mechatronic devices based on bistable dielectric elastomer actuators," *IEEE-ASME Transactions on Mechatronics*, 4(11), 448-456 (2006).
- [89] Plante, J. S., Devita, L. M., and Dubowsky, S., "A road to practical dielectric elastomer actuators based robotics and mechatronics: discrete actuation," in *Smart Structures and Materials & Nondestructive Evaluation and Health Monitoring 2007: Electroactive Polymer Actuators and Devices (EAPAD)* San Diego, CA, USA 652406 (2007).
- [90] Kofod, G., Kornbluh, R., Pelrine, R., and Sommer-Larsen, P., "Actuation response of polyacrylate dielectric elastomers," in *Proc. IEEE EAPAD*, Newport Beach, CA., 141-147 (2001).
- [91] Liu, C., Bar-Cohen, Y., and Leary, S. P., "Electrostatically stricted polymers (ESSP)," in *Smart Structures and Materials 1999: Electroactive Polymer Actuators and Devices*, Newport Beach, CA, USA, 186-190 (1999).
- [92] Carpi, F., Bauer, S., and De Rossi, D., "Stretching dielectric elastomer performance," *Science*, 6012(330), 1759-1761 (2010).
- [93] Barnes, A. Z., Liu, Q., Young, G. F., and Lu, T., "Evaluation of selected dielectric elastomers for use in an artificial muscle actuator," in *Proc. Australasian Conference on Robotics and Automaton*, Brisbane, Australia, 1-9 (2007).

- [94] Bakerjian, R. and Mitchell, P., *ool and manufacturing engineers handbook. Volume VI, Design for manufacturability : a reference book for manufacturing engineers, managers, and technicians*, 4th ed. Dearborn, Mich.: Society of Manufacturing Engineers (1992).
- [95] Rolland, J. P., Van Dam, R. M., Schorzman, D. A., Quake, S. R., and DeSimone, J. M., "Solvent-resistant photocurable "Liquid Teflon" for microfluidic device fabrication," *J. Am. Chem. Soc.*, 8(126), 2322-2323 (2004).
- [96] Schneider, F., Fellner, T., Wilde, J., and Wallrabe, U., "Mechanical properties of silicones for MEMS," *Journal of Micromechanics and Microengineering*, 6(18), 065008 (2008).
- [97] Gallone, G., Carpi, F., De Rossi, D., Levita, G., and Marchetti, A., "Dielectric constant enhancement in a silicone elastomer filled with lead magnesium niobate-lead titanate," *Materials Science & Engineering C-Biomimetic and Supramolecular Systems*, 1(27), 110-116 (2007).
- [98] Ha, S., Yuan, W., Pei, Q., Pelrine, R., and Stanford, S., "Interpenetrating polymer networks for high-performance electroelastomer artificial muscles," *Adv. Mater.*, 7(18), 887-891 (2006).
- [99] Ma, W. and Cross, L. E., "An experimental investigation of electromechanical response in a dielectric acrylic elastomer," *Applied Physics A-Materials Science & Processing*, 8(78), 1201-1204 (2004).
- [100] Mata, A., Fleischman, A. J., and Roy, S., "Characterization of polydimethylsiloxane (PDMS) properties for biomedical micro/nanosystems," *Biomedical Microdevices*, 4(7), 281-293 (2005).
- [101] Findley, W. N., Lai, J. S., and Onaran, K., *Creep and relaxation of nonlinear viscoelastic materials*. New York: Dover Publications Inc. 371 (1989).
- [102] Conway, B. E., *Electrochemical supercapacitors: Scientific fundamentals and technological applications*. New York: Plenum Press 698 (1999).
- [103] Rosset, S., Niklaus, M., Dubois, P., and Shea, H. R., "Large-stroke dielectric elastomer actuators with ion-implanted electrodes," *J. Microelectromech. Syst.*, 6(18), 1300-1308 (2009).
- [104] Plante, J. S. and Dubowsky, S., "On the performance mechanisms of dielectric elastomer actuators," *Sens. Actuators, A*, 1(137), 96-109 (2007).
- [105] Dubois, P., Rosset, S., Niklaus, M., Dadras, M., and Shea, H., "Voltage control of the resonance frequency of dielectric electroactive polymer (DEAP) membranes," *Journal of Microelectromechanical Systems*, 5(17), 1072-1081 (2008).
- [106] Pimpin, A., Suzuki, Y., and Kasagi, N., "Microelectrostrictive actuator with large out-of-plane deformation for flow-control application," *Journal of Microelectromechanical Systems*, 3(16), 753-764 (2007).
- [107] Loverich, J. J., Kanno, I., and Kotera, H., "Concepts for a new class of all-polymer micropumps," *Lab on a Chip*, 9(6), 1147-1154 (2006).
- [108] Bonwit, N., Heim, J., Rosenthal, M., Duncheon, C., and Beavers, A., "Design of commercial applications of EPAM technology," in *Proc., IEEE EAPAD*, San Diego, CA, USA 616805 (2006).
- [109] Figliola, R. S. and Beasley, D. E., *Theory and design for mechanical measurements*, 4th ed. Hoboken, N.J . John Wiley & Sons, Inc. 542 (2006).

- [110] Niemeyer, L., Pietronero, L., and Wiesmann, H. J., "Fractal dimension of dielectric breakdown," *Phys. Rev. Lett.*, 12(52), 1033 (1984).
- [111] Valente, M., Costa, L., Mendiratta, S., Henry, F., and Ramanitra, L., "Structural and electrical properties of polystyrene-carbon composites," *Solid State Commun.*, 2(112), 67-72 (1999).
- [112] Flandin, L., Chang, A., Nazarenko, S., Hiltner, A., and Baer, E., "Effect of strain on the properties of an ethylene-octene elastomer with conductive carbon fillers," *J. Appl. Polym. Sci.*, 6(76), 894-905 (2000).
- [113] Engel, J., Chen, J., Chen, N., Pandya, S., and Liu, C., "Multi-walled carbon nanotube filled conductive elastomers: Materials and application to micro transducers," in 19th IEEE International Conference on MEMS, 246-249 (2006).
- [114] Khosla, A. and Gray, B. L., "Preparation, characterization and micromolding of multi-walled carbon nanotube polydimethylsiloxane conducting nanocomposite polymer," *Mater. Lett.*, 13-14(63), 1203-1206 (2009).
- [115] Sandler, J., Kirk, J., Kinloch, I., Shaffer, M., and Windle, A., "Ultra-low electrical percolation threshold in carbon-nanotube-epoxy composites," *Polymer*, 19(44), 5893-5899 (2003).
- [116] Ji, L., Stevens, M., Zhu, Y., Gong, Q., Wu, J., and Liang, J., "Preparation and properties of multi-walled carbon nanotube/carbon/polystyrene composites," *Carbon*, 11(47), 2733-2741 (2009).
- [117] Worsley, M., Kucheyev, S., Kuntz, J., Hamza, A., Satcher, J., and Baumann, T., "Stiff and electrically conductive composites of carbon nanotube aerogels and polymers," *J. Mater. Chem.*, (19), 3370-3372 (2009).
- [118] Bumsuk, K., Jongjin, L., and Insuk, Y., "Electrical properties of single-wall carbon nanotube and epoxy composites," *J. Appl. Phys.*, 10(94), 6724-6728 (2003).
- [119] Blighe, F., Hernandez, Y., Blau, W., and Coleman, J., "Observation of percolation-like scaling - far from the percolation threshold - in high volume fraction, high conductivity polymer-nanotube composite films," *Adv. Mater.*, 24(19), 4443-4447 (2007).
- [120] De, S., Lyons, P. E., Sorel, S., Doherty, E. M., King, P. J., Blau, W. J., Nirmalraj, P. N., Boland, J. J., Scardaci, V., Joimel, J., and Coleman, J. N., "Transparent, flexible, and highly conductive thin films based on polymer - nanotube composites," *ACS Nano*, 3(3), 714-720 (2009).
- [121] Ham, H., Choi, Y., Chee, M., Cha, C., and Chung, I., "PEDOT-PSS/singlewall carbon nanotubes composites," *Polym. Eng. Sci.*, 1(48), 1-10 (2008).
- [122] Cong, H. and Pan, T., "Photopatternable conductive PDMS materials for microfabrication," *Adv. Funct. Mater.*, 13(18), 1912-1921 (2008).
- [123] Celzard, A., McRae, E., Marêché, J., Furdin, G., Dufort, M., and Deleuze, C., "Composites based on micron-sized exfoliated graphite particles: Electrical conduction, critical exponents and anisotropy," *J. Phys. Chem. Solids.*, 6-8(57), 715-718 (1996).
- [124] Srivastava, N. and Mehra, R., "Study of structural, electrical, and dielectric properties of polystyrene/foiliated graphite nanocomposite developed via in situ polymerization," *J. Appl. Polym. Sci.*, 6(109), 3991-3999 (2008).

- [125] Stankovich, S., Dikin, D. A., Dommett, G. H. B., Kohlhaas, K. M., Zimney, E. J., Stach, E. A., Piner, R. D., Nguyen, S. T., and Ruoff, R. S., "Graphene-based composite materials," *Nature*, 7100(442), 282-286 (2006).
- [126] Yang, L. J., Wang, H. H., Yang, P. C., Chung, Y. C., and Sheu, T. S., "New packaging method using PDMS for piezoresistive pressure sensors," *Sensors and Materials*, 7(19), 391-403 (2007).
- [127] Lee, J., Shin, D., Makotchenko, V., Nazarov, A., Fedorov, V., Kim, Y., Choi, J., Kim, J., and Yoo, J., "One-step exfoliation synthesis of easily soluble graphite and transparent conducting graphene sheets," *Adv. Mater.*, 21, 1-5 (2009).
- [128] Falcao, E., Blair, R., Mack, J., Viculis, L., Kwon, C., Bendikov, M., Kaner, R., Dunn, B., and Wudl, F., "Microwave exfoliation of a graphite intercalation compound," *Carbon*, 6(45), 1367-1369 (2007).
- [129] Wei, T., Fan, Z., Luo, G., Zheng, C., and Xie, D., "A rapid and efficient method to prepare exfoliated graphite by microwave irradiation," *Carbon*, 1(47), 337-339 (2009).
- [130] Chen, G., Weng, W., Wu, D., Wu, C., Lu, J., Wang, P., and Chen, X., "Preparation and characterization of graphite nanosheets from ultrasonic powdering technique," *Carbon*, 4(42), 753-759 (2004).
- [131] Yang, H., Tian, M., Jia, Q. X., Shi, J. H., Zhang, L. Q., Lim, S. H., Yu, Z. Z., and Mai, Y. W., "Improved mechanical and functional properties of elastomer/graphite nanocomposites prepared by latex compounding," *Acta Mater.*, 18(55), 6372-6382 (2007).
- [132] Atli, B., Gandhi, F., and Karst, G., "Thermomechanical characterization of shape memory polymers," *Journal of Intelligent Material Systems and Structures*, 1(20), 87-95 (2009).
- [133] Rosset, S., Niklaus, M., Dubois, P., and Shea, H. R., "Ion-implanted compliant electrodes for mm-size dielectric elastomer actuators," in *Smart Structures and Materials & Nondestructive Evaluation and Health Monitoring 2009: Electroactive Polymer Actuators and Devices (EAPAD)*, San Diego, CA, USA 72870C (2009).
- [134] Wang, G., Tao, X., and Wang, R., "Flexible organic light-emitting diodes with a polymeric nanocomposite anode," *Nanotechnology*, 14(145201) (2008).
- [135] Stankovich, S., Piner, R., Chen, X., Wu, N., Nguyen, S., and Ruoff, R., "Stable aqueous dispersions of graphitic nanoplatelets via the reduction of exfoliated graphite oxide in the presence of poly(sodium 4-styrenesulfonate)," *J. Mater. Chem.*, 16, 155-158 (2005).
- [136] Flandin, L., Hiltner, A., and Baer, E., "Interrelationships between electrical and mechanical properties of a carbon black-filled ethylene-octene elastomer," *Polymer*, 2(42), 827-838 (2001).
- [137] Cong, H. L. and Pan, T. R., "Photopatternable conductive PDMS materials for microfabrication," *Adv. Funct. Mater.*, 13(18), 1912-1921 (2008).
- [138] Lux, F., "Review - Models proposed to explain the electrical conductivity of mixtures made of conductive and insulating materials," *Mater. Sci.*, 2(28), 285-301 (1993).

- [139] Bokobza, L. and Rahmani, M., "Carbon nanotubes: exceptional reinforcing fillers for silicone rubbers," *Kautsch. Gummi Kunstst.*, 3(62), 112-117 (2009).
- [140] Guth, E., "Theory of filler reinforcement," *J. Appl. Phys.*, 1(16), 20-25 (1945).
- [141] Halpin, J., "Stiffness and expansion estimates for oriented short fiber composites," *J. Compos. Mater.*, 4(3), 732-734 (1969).
- [142] Celzard, A., McRae, E., Deleuze, C., Dufort, M., Furdin, G., and Marêché, J., "Critical concentration in percolating systems containing a high-aspect-ratio filler," *Phys. Rev. B.*, 10(53), 6209 (1996).
- [143] Bunch, J., van der Zande, A., Verbridge, S., Frank, I., Tanenbaum, D., Parpia, J., Craighead, H., and McEuen, P., "Electromechanical resonators from graphene sheets," *Science*, 5811(315), 490-493 (2007).
- [144] Park, S. and Ruoff, R. S., "Chemical methods for the production of graphenes," *Nature Nanotechnology*, 4(4), 217-224 (2009).
- [145] Fan, X. B., Peng, W. C., Li, Y., Li, X. Y., Wang, S. L., Zhang, G. L., and Zhang, F. B., "Deoxygenation of Exfoliated Graphite Oxide under Alkaline Conditions: A Green Route to Graphene Preparation," *Advanced Materials*, 23(20), 4490-4493 (2008).
- [146] Cai, D. and Song, M., "Preparation of fully exfoliated graphite oxide nanoplatelets in organic solvents," *J. Mater. Chem.*, 17), 3678-3680 (2007).
- [147] Zhang, R., Baxendale, M., and Peijs, T., "Universal resistivity-strain dependence of carbon nanotube/polymer composites," *Phys. Rev. B.*, 19(76), 195433 (2007).
- [148] Hu, L. B., Yuan, W., Brochu, P., Gruner, G., and Pei, Q. B., "Highly stretchable, conductive, and transparent nanotube thin films," *Appl. Phys. Lett.*, 16(94), 3 (2009).
- [149] Kim, K., Zhao, Y., Jang, H., Lee, S., Kim, J., Kim, K., Ahn, J., Kim, P., Choi, J., and Hong, B., "Large-scale pattern growth of graphene films for stretchable transparent electrodes," *Nature*, 7230(457), 706-710 (2009).
- [150] Rosset, S., Niklaus, M., Dubois, P., and Shea, H. R., "Metal Ion Implantation for the Fabrication of Stretchable Electrodes on Elastomers," *Advanced Functional Materials*, 3(19), 470-478 (2009).
- [151] Sekitani, T., Noguchi, Y., Hata, K., Fukushima, T., Aida, T., and Someya, T., "A rubberlike stretchable active matrix using elastic conductors," *Science*, 5895(321), 1468-1472 (2008).
- [152] Rosset, S., Niklaus, M., Stojanov, V., Felber, A., Dubois, P., and Shea, H., "Ion-implanted compliant and patternable electrodes for miniaturized dielectric elastomer actuators," 69270W (2008).
- [153] Chung, D., "Review graphite," *J. Mater. Sci.*, 8(37), 1475-1489 (2002).
- [154] Hummers, W. S. and Offeman, R. E., "Preparation of graphitic oxide," *J. Am. Chem. Soc.*, 6(80), 1339-1339 (1958).
- [155] Stankovich, S., Dikin, D., Dommett, G., Kohlhaas, K., Zimney, E., Stach, E., Piner, R., Nguyen, S., and Ruoff, R., "Graphene-based composite materials," *Nature*, 7100(442), 282-286 (2006).
- [156] Engel, J. M., Chen, J., Liu, C., and Bullen, D., "Polyurethane rubber all-polymer artificial hair cell sensor," *Journal of Microelectromechanical Systems*, 4(15), 729-736 (2006).

- [157] Menzel, D. H., *Fundamental formulas of physics* vol. 2. New York: Dover Publications (1960).
- [158] Chen, G., Weng, W., Wu, D., and Wu, C., "PMMA/graphite nanosheets composite and its conducting properties," *Eur Polym J*, 12(39), 2329-2335 (2003).
- [159] Viswanathan, R. and Heaney, M., "Direct imaging of the percolation network in a three-dimensional disordered conductor-insulator composite," *Phys. Rev. Lett.*, 24(75), 4433 (1995).
- [160] Kilbride, B. E., Coleman, J. N., Fraysse, J., Fournet, P., Cadek, M., Drury, A., Hutzler, S., Roth, S., and Blau, W. J., "Experimental observation of scaling laws for alternating current and direct current conductivity in polymer-carbon nanotube composite thin films," *J. Appl. Phys.*, 7(92), 4024-4030 (2002).
- [161] Quivy, A., Deltour, R., Jansen, A., and Wyder, P., "Transport phenomena in polymer-graphite composite materials," *Phys. Rev. B*, 2(39), 1026 (1989).
- [162] Ezquerra, T. A., Mohammadi, M., Kremer, F., Vilgis, T., and Wegner, G., "On the percolative behaviour of polymeric insulator-conductor composites: polyethylene oxide-polypyrrole," *J. Phys. C: Solid State Phys.*, 5(927) (1988).
- [163] Grimaldi, C. and Balberg, I., "Tunneling and nonuniversality in continuum percolation systems," *Phys. Rev. Lett.*, 6(96), 066602 (2006).
- [164] Balberg, I., "Tunneling and nonuniversal conductivity in composite materials," *Phys. Rev. Lett.*, 12(59), 1305 (1987).
- [165] Rosset, S., Niklaus, M., Stojanov, V., Felber, A., Dubois, P., and Shea, H. R., "Ion-implanted compliant and patternable electrodes for miniaturized dielectric elastomer actuators," in *Smart Structures/Nondestructive Evaluation for Health Monitoring + Diagnostics 2008: Electroactive Polymer Actuators and Devices (EAPAD)* San Diego, CA, USA 69270W (2008).
- [166] Liu, C. and Choi, J., "Patterning conductive PDMS nanocomposite in an elastomer using microcontact printing," *J. Micromech. Microeng.*, 8(085019) (2009).
- [167] Kujawski, M., Pearse, J. D., and Smela, E., "Elastomers filled with exfoliated graphite as compliant electrodes," *Carbon*, 9(48), 2409-2417 (2010).
- [168] Abot, J., L., Schulz, M., J., Song, Y., Medikonda, S., and Rooy, N., "Novel distributed strain sensing in polymeric materials," *Smart Mater. Struct.*, 8(19), 085007 (2010).
- [169] Hu, N., Karube, Y., Yan, C., Masuda, Z., and Fukunaga, H., "Tunneling effect in a polymer/carbon nanotube nanocomposite strain sensor," *Acta Mater.*, 13(56), 2929-2936 (2008).
- [170] Knite, M., Teteris, V., Kiploka, A., and Kaupuzs, J., "Polyisoprene-carbon black nanocomposites as tensile strain and pressure sensor materials," *Sens. Actuators, A*, 1-3(110), 142-149 (2004).
- [171] Product Data Sheet, All-Spec Industries, http://www.all-spec.com/downloads/circuitworks/CW2400_040609s.pdf, Accessed on April 17 (2011).
- [172] Kim, H. and Macosko, C. W., "Morphology and properties of polyester/exfoliated graphite nanocomposites," *Macromolecules*, 9(41), 3317-3327 (2008).
- [173] Afanasov, I. M., Morozov, V. A., Kepman, A. V., Ionov, S. G., Seleznev, A. N., Tendeloo, G. V., and Avdeev, V. V., "Preparation, electrical and thermal

- properties of new exfoliated graphite-based composites," *Carbon*, 1(47), 263-270 (2009).
- [174] Product Datasheet, Asbury Carbons Inc., <http://www.asbury.com/Expandable-Flake-Graphite.html>, Accessed on March 29 (2011).
- [175] Material Safety Data Sheet, Environmolds, http://www.artmolds.com/pdf/MSDS_407_Latex.pdf, Accessed on March 29 (2011).
- [176] Frogley, M. D., Ravich, D., and Wagner, H. D., "Mechanical properties of carbon nanoparticle-reinforced elastomers," *Compos. Sci. Technol.*, 11(63), 1647-1654 (2003).
- [177] Kovacs, G. T. A., *Micromachined Transducers Sourcebook*. Boston, M.A.: McGraw- Hill (1998).
- [178] Pang, H., Chen, T., Zhang, G., Zeng, B., and Li, Z., "An electrically conducting polymer/graphene composite with a very low percolation threshold," *Mater. Lett.*, 20(64), 2226-2229 (2010).
- [179] Pham, G. T., Park, Y., Liang, Z., Zhang, C., and Wang, B., "Processing and modeling of conductive thermoplastic/carbon nanotube films for strain sensing," *Composites Part B*, 1(39), 209-216 (2008).
- [180] He, D. and Ekere, N. N., "Effect of particle size ratio on the conducting percolation threshold of granular conductive-insulating composites," *J. Phys. D: Appl. Phys.*, 13(37), 1848 (2004).
- [181] da Silva, J. G., de Carvalho, A. A., and da Silva, D. D., "A strain gauge tactile sensor for finger-mounted applications," *Proc. IEEE Trans. on Instrumentation and Measurement*, 1(51), 18-22 (2002).
- [182] Kazi, I. H., Wild, P. M., Moore, T. N., and Sayer, M., "The electromechanical behavior of nichrome (80/20 wt.%) film," *Thin Solid Films*, 1-2(433), 337-343 (2003).
- [183] Aslam, M., Taher, I., Masood, A., Tamor, M. A., and Potter, T. J., "Piezoresistivity in vapor-deposited diamond films," *Appl. Phys. Lett.*, 23(60), 2923-2925 (1992).
- [184] Hay, G. I., Southee, D. J., Evans, P. S. A., Harrison, D. J., Simpson, G., and Ramsey, B. J., "Examination of silver-graphite lithographically printed resistive strain sensors," *Sens. Actuators, A*, 2(135), 534-546 (2007).
- [185] Yasin, S. F., Zihlif, A. M., and Ragosta, G., "The electrical behavior of laminated conductive polymer composite at low temperatures," *J. Mater. Sci. - Mater. Elect.*, 2(16), 63-69 (2005).
- [186] Wen, S., Wang, S., and Chung, D. D. L., "Carbon fiber structural composites as thermistors," *Sens. Actuators, A*, 2-3(78), 180-188 (1999).
- [187] Tang, Q., Chan, Y. C., and Zhang, K., "Fast response resistive humidity sensitivity of polyimide/multiwall carbon nanotube composite films," *Sens. Actuators, B*, 1(152), 99-106 (2011).
- [188] Yu, H., Cao, T., Zhou, L., Gu, E., Yu, D., and Jiang, D., "Layer-by-Layer assembly and humidity sensitive behavior of poly(ethyleneimine)/multiwall carbon nanotube composite films," *Sens. Actuators, B*, 2(119), 512-515 (2006).

- [189] Yoo, K., Lim, L., Min, N., Lee, M., Lee, C. J., and Park, C., "Novel resistive-type humidity sensor based on multiwall carbon nanotube/polyimide composite films," *Sens. Actuators, B*, 1(145), 120-125 (2010).
- [190] Luheng, W., Tianhuai, D., and Peng, W., "Thin flexible pressure sensor array based on carbon black/silicone rubber nanocomposite," *IEEE Sens. J.*, 9(9), 1130-1135 (2009).
- [191] Luheng, W., Tianhuai, D., and Peng, W., "Effects of conductive phase content on critical pressure of carbon black filled silicone rubber composite," *Sens. Actuators, A*, 2(135), 587-592 (2007).
- [192] Vilčáková, J., Sáha, P., Kresálek, V., and Quadrat, O., "Pre-exponential factor and activation energy of electrical conductivity in polyester resin/carbon fibre composites," *Synth. Met.*, 1-2(113), 83-87 (2000).
- [193] Psarras, G. C., "Hopping conductivity in polymer matrix-metal particles composites," *Composites Part A*, 10(37), 1545-1553 (2006).
- [194] Banerjee, S. and Chakravorty, D., "Alternating current conductivity and dielectric dispersion in copper-silica nanocomposites synthesized by electrodeposition," *J. Appl. Phys.*, 2(84), 799-805 (1998).
- [195] King, R. J., "Dynamic Mechanical Properties of Resilin," in *Engineering Science and Mechanics*. vol. Masters of Science In Engineering Mechanics: Virginia Polytechnic Institute, 2010, p. 33.